THE UNIVERSITY OF ALBERTA

RELEASE FORM

NAME OF AUTHOR   Gordon Edwin Blinston

TITLE OF THESIS   Spectral Analysis of Motor Unit Responses

in Toad Skeletal Muscle

DEGREE FOR WHICH THESIS WAS PRESENTED. Doctor of Philosophy

YEAR THIS DEGREE GRANTED   1976

Permission is hereby granted to THE UNIVERSITY OF ALBERTA LIBRARY to reproduce single copies of this thesis and to lend or sell such copies for private, scholarly or scientific research purposes only.

The author reserves other publication rights, and neither the thesis nor extensive extracts from it may be printed or otherwise reproduced without the author's written permission.

THE UNIVERSITY OF ALBERTA

SPECTRAL ANALYSIS OF MOTOR UNIT RESPONSES
IN TOAD SKELETAL MUSCLE

by

Gordon Edwin Blinston (C)

A THESIS

SUBMITTED TO THE FACULTY OF GRADUATE STUDIES AND RESEARCH

IN PARTIAL FULFILMENT OF THE REQUIREMENTS FOR THE DEGREE

OF DOCTOR OF PHILOSOPHY

DEPARTMENT OF ELECTRICAL ENGINEERING

EDMONTON, ALBERTA

SPRING 1976

THE UNIVERSITY OF ALBERTA

FACULTY OF GRADUATE STUDIES AND RESEARCH

The undersigned certify that they have read, and recommend to the Faculty of Graduate Studies and Research, for acceptance, a thesis entitled Spectral Analysis of Motor Unit Responses in Toad Skeletal Muscle submitted by Gordon Edwin Blinston in partial fulfilment of the requirements for the degree of Doctor of Philosophy.

ABSTRACT

The effectiveness of spectral analysis in studying the
responses of single motor units was investigated for motor units in the
iliofibularis muscle of the toad *Xenopus laevis*.

Isolated motor axons were electrically stimulated with
narrow, supramaximal pulses. Motor units which displayed a twitch-like
contraction in response to a single stimulus pulse were classified as
fast motor units, and those which did not display such a contraction
were classified as slow motor units. On the basis of their isometric
tension responses to stimulation with trains of evenly-spaced pulses,
the fast motor units were further subdivided into three types, and the
slow units were subdivided into two types.

The histochemistry of muscle fibres from several isolated
motor units was studied. The results of such studies support the
hypothesis that each unit contains only a single type of muscle fibre.
Each motor unit type was matched with one of five muscle fibre types.

Spectral analysis methods were used to study the responses
of each type of motor unit to trains of randomly-occurring pulses.
Transfer function and coherence estimates which related the low freq-
uency components of the random stimulus train to the resulting isometric
muscle tension were calculated. These estimates indicated that for
frequencies in the range 0.5-25 Hz, the response of a slow motor unit
to random stimulation is poorly represented by the response of a linear,
noise-free system, and the response of a fast motor unit is similar to
that of a second-order low-pass filter with an added time delay.
Curves representing the responses of such linear systems were fitted to

transfer function estimates for fast motor units, and confidence inter-
vals for the parameters defining these fitted curves were estimated.

For a given motor unit, these parameters depended systematically upon

such factors as muscle length and mean stimulus rate. Computer

simulations of fast motor units, based on the experimentally-observed

linear models, were used to demonstrate the effects of various modif-

ications to the spectral analysis procedure.

The linear models for the responses of fast motor units to

random stimulation were only approximate and were subject to many

restrictions. However, such models were found to be useful as a

standard basis for describing motor unit responses. They also provided

information about motor unit function which supplemented the results of

studies involving stimulation with trains of regularly-occurring pulses.

ACKNOWLEDGMENT

TABLE OF CONTENTS

Chapter

* * *

LIST OF TABLES

LIST OF FIGURES

CHAPTER 1

INTRODUCTION

Studies of input-output relationships for the elements of a
control system often involve the development of mathematical models
from experimental observations. Linear relationships can be modeled
in this way by fitting transfer functions to frequency response plots
based on experimental data [1,2,3], and, in many situations, nonlinear
relationships may be approximated by such linear transfer functions.
Attempts have been made to use this approach in studying various
elements of the system which controls movement in animals (the motor
control system), but the use of linear transfer functions in such
situations is complicated by the fact that many of the signals which
are encountered appear as trains of identical, narrow spikes [4],
whereas the behavior of a linear system is generally described in
terms of its transfer function for continuous sinusoidal signals.

A skeletal muscle is composed of many muscle fibres arranged
into individually-controllable groups called motor units. These fibres
contract when the nerve serving the muscle is electrically stimulated
with a train of narrow pulses. A mathematical model describing the
relationship between the electrical stimulus and the resulting muscle
tension for single motor units would be a useful component of any
analysis of the entire motor control system; but, if such a model is
to be determined, a means of analytically relating the pulse train to
the continuously changing muscle tension must be devised. Partridge
[5], who studied the frequency response of the whole triceps surae
muscle in the cat, approached this problem by using pulse trains for
which the interpulse intervals were sinusoidally modulated. Frequency

1

response plots expressing the relationship between the modulating signal and the muscle tension were produced, and transfer functions were fitted to these plots. A similar approach was used by Rosenthal et al. [6] for the cat gastrocnemius muscle.

Pulse trains with sinusoidally modulated interpulse intervals have certain disadvantages when used as inputs to measure the frequency response of nerve-muscle preparations. The production of a frequency response plot requires measurement of the responses to a large number of different sinusoidally modulated signals, and this means that the preparation must be subjected to long periods of stimulation which could cause muscle fatigue. In addition, because such pulse trains contain power only at discrete frequencies [7], any nonlinearities arising from the effects of intermodulation could not be detected.

In order to overcome these disadvantages, spectral analysis methods have been used to relate spike trains to continuous signals for both sensory [8-10] and motor [11,12] elements of the neuromuscular system. For the nerve-muscle preparation, a train of randomly occurring pulses is used as the input signal, and the resulting transfer function estimate relates the frequency components of this pulse train to the corresponding frequency components in the continuous signal representing muscle tension. The input pulse train can be tailored so that it contains power at all frequencies within the band of interest, thereby insuring that any potential intermodulation effects will occur. If the system is not perfectly linear and noise-free, the transfer function estimate will represent the response of the linear, noise-free system which describes with minimum mean-squared error [13] the

actual system response. The degree to which this linear system contributes to the actual system response is apparent from the coherence estimate which is readily calculated from the same data used in determining the transfer function estimate [14].

Several approaches are available for the spectral analysis of random pulse trains: the pulse train may be viewed as a realization of a stochastic point process and analyzed accordingly [15-18], it may be viewed as a train of unit impulses [19], or it may be filtered with a low-pass filter to produce a continuous, band-limited signal [8,9]. The filtering approach is attractive for the study of nerve-muscle preparations because special hardware to measure the occurrence times of the impulses is not required, and because the continuous signal appearing at the filter output may be processed with the fast Fourier transform [20-22] in the same manner as the continuous signal representing the system output [14,23,24].

In considering the application of spectral analysis to the study of input-output relationships for single motor units, several questions may be posed.

1. What spectral analysis procedures should be used for this application?

2. Can the results of such studies be readily interpreted?

3. How are the transfer function estimates related to the responses resulting from stimulation with trains of evenly-spaced pulses?

4. How does the structure of the muscle affect the observed input-output relationships?

5. How does a study of the input-output relationships for
    single motor units contribute to our knowledge of motor
    unit organization?

Beginning with reviews of some of the relevant areas of muscle
physiology and spectral analysis in Chapters 2 and 3 respectively, this
thesis is an attempt to answer the above questions for motor units in a
muscle of the hind limb of the amphibian *Xenopus laevis*. When this
project was begun, it was not known whether spectral analysis methods
could be successfully used in such an application, but, since that time
the results of a few studies demonstrating the feasibility of such an
approach have appeared [11,12,25]. Therefore, although the problems
involved in implementing the technique are considered here, much of the
emphasis is placed on the interpretation of the resulting transfer
function estimates with the aim of determining whether these results
provide enough information to justify the considerable effort required
to obtain them.

CHAPTER 2

MUSCLE FIBRES AND MOTOR UNITS

2.1   Vertebrate Skeletal Muscle

2.1.1 Structure

According to current physiology textbooks [27-29], vertebrate
skeletal muscle is composed of an aggregation of cylindrical muscle
fibres held together with connective tissue. These fibres are
arranged longitudinally, and they often run the full length of the
muscle. Unfortunately, most of these sources imply that vertebrate
skeletal muscle is composed of identical muscle fibres when, in fact,
several types of muscle fibre have been described, both in mammals
[30-33,49] and in amphibia [34-37]. The contractile properties of
individual muscle fibres can vary greatly from fibre to fibre in the
same muscle, and the distribution of fibre types varies from muscle to
muscle in the same individual. However, the structure of a particular
muscle is remarkably similar in different individuals of the same
species.

Muscle fibres are composed of bundles of cylindrical fibrils,
and each fibril is composed of many longitudinally arranged filaments
which are organized into distinct bands [38]. A system of nomenclature
to describe this band-like structure has arisen (Figure 2.1). The A
(anisotropic) band is composed of thick parallel filaments 100-120 $\overset{o}{A}$
in diameter and 1.6 μm long. The I (isotropic) band filaments, which
are generally attached at their mid-point to a structure known as the
Z line, are thinner (60-70 $\overset{o}{A}$ in diameter). The two sets of filaments
overlap within much of the A band, and they are generally arranged so
that each A filament is surrounded by six I filaments; but other
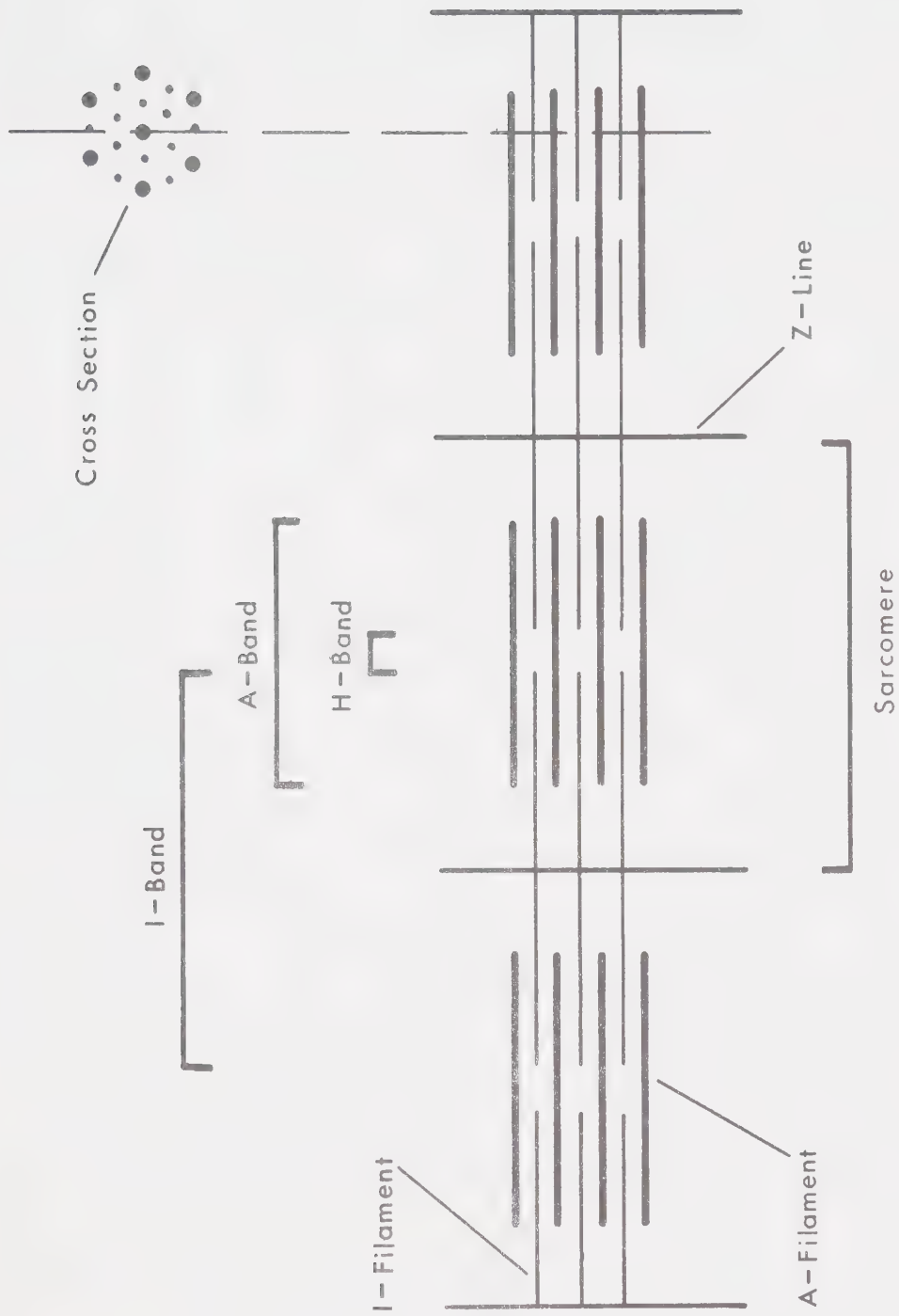
FIGURE 2.1 Structure of Skeletal Muscle

alignments do occasionally occur. The region within the A band where the two sets of filaments do not overlap is known as the H (Hensen's) band, and the portion of the fibril delineated by two Z lines is called a sarcomere. This arrangement is repeated along the length of the fibril.

An important component of every muscle fibre is called the sarcoplasmic reticulum [39]. This structure is a continuous, membrane-limited system of tubules which form a close network around each fibril. The finger-like tubules which surround the myofibrils are longitudinally oriented, and they periodically converge to form dilated circumferential structures known as terminal cisternae. Another system of tubules within the muscle fibre is in close contact with, but separate from, the terminal cisternae. These tubules, which appear to be open to the extracellular space at the cell membrane [40], run transversely through most of the muscle fibre and are therefore called transverse or T-tubules. The arrangement of the sarcoplasmic system and the T-tubules is such that certain characteristic features known as triads occur in every sarcomere. A triad consists of a T-tubule and two terminal cisternae arranged so that a longitudinal section through the muscle would reveal the T-tubule between the two terminal cisternae aligned along an axis parallel to the myofibrils. In most mammals, the triad is centered near the A-I junction, but in frogs, it coincides with the Z line [41].

As well as the more or less regularly arranged myofibrils and membrane systems, the muscle fibre contains many irregularly placed bodies. Scattered throughout each muscle fibre are structures known

as mitochondria which are involved in the synthesis of adenosine triphosphate (ATP). Glycogen and droplets containing fat act as sources of energy for this process. Every muscle fibre also contains many peripherally-placed nuclei [38].

2.1.2 Muscle Contraction

A motor nerve cell (motoneuron) transmits information from the central nervous system to the skeletal muscles by means of action potentials (temporary depolarizations of the nerve cell membrane) [49]. These action potentials travel along a thread-like extension of the cell body known as the nerve axon. A structure called a synapse is located at the junction of a motor nerve axon and a muscle fibre [45]. When an action potential arrives at the synapse, a small quantity of the chemical acetylcholine is released. The acetylcholine causes a local depolarization of the muscle fibre's surface membrane, and, in most muscle fibres, this depolarization develops into an action potential which is transmitted along the fibre. A release of calcium ions by the sarcoplasmic reticulum is associated with the depolarization of the surface membrane [46], and these calcium ions catalyse a chemical reaction involving ATP which causes the interdigitated A and I filaments to slide together producing tension [41]. After a short time, the calcium ions are sequestered by the sarcoplasmic reticulum, and the muscle tension drops back to its initial level [47]. Thus a single depolarizing pulse applied to the motoneuron causes a single muscle twitch. If the motoneuron is stimulated by a series of pulses, the individual twitches tend to sum; and if the frequency of stimulation

is high enough, a smooth sustained muscular contraction results. This type of contraction is called a tetanic contraction.

Although the above description of the mechanism for muscle contraction holds for a large proportion of muscle fibres, the response of certain amphibian muscle fibres does not follow this pattern. The local depolarization induced by the release of acetylcholine at the synapse does not result in the generation of a propagated action potential [48]. Therefore the muscle fibre contracts only in the region of the synapse rather than over its whole length, and it does not produce a twitch in response to a single stimulating pulse applied to the motoneuron. If the motoneuron is stimulated by a series of pulses, however, a smooth sustained contraction is observed [50].

The tension developed by muscles is used mechanically in several ways. The muscle may shorten and produce movement, it may oppose a constant force (such as gravity) without changing length, or it may oppose some external force or antagonistic muscle while it is being stretched. Although the muscle can develop tension over a wide range of lengths and external forces, normally two standard modes of contraction--isometric and isotonic--are used in the study of the gross contractile properties of muscle [52-54]. Isometric contraction refers to contraction at a fixed length, and isotonic contraction refers to contraction with a constant load.

The human body contains approximately 2.5×10^8 muscle fibres but only about 4×10^5 motoneurons [55], and similar ratios of muscle fibres to motoneurons are apparent in all vertebrates. Therefore, one motoneuron must innervate many different muscle fibres. Since the control of a muscle is achieved via the motoneurons, the smallest

discrete unit which can be controlled by the central nervous system consists of all of the muscle fibres innervated by the branches of a single motoneuron. This group of muscle fibres, together with its motoneuron is known as a motor unit. Some small motor units contain only a few muscle fibres [56], but larger motor units containing several hundred muscle fibres are not uncommon [57].

2.2 Amphibian Skeletal Muscle

2.2.1 Response to Stimulation

Differences between the muscle fibres in amphibia were first noted in 1944 by Tasaki and Mizutani [58]. They observed differences in the contractile properties of the muscle when various isolated motor axons were stimulated. Kuffler et al. [50,59] found that stimulation of the larger diameter motoneurons resulted in the familiar propagated action potential and resulting twitch, but selective stimulation of the smaller diameter motoneurons resulted in a slow local contraction and a non-propagated depolarization in the area of the local contraction. The two different responses were observed in the gastrocnemius, peroneus, and tibial interossei muscles, but not in the sartorius or adductor longus. The so-called "small nerve system" was especially prevalent in the iliofibularis and semitendinosus, and a bunching of the small nerve activated muscle fibres was noted in the iliofibularis. This bundle, which had earlier been called the "tonus bundle" by Sommerkamp [60] was composed of reddish-colored fibres. When the tonus bundle was subjected to the same stimulation procedure previously applied to the whole muscle, both propagated large nerve contractures and local small nerve contractures were observed.

Kuffler [61] continued to study the properties of muscle fibres innervated by small-diameter motoneurons. He found that the muscle fibres possessed many terminal contacts with motoneurons, that these contacts were distributed along the whole fibre length, and that the contacts on an individual fibre did not all originate from the same axon. He also noted that the membrane potential was smaller than that of the fast, twitch producing fibres and that propagated action potentials never occurred in the slow fibres. These results were later confirmed by Burke and Ginsborg [48]. Kuffler also concluded that no individual muscle fibre can exhibit both "fast" and "slow" types of response. Kuffler and Williams [62] noted that although the slow fibres were incapable of developing large tensions, they could, when continuously stimulated, maintain large tensions originally produced by twitches.

Nasledov [63] studied the electrical excitability of fibres in the sartorius and in the tonic bundle of the iliofibularis. He found that the sartorius was composed exclusively of fast fibres and that the tonic bundle of the iliofibularis contained two types of fast fibres in addition to the slow fibres. One of these fast fibre types had properties similar to those noted in the sartorius, but the other type of fast fibre did not always develop an action potential in response to a single stimulation of the nerve. This type of fibre probably corresponds to those noted by Ralston and Libet [64] and by Kuffler and Williams [62] in which the development of action potentials is facilitated by stretch or multiple stimuli. Orkand [65] proposed that the reason for the low excitability of such fibres is

the small quantity of transmitter released at the motor endplate by an individual nerve impulse.

2.2.2 Structure

Although much of the early evidence for the existence of more than one type of muscle fibre was obtained from studies of a muscle's response to electrical stimulation, observations by microscopists also indicated the existence of at least two structurally different types of muscle fibre. Kruger's [66] classification of amphibian muscle fibre structures into two types, *fibrillenstruktur* and *felderstruktur*, was confirmed by Hess in 1960 [67]. *Fibrillenstruktur* fibres contain lipid droplets, have many sarcoplasmic granules and possess individual fibres surrounded by sarcoplasm. The Z lines of such fibres appear straight across the width of the fibrils. *Felderstruktur* fibres, on the other hand, contain no lipid droplets and fewer sarcoplasmic granules. Their fibres appear to clump together, and the Z lines appear wavy across the width of the fibre.

Two distinct types of motor end-plate (junction of nerve and muscle) were observed by Gray [68] in 1956 and this observation was confirmed and expanded upon by Hess [67]. Hess stated that the nerve endings were either of *en plaque* or *en grappe* type. *En plaque* endings are branching, ribbon-like structures originating from large-diameter axons, whereas *en grappe* endings appear as clusters of tiny balls originating from branches of the smaller axons. Variations between the *en plaque* endings of fibres within the tonus bundle and those not contained within the tonus bundle were noted. *En grappe* endings were found only on fibres within the tonus bundle, and many such endings

were observed closely spaced on each muscle fibre. Generally only one *en plaque* ending could be seen per muscle fibre, and when more than one such ending was observed on a single fibre, the multiple endings were widely spaced. Both types of motor end-plate could not be seen on the same fibre. Direct observation showed that muscle fibres with *en plaque* endings are of *fibrillenstruktur* type only, and that *en grappe* endings occur on fibres of *felderstruktur* type. It thus appeared that the fast muscle fibres are of *fibrillenstruktur* type with *en plaque* endings and the slow muscle fibres are of *felderstruktur* type with *en grappe* endings.

Further structural differences between slow and fast muscle fibres were documented by Peachey and Huxley [69]. They observed that the fast fibres are composed of myofibrils well-delineated by sarco-plasmic elements. The M band (a swelling of the thick filaments occurring in the middle of the A band) is well-defined, and triads are visible. In contrast, slow fibres are composed of larger ribbon-like myofibrils, often fused together; they have no visible M bands and no triads; and the Z bands of such fibres are thicker. In addition, the slow muscle fibres possess more mitochondria than do the fast fibres. Page [70] agreed with most of these observations, but, unlike Peachey and Huxley, she was able to detect triads occurring at every fifth or sixth Z line in the slow fibres.

Smith and Ovalle [34] have carried the structural classifica-tion of muscle fibre types a step further by staining serial sections of the same muscle for two different enzymes, succinic dehydrogenase and myosin adenosine triphosphatase, and correlating the histochemical profiles with the fibres' ultrastructural characteristics. With this

technique, they were able to distinguish five types of muscle fibre that they have designated numerically. A summary of their results is presented in Table 2.1. The sartorius muscle, which contains no slow muscle fibres is composed solely of types 1 and 2 fibres as is the outer portion of the iliofibularis. The centre portion of the iliofibularis is composed of types 3, 4 and 5 muscle fibres. Smith and Ovalle feel that the muscle fibre types designated 1, 2 and 3 belong to the population of fast muscle fibres and that types 4 and 5 are slow muscle fibres.

2.2.3 Relationship Between Structure and Function

The functional properties of the various types of muscle fibres in the iliofibularis were studied by Lännergren and Smith [35]. They found that the fibres outside the tonus bundle possess a moderate content of lipids and oxidative enzymes, and that these fibres fatigue rapidly if stimulation is maintained. They also found that some of the fast fibres within the tonus bundle possess a high content of lipids and oxidative enzymes and do not fatigue rapidly. The oxidative enzyme and lipid content of the slow fibres was found to be very low. Similar histochemical results were obtained by Asmussen and Kiessling [71]. They identified two types of fast muscle fibre and observed that the tonus bundle of the iliofibularis is composed of two fibre types-- slow fibres with an extremely low content of oxidative mitochondrial enzymes and thin, fast fibres with many mitochondria.

Recently, Zagorska [37] has classified fibres in the eye muscles of various species of frogs and toads into four groups. This classification, based on structural criteria, includes three fast

Muscle fibre types ... Numerical designation ...	Large pale 1	Large dark 2	Small dark 3	Small pale 4	Small clear 5
Myosin ATPase staining	Dark	Dark	Dark	Pale	Clear
SDHase staining	Pale	Dark	Very dark	Pale	Clear
Muscle fibre diameter (μm)	169.0±17.8	145.0±17.6	76.7±12.1	60.7±5.4	44.0±7.7
Myofibril cross-section area (μm2)	3.3±1.0	1.1±0.3	0.7±0.2	2.8±1.2	5.4±2.5
Mitochondrial volume(%)	2.5	11.1	17.4	4.1	1.3
Glycogen and lipid droplet content	Low	High	Very high	Low	Very low
Z band	Thin; square lattice; straight	Moderately thick; square lattice; straight	Moderately thick; square lattice; straight	Thick; square lattice; jagged	Thick; irregular lattice; jagged
M band	Straight	Straight	Straight	Irregular when present	Absent
Sarcotubular system	Well developed	Well developed	Moderately developed	Poorly developed	Poorly developed

TABLE 2.1

Characteristics of Muscle Fibre Types

muscle fibre types and a single slow fibre type. Species-related
differences were noted in the proportions of the various fibre types in
each eye muscle, and these differences agree with the proposition that
the muscles are constructed to suit the particular way of life of each
species.

A study by Smith and Lännergren [72] of the properties of
individual motor units in the iliofibularis identified four types of
motor units--two fast and two slow. The fast motor units composed of
fibres in the outer part of the muscle fatigue rapidly in comparison to
the fast motor units near the centre of the muscle. The two slow motor
unit types can be differentiated according to the rate of rise of
tension in response to a train of stimulus pulses. Both types of slow
motor unit are located near the centre of the muscle. The fact that the
location of single motor units within the muscle corresponds to the
location of a given type of muscle fibre indicates that motor units may
possibly be homogeneous in composition. Further support for this pro-
position is provided by the fact that the functional properties of
single motor units and individual muscle fibres are remarkably similar.

2.3 Summary

Skeletal muscles in vertebrates are composed of muscle fibres
which are not all similar, either in terms of their structure or their
function. Muscle fibres in frogs and toads can be broadly classified
into two groups--fast and slow--and evidence indicating the existence of
a total of five sub-classifications has been presented. The muscle
fibres are organized into motor units having a variety of functional
properties. Because each motor unit appears to be homogeneous in

composition, the possibility of a one-to-one correspondence between motor unit types and muscle fibre types is evident. The demonstration of such a relationship would be a worthwhile expansion of the current knowledge concerning the functioning of amphibian muscle.

CHAPTER 3

SPECTRAL ESTIMATION

3.1 The Power Spectrum

The autocovariance function $R_{xx}(\tau)$ of a stationary random process $x(t)$ is defined as

$$R_{xx}(\tau) = \lim_{T \to \infty} \frac{1}{T} \int_{-T/2}^{T/2} x(t) \cdot x(t+\tau) d\tau \tag{3.1}$$

A random process is stationary if its statistical properties are unaffected by any translation of the time origin. The Fourier transform of $R_{xx}(\tau)$ is known as the power spectrum of $x(t)$:

$$S_{xx}(f) = \int_{-\infty}^{\infty} R_{xx}(\tau) e^{-j2\pi f\tau} d\tau \tag{3.2}$$

This quantity is a measure of the power per unit bandwidth (in Hz) centred at frequency f. Although the Fourier transform of a signal is generally a complex quantity, the power spectrum is real because $R_{xx}(\tau)$ is symmetrical about the $\tau=0$ axis.

In order to evaluate the power spectrum of a signal with Equation (3.2), an infinitely long sample of the signal is required. In practical situations, only samples of finite length are available, and the power spectrum must be estimated from such samples.

3.1.1 Power Spectrum Estimation

In 1958, Blackman and Tukey [73] described an indirect procedure for calculating spectral estimates based on the Fourier transformation of autocovariance functions evaluated over the sample

18

length. This procedure was popular until the development of the fast Fourier transform algorithm in the middle 1960's [20-22,92]. With this algorithm, spectral estimates can be calculated directly by Fourier transforming the finite-length sample of the process. Because it is much faster than the indirect procedure, the direct procedure is now used almost exclusively.

A finite sample of the random process $x(t)$ will be denoted as $x_T(t)$ where

$$x_T(t) = \begin{cases} x(t) & 0 \leq t \leq T \\ 0 & t < 0, \ t > T \end{cases} \tag{3.3}$$

A direct estimate of the power spectrum of $x(t)$ based on $x_T(t)$ is

$$\hat{S}_{xx}(f) = \frac{1}{T} |X_T(f)|^2 \tag{3.4}$$

where $X_T(f)$ is the Fourier transform of $x_T(t)$ [23].

If $S_{xx}(f)$ is approximately constant over a frequency band of width $1/T$, the expected value of $\hat{S}_{xx}(f)$ is $S_{xx}(f)$ [23]. However, as T becomes large, the variance of the spectral estimator approaches $S_{xx}^2(f)$ rather than zero [23]. The probability distribution of the spectral estimator $\hat{S}_{xx}(f)$ is proportional to that of a chi-squared distribution with two degrees of freedom [23].

Because the variance of $\hat{S}_{xx}(f)$ does not approach zero as the record length increases, $\hat{S}_{xx}(f)$ is an inconsistent estimator of the true power spectrum, and often the variance of such an estimate is so high that the estimate is useless. A further refinement of the analysis procedure is required in order to eliminate this inconsistency and reduce the variance to an acceptable value. If n independent evaluations of $\hat{S}_{xx}(f)$ are calculated and then averaged, the result is called a smoothed spectral estimate. These n independent evaluations

may be obtained from $x_T(t)$ by dividing this record into n non-overlapping sub-records each of length L and then calculating a separate spectral estimate for each sub-record. For such a situation, n=T/L and the smoothed spectral estimate $\hat{\hat{S}}_{xx}(f)$ [74] is

$$\hat{\hat{S}}_{xx}(f) = \frac{L}{T} \sum_{i=1}^{i=\frac{T}{L}} \hat{S}_{xx_i}(f) \qquad (3.5)$$

A particular sub-record $x_L(t)$ may be viewed as the product of $x(t)$ and $w_D(t)$ where

$$w_D(t) = \begin{cases} 1 & t_1 \leq t \leq t_2 \\ 0 & t > t_1, \ t > t_2 \end{cases} \qquad (3.6)$$

and $t_2 - t_1 = L$. $w_D(t)$ is known as a rectangular data window, and its Fourier transform, $W_D(f)$ is called a frequency window. Multiplication of $x(t)$ by a data window is equivalent to the convolution of $X(f)$ with the corresponding frequency window [75]. That is,

$$X_L(f) = \int_{-\infty}^{\infty} W_D(f-g) \cdot X(g) dg \qquad (3.7)$$

This convolution results in a leakage between frequency bands which is generally undesirable, so the shape of the data window is often modified to reduce the leakage. If the abrupt jumps at the ends of the rectangular data window are smoothed out, the side lobes of the resulting frequency window will be lower than those of the frequency window corresponding to the rectangular data window, and the leakage between widely separated frequency bands will therefore be less [23]. Some commonly used data windows and their corresponding frequency windows are listed in Table 3.1 and illustrated in Figure 3.1 [23]. The effects of leakage through these and other data windows are illustrated by Ramirez [76].

DESCRIPTION	DATA WINDOW	FREQUENCY WINDOW
RECTANGULAR	$w_R(\tau) = \begin{cases} 1 & |\tau| \leq \dfrac{T}{2} \\ 0 & |\tau| > \dfrac{T}{2} \end{cases}$	$W_R(f) = T\left(\dfrac{\sin \pi f T}{\pi f T}\right)$ $\qquad -\infty \leq f \leq \infty$
BARTLETT	$w_B(\tau) = \begin{cases} 1 - 2\dfrac{|\tau|}{T} & |\tau| \leq \dfrac{T}{2} \\ 0 & |\tau| > \dfrac{T}{2} \end{cases}$	$W_B(f) = \dfrac{T}{2}\left(\dfrac{\sin \pi f T/2}{\pi f T/2}\right)$ $\qquad -\infty \leq f \leq \infty$
HANNING	$w_H(\tau) = \begin{cases} \dfrac{1}{2}\left(1 + \cos\dfrac{2\pi\tau}{T}\right) & |\tau| \leq \dfrac{T}{2} \\ 0 & |\tau| > \dfrac{T}{2} \end{cases}$	$W_H(f) = \dfrac{T}{2}\left(\dfrac{\sin \pi f T}{\pi f T}\right)\left(\dfrac{1}{1-(fT)^2}\right)$ $\qquad -\infty \leq f \leq \infty$

TABLE 3.1

Windows for Spectral Analysis

Data Windows
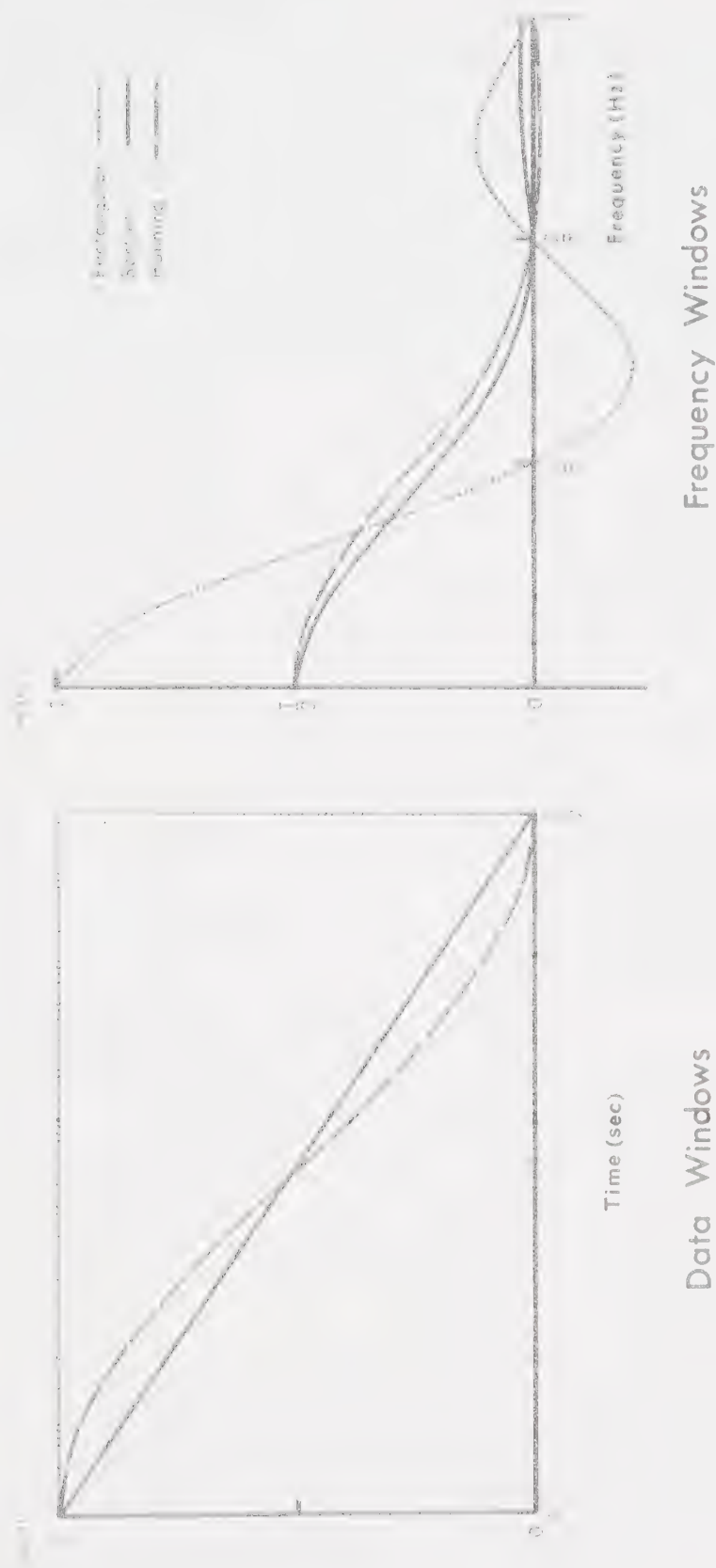
Frequency Windows

FIGURE 3.1   Data and Frequency Windows

3.2 The Discrete Power Spectrum

In practice, spectral estimates calculated according to the above procedure are produced with the aid of a digital computer. Therefore, a continuous signal must be expressed as a series of discrete values which generally represent samples of the signal amplitude collected at evenly spaced time intervals. If the process x(t) is sampled in such a manner and Fourier transformed as in Equation (3.2), the result is

$$X_s(f) = \frac{1}{\Delta} \sum_{n=-\infty}^{\infty} X(f - \frac{n}{\Delta}) \tag{3.8}$$

where Δ is the time (in seconds) between samples [75]. If $X(f) = 0$ when $|f| > 1/2\Delta$, then

$$X_s(f) = \begin{cases} \frac{1}{\Delta} \cdot X(f) & 0 \leq f \leq \frac{1}{2\Delta} \\ \frac{1}{\Delta} \cdot X(1 - \frac{1}{\Delta}) & \frac{1}{2\Delta} \leq f \leq \frac{1}{\Delta} \end{cases} \tag{3.9}$$

This means that the Fourier transform of a process x(t) may be separated from the Fourier transform of the sample values whenever the magnitude of X(f) is zero for all frequencies greater than the so-called Nyquist frequency which is equal to $1/2\Delta$ Hz.

If the signal is not band-limited in this way, components with frequencies higher than the Nyquist frequency will appear at some frequency below the Nyquist frequency because of the summation in Equation (3.8). This effect is referred to as aliasing.

3.2.1 The Discrete Fourier Transform

If $X_s(f)$ is to be evaluated digitally, Equation (3.2) cannot be applied directly. Instead, the discrete Fourier transform is employed. The discrete Fourier transform of a series of numbers

x_0, x_1, x_2...x_{N-1} is [22]

$$X_k = \frac{1}{N} \sum_{q=0}^{N-1} x_q \, e^{-j2\pi kq/N} \qquad (3.10)$$

where $k = 0, 1,...N-1$ and $j = \sqrt{-1}$. The result of this operation is a series of N evenly spaced samples of $X(f)$ spanning the frequency range between 0 and $1/\Delta$ Hz. Only the first $N/2 + 1$ points of this series are unique. As Equation (3.9) shows, the remaining points are the complex conjugates of the first half of the series.

Signals encountered in practical situations are not ideally band-limited as the sampling theorem requires. If, however, the magnitude of the high frequency components decreases with increasing frequency, the effect of aliasing can be minimized by sampling the signal at a rate high enough to insure that the magnitudes of the components above the Nyquist frequency are negligible in comparison to the magnitudes of the low frequency components. This requirement can be satisfied for any signal by passing the signal through an electronic low-pass filter before it is sampled. The cut-off frequency of the low-pass filter and the sampling rate are selected to yield a Fourier transform which covers the entire frequency range of interest with a minimum of aliasing.

If this procedure is not acceptable for a particular signal, a specific procedure which is applicable only to that signal may often be implemented in order to reduce aliasing. An example of such a procedure is the technique proposed by French and Holden [19] for sampling neuronal spike trains. The spike train, which is treated as a series of delta functions, is digitally filtered in order to generate a series of alias-free, evenly-spaced sample values.

A further error in the evaluation of discrete Fourier transforms is introduced when the sample values of the continuous signal are digitized for computer processing. Each sample value must be represented by a discrete binary number (quantization level) with a value which matches that of the sample value as closely as possible. The error introduced by this procedure, called quantization error, can be viewed as noise which has been added to the original signal. Bendat and Piersal [14] show that the RMS value of this quantization noise is equal to 0.29 times the minimum possible difference between two quantization levels. This means that the RMS signal-to-noise ratio is equal to m/0.29 where m is the number of possible quantization levels within the amplitude range covered by the signal. Therefore, the allowable signal-to-noise ratio determines the number of quantization levels required for a particular signal. Tufts, Hersey and Mosier [78] have shown that the effects of quantization noise on the Fourier transform are negligible when 256 or more quantization levels are available.

Evaluation of the discrete Fourier transform of a series of N points according to Equation (3.10) requires approximately N^2 arithmetic operations. If, however, a fast Fourier transform algorithm is used, the number of operations required can be reduced to approximately $2N \cdot \log_2 N$ [79]. This reduction in computational effort is achieved by judiciously factoring Equation (3.10). Fast Fourier transform algorithms are applied to time series for which N is an integral power of 2, but algorithms for transforming time series of other lengths are available if required [80]. Otherwise, a time series may be extended to the desired length by attaching a train of zeroes to either end [80].

3.2.2 The Periodogram

The square of the magnitude of a discrete Fourier transform is called a periodogram, and when this quantity is scaled correctly, it provides an estimate of the power spectrum. If $X(f_k)$ is the discrete Fourier transform based on a series of N samples of the process $x(t)$ which has been modified by a data window $w(t)$ and extended to length N' with a train of zeroes, it can be shown [80] that the resulting modified periodogram is

$$\hat{S}_{xx}(f_k) = \frac{N^2}{N'U} |X(f_k)|^2 \qquad (3.11)$$

where

$$U = \frac{1}{N'} \sum_{q=0}^{N'-1} w(q\Delta) \qquad \begin{array}{l} f_k = q/N \\ q = 0, 1, \ldots N/2 \end{array} \qquad (3.12)$$

The expected value of the modified periodogram is approximately $S_{xx}(f_k)$ and its variance depends upon the shape of the data window [81]. For the rectangular window,

$$\text{Var}[\hat{S}_{xx}(f_k)] = S_{xx}^2(f_k) \qquad (3.13)$$

Windowing with a tapered data window tends to reduce the effective length of a data segment because equally important data points are weighted unequally, and as a result, the variance of the periodogram is slightly inflated. However, Durrani and Nightingale [82] evaluated the variances of periodograms resulting from the application of various reasonable data windows to Gaussian data, and they found that, even for a severely tapered data window, the variance is inflated by only about 10% over the value predicted by Equation (3.13).

The expected value and variance of a periodogram calculated from a particular time series are not affected if the time series is extended with zeroes before the periodogram is evaluated [80]. However, the correlation between adjacent periodogram ordinates increases as more zeroes are added to the time series [80]. The addition of extra zeroes reduces the spacing between periodogram ordinates without changing the shape of the spectral window. Jenkins and Watts [23] show that the covariance between two spectral estimates at different frequencies is proportional to the amount of overlap of the spectral windows centred at these frequencies. The term "spectral window" is normally associated with spectral estimates derived from the Fourier transform of the auto-covariance function. For this situation

$$W_L(f) = | W_D(f) |^2 \qquad (3.14)$$

where $W_L(f)$ is the spectral window and $W_D(f)$ is the frequency window [83].

3.2.3 Smoothed Spectral Estimates

A smoothed spectral estimate may be evaluated by averaging several modified periodograms (Equation (3.11)) from the same stationary process [84]

$$\hat{\hat{S}}_{xx}(f_k) = \frac{1}{n} \sum_{i=1}^{n} S_{xx_i}(f_k) \qquad (3.15)$$

The expected value of the smoothed spectral estimate [84] is

$$E[\hat{\hat{S}}_{xx}(f_k)] = \int_{-1/2}^{1/2} H(f) \, S_{xx}(f-f_k) df \qquad (3.16)$$

where $S_{xx}(f)$ is the true power spectrum of $x(t)$ and

$$H(f) = \frac{1}{N'U} \left| \sum_{q=0}^{N'-1} w(q\Delta)e^{j2\pi fq} \right|^2 \qquad (3.17)$$

Thus the spectral estimate at a particular frequency is influenced (biased) by the power spectrum at other frequencies. The effect of this bias may be viewed as a decrease in spectral resolution, and its extent is dependent upon the width of the frequency band influenced by $H(f)$.

The variance of this smoothed spectral estimate [84] is

$$\text{Var}[\hat{\hat{S}}_{xx}(f_k)] = \frac{1}{n} \cdot \text{Var}[\hat{S}_{xx}(f_k)]. \qquad (3.18)$$

Therefore, if enough data is available, the variance can be reduced as much as desired simply by averaging over the required number of periodograms. The evaluation of a spectral estimate from a fixed amount of data involves a trade-off between variance and spectral resolution. If many periodograms are calculated from short, non-overlapping data segments and averaged, the variance of the resulting spectral estimate will be low. However, because the periodograms are calculated from short data segments, only a few sample values of the power spectrum will result, and therefore they will be widely spaced over the frequency band between 0 Hz and the Nyquist frequency. On the other hand, if periodograms are calculated from longer data segments in order to improve the spectral resolution, fewer periodograms will be available and the variance of the estimate will be higher.

Welch [84] has shown that a decrease in the variance of a spectral estimate evaluated from a fixed amount of data may be achieved by averaging periodograms calculated from overlapping data segments. Such overlapping will increase the number of periodograms available

from a given amount of data, but, because the segments are not independent, the reduction in variance will not be as great as the reduction which could be achieved by averaging periodograms calculated from the same number of independent segments. The actual variance reduction for a particular overlap depends upon the shape of the data window, but Welch has suggested that if the segments overlap by half their length, a near maximum reduction in variance can be achieved for any particular window. For a data window similar to the Hanning window and an overlap of 50% of the segment length, the variance of the spectral estimate is reduced by approximately 40%. If periodograms from the same number of independent segments were averaged, the reduction in variance would be 50%.

The multiplication of a time series by a data window or the convolution of its Fourier transform with a frequency window is referred to as linear modification. A similar procedure, called quadratic modification, may be applied to the autocovariance function or to its Fourier transform, the periodogram. With quadratic modification, a smoothed spectral estimate may be calculated by convolving a periodogram with a function known as a spectral window [23]. This is equivalent to multiplying the autocovariance function by a so-called lag window, the inverse Fourier transform of the spectral window. When spectral estimates are calculated from the autocovariance function, smoothing is accomplished by weighting the autocovariance function with lag windows similar to the functions used as data windows [27]. The resulting spectral windows are similar to the frequency windows illustrated in Figure 3.1. Spectral windows with much simpler shapes,

generally triangular, are now most often used when smoothing is carried out by means of convolution in the frequency domain [81].

The expected value of a spectral estimate smoothed by quadratic modification is [23]

$$E[\hat{S}_{xx}(f_k)] = \int_{-1/2}^{1/2} W_L(f) S_{xx}(f-f_k) df \qquad (3.19)$$

where $W_L(f)$ is the spectral window. This expression is equivalent to Equation (3.16) if $W_L(f) = H(f)$.

The variance of a quadratically modified spectral estimate depends upon the shape and width of the lag window, $w_L(t)$ [23]

$$Var[\hat{S}_{xx}(f_k)] \approx \frac{S_{xx}^2(f_k)}{T} \int_0^\infty w_L(t) dt \qquad (3.20)$$

where T is the total record length.

Therefore, if the variance is to be low, the lag window must be narrow, but a narrow lag window corresponds to a wide spectral window. Since multiplication of the autocovariance function by a lag window is equivalent to convolution of the power spectrum by the cor-responding spectral window, this means that for a fixed amount of data, a trade-off exists between variance and resolution similar to the trade-off encountered in spectral estimates smoothed by averaging.

Sloan [83], who compared the effects of linear and quadratic modification on a single periodogram derived from Gaussian data, found that linear modification results in a decrease in spectral resolution without a compensating decrease in variance, whereas the decrease in resolution due to quadratic modification is compensated by a comparable decrease in variance. He does concede, however, that linear

modification is useful in reducing leakage when applied to data which is not Gaussian; and Otnes and Enochson [85] state that, for many practical situations, linear modification is a useful procedure because of its leakage-suppression properties.

Jenkins and Watts [23] show that, for Gaussian white-noise processes, the probability distribution of a smoothed spectral estimate is proportional to a chi-squared distribution. The number of degrees of freedom for the distribution is

$$\nu = \frac{2\{E\{\hat{S}_{xx}(f_k)\}\}}{Var\{\hat{S}_{xx}(f_k)\}} \quad (3.21)$$

Thus the number of degrees of freedom of the approximating chi-squared distribution depends upon the variance of the spectral estimate which in turn depends upon the smoothing procedure. Olshen [86] has shown that such a chi-squared approximation may be applied to a spectral estimate from any process representable as a moving average of independent (finite variance) random variables. Based on this chi-squared distribution, an approximate confidence interval for a particular spectral estimate may be calculated [23].

3.3 The Cross Spectrum

The relationship between components of the same frequency in two signals determines the value of the cross-spectrum at that frequency [23]. If $x(t)$ and $y(t)$ are two stationary processes, their cross covariance function, $R_{xy}(\tau)$ is

$$R_{xy}(\tau) = \lim_{T\to\infty} \frac{1}{T} \int_{-T/2}^{T/2} x(t)y(t+\tau)d\tau \quad (3.22)$$

The cross spectrum is the Fourier transform of $R_{xy}(\tau)$

$$S_{xy}(f) = \int_{-\infty}^{\infty} R_{xy}(\tau) e^{-j2\pi f\tau} d\tau \tag{3.23}$$

Procedures for estimating the cross spectrum between two signals are similar to those for estimating the power spectrum of a single signal [81]. Fourier transforms $X_T(f_K)$ and $Y_T(f_K)$ are evaluated according to Equation (3.10) from time series of length N which represent trains of simultaneous samples of the two signals $x(t)$ and $y(t)$. The cross periodogram $\hat{S}_{xy}(f_k)$ is given by

$$\hat{S}_{xy}(f_k) = \frac{N}{U} [X_T^*(f_k) \cdot Y_T(f_k)] \tag{3.24}$$

where $X_T^*(f_k)$ is the complex conjugate of $X_T(f_k)$ and U is given by Equation (3.12). A smooth cross spectrum estimate may be obtained by averaging several such periodograms or by convolving a single cross periodogram with a suitable spectral window. The expected value of a cross spectrum estimate is approximately $S_{xy}(f)$, and the accuracy of this approximation improves if the width of the data window is increased [23].

In contrast to the power spectrum, which is always a real quantity, the cross spectrum at a particular frequency must generally be expressed as a complex number

$$\hat{\hat{S}}_{xy}(f_k) = \hat{\hat{M}}_{xy}(f_k) e^{j\hat{\hat{Q}}_{xy}(f_k)} \tag{3.25}$$

where $\hat{\hat{M}}_{xy}(f_k)$ is the magnitude of the complex number and $\hat{\hat{Q}}_{xy}(f_k)$ is its phase angle. For unmodified smoothed cross spectrum estimates [23,74]

$$\text{Var}[\hat{\hat{M}}_{xy}(f_k)] \approx \frac{1}{2n} M_{xy}^2(f_k) \left[1 + \frac{1}{\gamma_{xy}^2(f_k)} \right] \tag{3.26}$$

and

$$\text{Var}[\hat{Q}_{xy}(f_k)] \approx \frac{1}{2n}\left[\frac{1}{\gamma^2_{xy}(f_k)} - 1\right] \tag{3.27}$$

where n is the number of cross periodograms averaged to produce the smoothed cross spectrum estimated, M_{xy} is the true cross spectrum magnitude and γ^2_{xy} is a quantity known as coherence given by [14]

$$\gamma^2_{xy}(f_k) = \frac{|S_{xy}(f_k)|^2}{S_{xx}(f_k) \cdot S_{yy}(f_k)} \tag{3.28}$$

The number of periodograms which must be averaged in order to achieve a desired variance therefore, depends to a large extent upon the value of the coherence, a quantity which always falls between 0 and 1.

3.4 Coherence

The linear correlation between two processes $x(t)$ and $y(t)$ at frequency f is given by the coherence, $\gamma^2_{xy}(f)$. A coherence of 1 occurs for situations where $x(t)$ and $y(t)$ are linearly related, and a coherence of zero indicates that the two processes are completely unrelated. A coherence greater than zero but less than unity indicates that the apparent relationship between the two processes is nonlinear either because a truly nonlinear relationship exists or because the relationship is contaminated by extraneous noise [14]. The coherence value provides a measure of the degree of this apparent nonlinearity.

Because the value of a coherence estimate based on unsmoothed spectral estimates will always be unity no matter what the true coherence is [9], a smoothed coherence estimate, $\hat{\gamma}^2_{xy}(f_k)$, must be evaluated according to

$$\hat{\gamma}^2_{xy}(f_k) = \frac{|\hat{\hat{S}}_{xy}(f_k)|^2}{\hat{\hat{S}}_{xx}(f_k) \cdot \hat{\hat{S}}_{yy}(f_k)} \tag{3.29}$$

Benignus [87] experimentally evaluated confidence intervals for such a coherence estimate, and his results were confirmed by Carter et al. [88]. Benignus [89] also demonstrated that the confidence intervals are not greatly dependent on the probability distribution for the population of sample values used in calculating the coherence estimate. Carter et al. [88] showed that the bias for coherence estimates increases as the true coherence approaches zero and as the number of degrees of freedom associated with the spectral estimates decreases. When n, the number of periodograms averaged, is large (say greater than 30) the bias is

$$B[\hat{\gamma}^2_{xy}(f_k)] \simeq \frac{1}{n}[1-\gamma^2_{xy}(f_k)]^2 \tag{3.30}$$

The variance of the estimate under similar conditions is

$$Var[\hat{\gamma}^2_{xy}(f_k)] \simeq \begin{cases} \dfrac{1}{n^2} & \gamma^2_{xy}(f_k) = 0 \\[2mm] \dfrac{2\gamma^2_{xy}(f_k)}{n} \cdot [1-\gamma^2_{xy}(f_k)]^2 & 0 < |\gamma^2_{xy}(f_k)| \le 1 \end{cases} \tag{3.31}$$

Plots showing the exact bias and variance for various values of n and $\hat{\gamma}^2_{xy}(f_k)$ are presented by Carter et al. [88].

Theoretically, the coherence between two signals is not affected if the signals are subjected to linear filtering operations [90]. As Foster and Guinzy [90] demonstrate, however, this statement only applies to the sample coherence defined in Equation (3.29) if the filter transfer functions are identical or slowly varying over the length of the spectral window. If u(t) and v(t) are filtered versions of x(t) and y(t) where the respective filter transfer functions are A(f) and B(f), then

$$\hat{\gamma}_{uv}(f) = \hat{\gamma}_{xy}(f) \frac{\left| \int_{-1/2}^{1/2} W_L(f-\lambda) \ B(\lambda)A*(\lambda)d\lambda \right|^2}{\int_{-1/2}^{1/2} W_L(f-\lambda)|A(\lambda)|^2 d\lambda \int_{-1/2}^{1/2} W_L(f-\lambda)|B(\lambda)|^2 d\lambda} \tag{3.32}$$

$W_L(f)$ is the spectral window, and $A*(f)$ denotes the complex conjugate of $A(f)$.

3.5   The Transfer Function Estimate

If the two processes $x(t)$ and $y(t)$ are related by a linear system with a transfer function $H(f)$, the following relationships apply [9,91]:

$$S_{xy}(f) = H(f) \cdot S_{xx}(f) \tag{3.33}$$

$$S_{yy}(f) = |H(f)|^2 \cdot S_{xx}(f) \tag{3.34}$$

Based on these relationships, $\hat{H}(f_k)$, an estimate for the transfer function, may be calculated from estimates of the auto and cross spectra.

$$\hat{H}(f_k) = \frac{\hat{S}_{xy}(f_k)}{\hat{S}_{xx}(f_k)} \tag{3.35}$$

$\hat{H}(f_k)$ is a complex number which may be expressed as

$$\hat{H}(f_k) = \hat{G}(f_k)e^{j\hat{P}(f_k)} \tag{3.36}$$

where

$$\hat{G}(f_k) = \frac{\hat{M}_{xy}(f_k)}{\hat{S}_{xx}(f_k)} \tag{3.37}$$

and

$$\hat{P}(f_k) = \hat{Q}_{xy}(f_k) \tag{3.38}$$

$\hat{G}(f)$ represents the gain of the transfer function, and $\hat{P}(f)$ describes

the phase spectrum. Approximate confidence limits for gain and phase are given by Jenkins and Watts [23].

If the relationship between x(t) and y(t) is nonlinear, the quantity H(f) is the linear operator that best approximates y(t) in a least squares sense by acting on x(t) [13]. The coherence for such a system can be interpreted as a measure of the degree to which each frequency component of y(t) is related to the corresponding component of x(t) by a linear, time-invariant system.

CHAPTER 4

SPECTRAL ANALYSIS APPLIED TO SINGLE MOTOR UNITS

4.1 Input-Output Relationship

One approach to the development of a mathematical model for a physical system requires a set of experimental measurements of the system's input-output characteristics. In many cases, especially for complex systems, such measurements provide the only available basis for a model. It is therefore important that the experimental procedure be designed to reveal the response of the system under conditions which are as natural as possible.

The axon and muscle fibres of a single motor unit are components of a system which produces tension in response to electrical stimulation. In the body, the input signals to this system are trains of narrow spikes originating at the cell body of the motoneuron. Experimental measurements which are to be used in modeling the system should therefore be obtained for input signals of this form. Although it may be possible to develop a model for the response to signals other than spike trains, such a model would be of little use in illustrating the physiological behavior of the system.

The tension developed by a group of muscle fibres depends upon such factors as stimulus rate [54,72], the length of the muscle [54,93,94] and the rate at which the length is changing [95]. The tension can also vary with time because of potentiation effects [72] or muscle fatigue [96,97]. Measurements from an experiment in which all of these factors are simultaneously varied would be difficult to interpret. A more reasonable approach would be to study the effects of varying one factor at a time. Measurements of isometric tension are particularly

suited to such an approach because the muscle length is fixed. Since the effects of fatigue or potentiation may be minimized by keeping the period of stimulation short, it should be possible to develop a model illustrating the effects on isometric muscle tension of stimulating the axon with a train of narrow pulses.

A sigmoid-shaped curve relating isometric muscle tension to stimulus rate results when a group of motor nerve fibres [54,93] is stimulated with a series of evenly-spaced pulses. Although the slope of this curve is higher for intermediate stimulus rates than for low or high rates, the response to small fluctuations in stimulus rate is approximately linear. Presumably, a similar linear relationship applies for single motor units. If so, the system's frequency response may be determined for a variety of muscle lengths and mean stimulus rates, and a set of linear models relating changes in stimulus rate to changes in muscle tension may be developed.

Muscles respond well to signals which have components at the low frequencies associated with normal movement [12]. However, the response to components with frequencies above about 8 Hz is weak, and for higher frequencies, the response is weaker still. If single motor units respond similarly, their overall behavior would be well-represented by frequency response plots covering a band of frequencies with some upper limit.

An approximate value for this limit can be determined from a study of the motor unit's twitch response. A nerve action potential and the resulting isometric muscle tension for a typical motor unit are illustrated in Figure 4.1. The magnitude of the transfer function (gain) calculated from the Fourier transforms of these two waveforms is
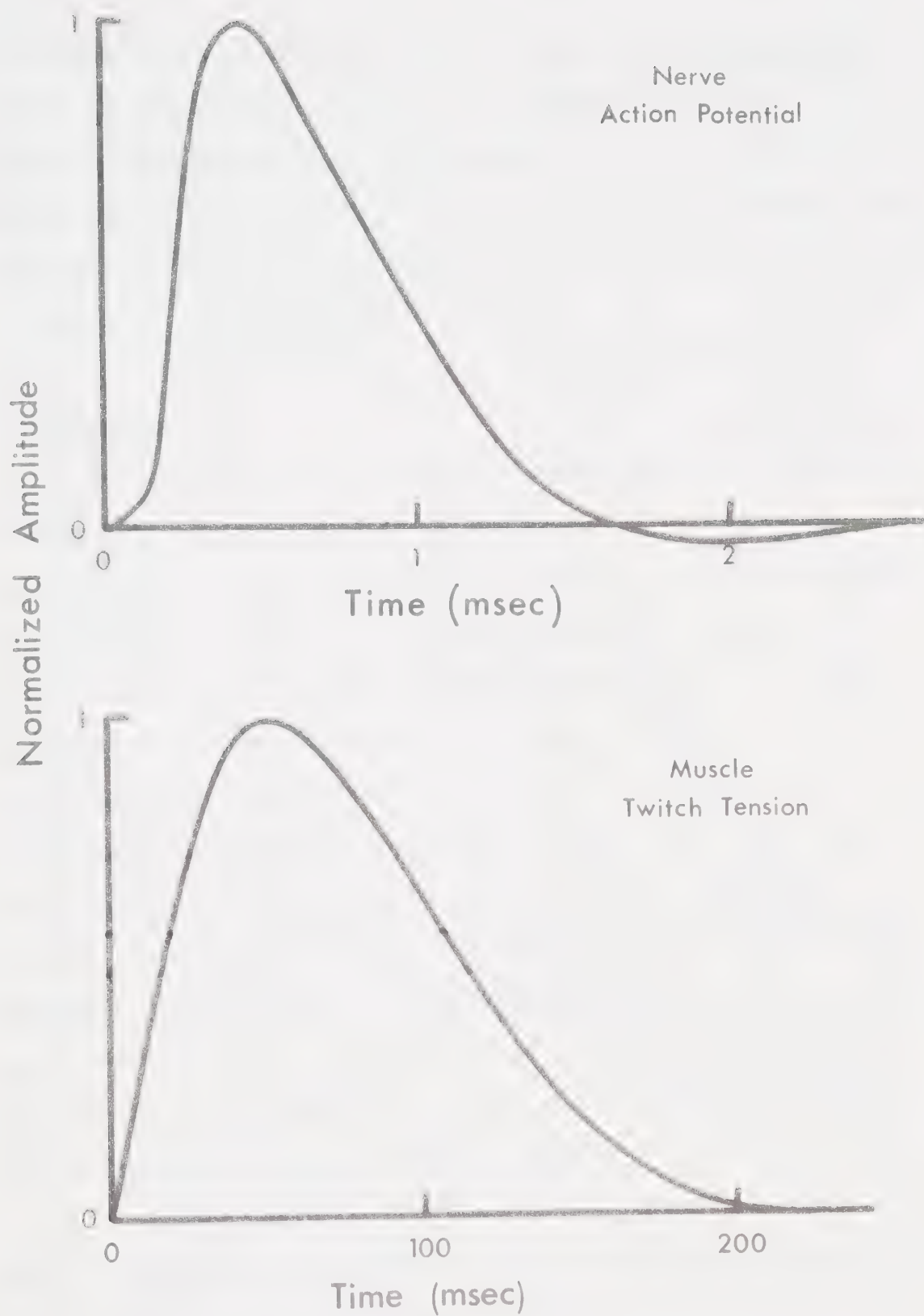
FIGURE 4.1 Nerve Action Potential and Isometric Twitch Waveforms

illustrated in Figure 4.2. From this plot, which has been normalized

so that the gain approaches unity at low frequencies, it can be seen

that the gain drops off rapidly as frequency increases. For frequencies

greater than 20 Hz, the gain is less than 3% of the low frequency gain.

Therefore, 20 Hz appears to be a reasonable upper limit for modeling

the frequency response of a single motor unit.

4.2 Input Signals

The conventional approach to the measurement of a system

transfer function involves recording the responses to a series of

constant-frequency signals applied at the input. However, this approach

cannot be applied to the study of single motor units because a pulse

train containing only a single frequency component cannot be created.

Therefore, a means for separating the frequency components of both the

input pulse train and the output tension record is required. The

spectral analysis techniques described in Chapter 3 can be used for

this purpose. If the system is linear for the input signals of

interest, the resulting transfer function can be used to predict the

response to any pulse train. If the system is nonlinear or noisy, the

coherence estimate will indicate the degree of these effects and the

transfer function estimate will provide the best linear approximation

for the output in response to a train of pulses.

Blackman and Tukey [73] state that the power spectrum of a

signal which is to undergo spectral analysis should be reasonably flat.

This criterion is quite well satisfied so long as the power spectrum

does not change appreciably over the width of the spectral window.

This means that the power spectrum of the input signal should not
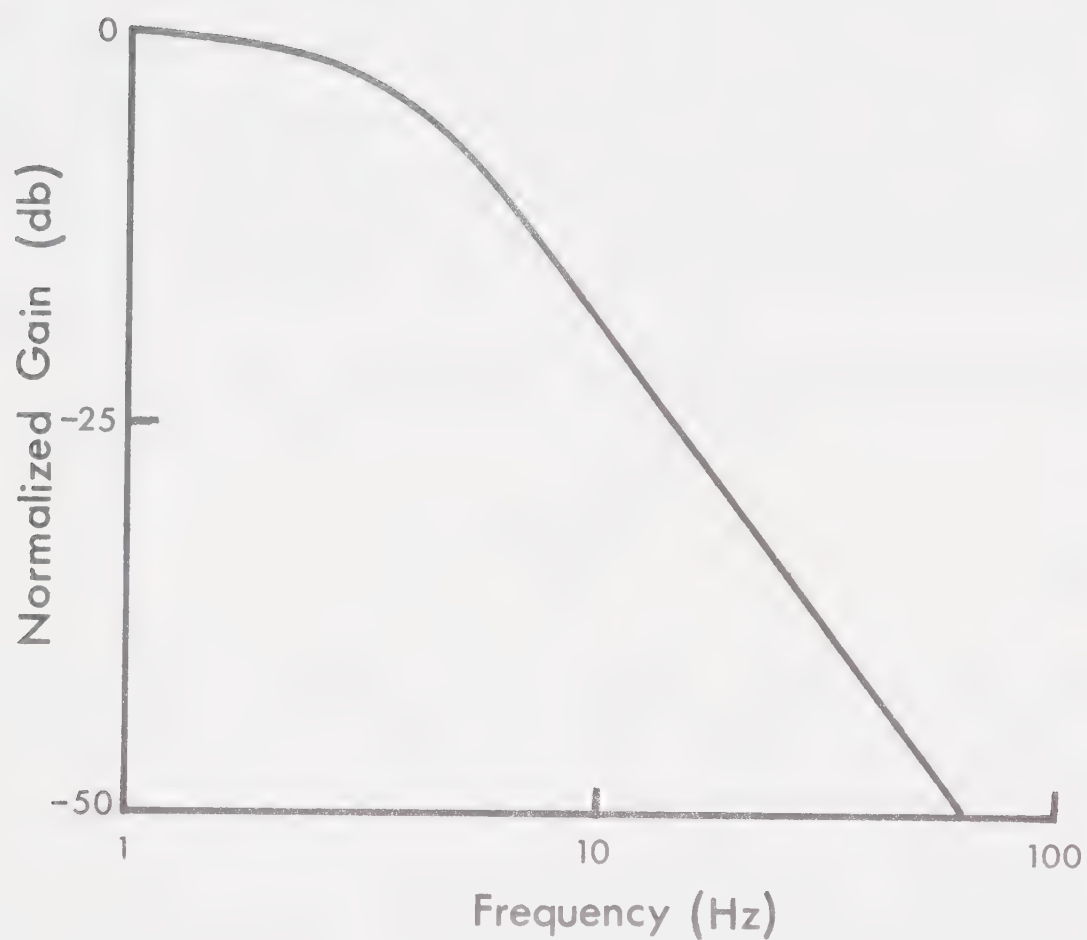
FIGURE 4.2 Gain Plot Based on Motor Unit
             Twitch Response

contain any sharp peaks or valleys. A train of pulses with interpulse intervals which are periodically related is therefore not a desirable input signal. Bayly [100] has demonstrated that the power spectrum of such a pulse train would contain sharp peaks at frequencies dependent upon the periodically related interpulse intervals. A pulse train with random interpulse intervals is therefore more suitable as an input signal for the measurement of the motor unit transfer function. However, the probability distribution of the interpulse intervals must be chosen so that a pulse train with a reasonably flat power spectrum results.

The class of distributions known as gamma distributions can be used in this situation. For such a distribution

$$p(t) = \frac{\beta^g t^{g-1} e^{-\beta t}}{\Gamma(g)} \tag{4.1}$$

where $p(t)$ is the probability of an interpulse interval of time t, g is the order of the distribution, β is a scale factor, and $\Gamma(g)$ is the gamma function of g.

Nelsen [98] has shown that the power spectrum of a train of impulses with interpulse intervals which are independently distributed is

$$S_{xx}(f) = \frac{1}{\bar{t}} \cdot \left[\frac{1 - |M_t(f)|^2}{|1 - M_t(f)|^2} \right] \tag{4.2}$$

where $\bar{t}$ is the average interpulse interval and $M_t(f)$ is the characteristic function corresponding to the probability distribution $p(t)$

$$M_t(f) = E[e^{j2\pi ft}] = \int_0^\infty p(\tau) e^{j2\pi f\tau} d\tau \tag{4.3}$$

At f=0 the power spectrum includes an impulse of size $1/\bar{t}^2$. If the 0 Hz component is subtracted before the signal is Fourier transformed, this impulse will have no effect on the results of the spectral analysis.

The plots in Figure 4.3 of the power spectra evaluated according to Equation (4.3) for various gamma distributions illustrate that for low values of g, the spectra vary slowly with frequency. In fact, when g=1, the power spectrum is flat. A first-order gamma distribution is equivalent to an exponential distribution, and the power spectrum for such a distribution has been evaluated by Rice [99] for the case where the pulses have finite width. Neglecting the 0 Hz component, this power spectrum is

$$S_{xx}(f) = \beta G_{xx}(f) \tag{4.4}$$

where $G_{xx}(f)$ is the power spectrum of a single pulse and β is the scale factor for the gamma distribution.

The input signal applied to the motoneuron is transmitted to the muscle fibres as a series of action potentials. Therefore, the power spectrum of each input pulse should be similar to that of an action potential. A train of narrow, rectangular pulses can be produced with little difficulty, and if the width of these pulses is chosen correctly, the difference between the power spectrum of the pulse and that of an action potential is negligible at low frequencies. The power spectrum of a typical nerve action potential is flat within 1% over the frequency range 0-20 Hz, and the power spectrum of a 3 msec rectangular pulse is a $(\sin x)/x$ function which decreases monotonically to about 99% of its low frequency value at a frequency
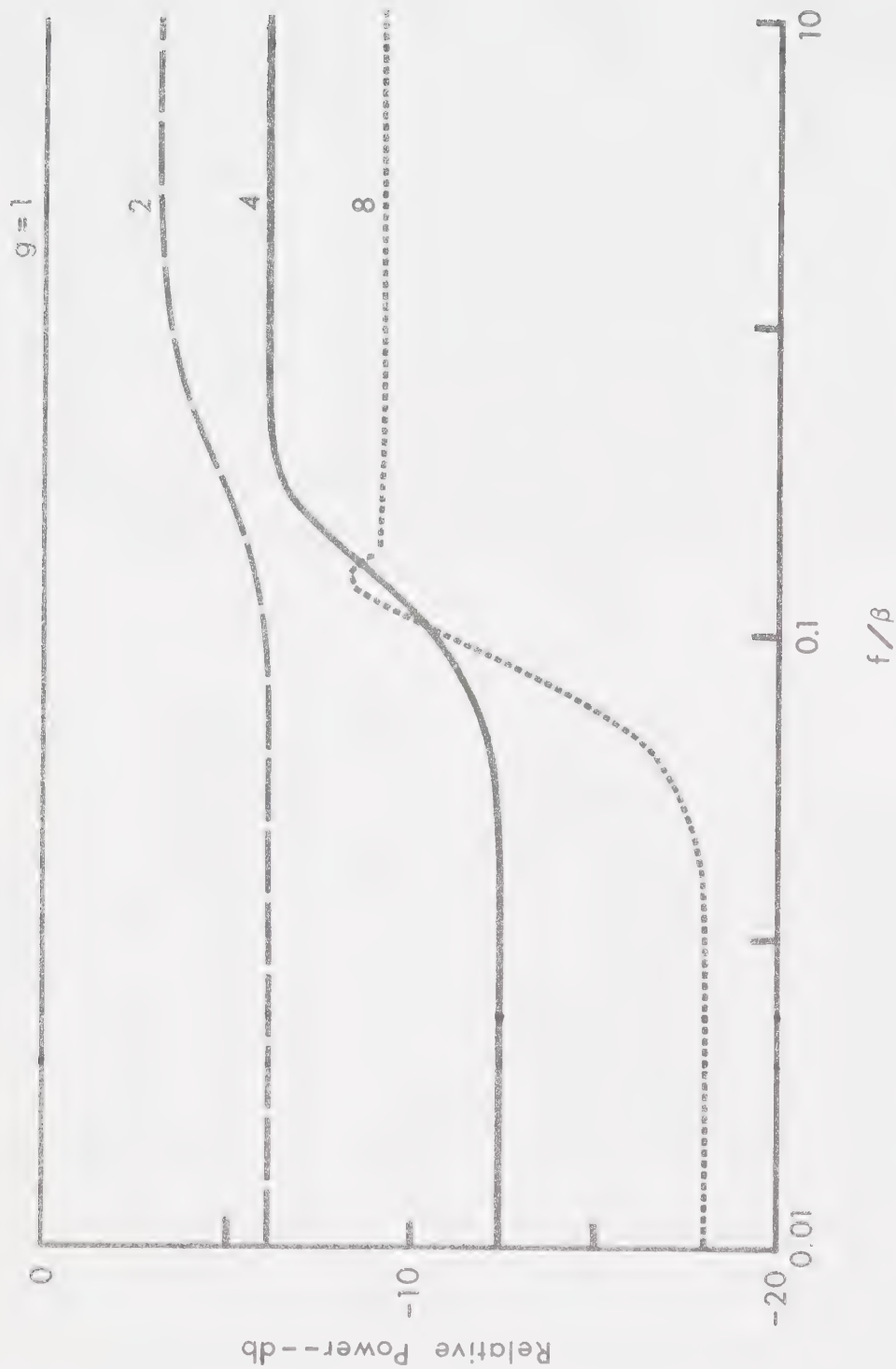
FIGURE 4.3 Power Spectra of Point Processes with Intervals Described by
Gamma Distributions of Various Orders

of 20 Hz. Therefore, if the transfer function is to be estimated over a frequency range of 0-20 Hz, a train of 3 msec rectangular pulses is a suitable test signal, because the difference between the two power spectra over this frequency range is never greater than 1%.

A frequency response plot based on the use of such an input signal must be scaled according to the pulse amplitude. The scaling is required because the magnitude of a transmitted action potential is independent of the size of the pulse which initiated it; and, since the gain is measured with respect to the input pulse train, the measured gain will be inversely proportional to the magnitude of the stimulating pulses.

4.3 Spectral Analysis Procedure

The development of a specific procedure for the measurement of motor unit transfer functions by means of spectral analysis must include a certain amount of trial and error adjustment. An initial procedure, based on the available knowledge of the motor unit's freq-uency response may be devised, but the results of applying this proced-ure will probably indicate the need for modifications. Any such procedure must, of course, work within the limits of the available instrumentation and computing facilities; and, if possible, the results of each transfer function measurement should be immediately available.

Because of its greater speed, the direct method for spectral estimation is preferable to the indirect method in this application. With the direct method, smoothing can be achieved either by averaging several consecutive periodograms or by convolving a single long per-iodogram with a suitable spectral window. Since the calculation of a

long periodogram with the fast Fourier transform requires more computer core memory than does the calculation of several short periodograms, the averaging approach is preferable. If a means of displaying the spectral estimate is available, this display may be continually updated as more periodograms are added to the average, and the decision to stop sampling may then be based on the smoothness of the displayed estimate.

The maximum frequency for which the transfer function estimate is to be evaluated determines the required sampling rate. Since the desired input signal contains significant components at frequencies above the desired Nyquist frequency, some form of low-pass filtering must be used to prevent aliasing.

The method of French and Holden [19] would be suitable for eliminating this aliasing in the input pulse train, but this method requires special hardware to accurately measure the time of occurrence of each pulse. When this hardware is not available, an electronic low-pass filter may be used. Koles[9] has shown that a filter consisting of two cascaded second-order filters with Butterworth characteristics is suitable for this application. If the corner frequencies of the Butterworth filters are equal to 60% of the Nyquist frequency, the aliasing error for a signal with a flat power spectrum is no higher than 6% at all frequencies below 80% of the Nyquist frequency. There-fore, a Nyquist frequency of 25 Hz and a filter corner frequency of 15 Hz are suitable for measuring the frequency response of a motor unit for frequencies below 20 Hz.

Only a limited amount of time is available for sampling the response of a motor unit subjected to continuous stimulation. Since motor units fatigue when thay are repetitively stimulated, the total

sampling time should be shorter than the time required for the effects of fatigue to become apparent; but, from the results of Smith and Lännergren [72], it appears that this time can be as short as 3 seconds. With a Nyquist frequency of 25 Hz, only 150 samples can be collected during this period of time, and if several periodograms are to be calculated from these samples, the frequency resolution will be very low. However, because the motor unit quickly recovers from the effects of a short burst of stimulation, the frequency resolution may be improved by averaging individual periodograms calculated from the response to widely separated short bursts of stimulation. With a stimulus burst 2.56 seconds in length and a sampling interval of 20 msec, independent periodogram coefficients may be calculated for 65 frequencies spanning the range 0-25 Hz.

When the power spectrum of a signal is reasonably flat over the width of the spectral window, the effects of leakage will be similar for all periodogram coefficients. The relative magnitudes of the coefficients will therefore be unaffected. If an input signal with a flat power spectrum is used in studying the responses of single motor units, the effects of leakage between nearby coefficients will not be apparent. However, because the system severely attenuates the high frequency components of the input signal, leakage between widely spaced periodogram coefficients could noticeably affect the spectral estimate for the output signal. The Hanning window, with its wide major lobe and very small minor lobes therefore appears to be a suitable choice as a data window. However, if the Fourier transformed samples are to be stored for further analysis, the rectangular data window is the most appropriate choice. With this approach, the stored

values may be subsequently convolved with any desired frequency window to reduce leakage.

4.4 Summary

The above discussion may be summarized as follows:

1. The portion of a motor unit consisting of the axon coupled to the muscle fibres may be regarded as a single-input, single-output system.

2. Although this system could conceivably respond to a variety of input signals, any model of the system's *in vivo* behavior should be concerned only with the response to trains of narrow pulses.

3. The relationship between stimulus rate and muscle tension is influenced by many factors, and this relationship is, in general, nonlinear. However, a set of linear models relating isometric tension to the low frequency components of the input spike train may possibly be developed.

4. Such models would be derived from plots of the system's low frequency response. Spectral analysis techniques may be used for such frequency response measurements.

5. A suitable input signal for such studies is a train of narrow, rectangular pulses. The probability distribution of the interpulse intervals can be similar to that of a low-order gamma distribution.

CHAPTER 5

PROCEDURE

5.1 The Nerve-Muscle Preparation

All experiments were performed on iliofibularis muscles taken from adult female specimens of *Xenopus laevis*. One end of this long, thin muscle which runs along the back of the thigh, is attached to the pelvis at the ilium, and the other end is joined to both the lower end of the femur and the upper end of the tibio-fibula by means of a split tendon. The muscle contains approximately 600 fibres of various types arranged into distinct zones. The lengths of the muscles used in the experiments, measured with the hind limb in a normal, relaxed position, ranged from 28-35 mm.

The portion of the animal including the pelvis and the hind limbs was separated from the rest of the body, skinned and placed in a dissecting tray containing enough Ringer's solution* to cover it. The iliofibularis muscle in one limb was exposed, and its length was measured with the limb in a natural relaxed position. The muscle was then removed from the limb together with the portion of sciatic nerve approximately 4 cm in length beginning at the sciatic plexus and running to a point approximately 1 mm distal from the exit of the nerve branch serving the iliofibularis. This dissection was performed carefully to insure that the nerve branch entering the muscle was not stretched or otherwise damaged. The nerve-muscle preparation was then placed in a shallow plexiglass container filled with Ringer's solution. A small

---

*The Ringer's solution had the following composition (mM): NaCl-112.0, KCl-2.5, $CaCl_2$-2.0, $NaHCO_3$-2.5, and glucose-5.5. The solution was saturated with a mixture of 95% O_2 and 5% CO_2.

hole was made in the tendon at each end of the muscle, and the muscle was fixed between two stainless steel hooks inserted through these holes. The nerve branch was supported on a thin plexiglass ledge fastened to the bottom of the container. The connective tissue sheath covering the sciatic nerve was slit longitudinally at the distal end over a distance of about 3 mm and peeled back in order to expose the cut ends of the nerve fibres within. All of these ends were then carefully pulled back until only the intact fibres which entered the iliofibularis remained, and a dissecting needle was used to cut all but one of these intact fibres.

A small plexiglass block with a concave depression in the top was placed in the container with the nerve-muscle preparation. The proximal end of the sciatic nerve was placed in the depression, and the depression was filled with Ringer's solution. A seal of petroleum jelly was placed across the nerve and the plexiglass block immediately distal to the point where the nerve entered the depression in the block. The whole container was fastened to a small table inside a Faraday cage, and the wire hook passing through one end of the muscle was replaced by a thin stainless steel wire hook attached to a Devices Instruments type 2ST02 isometric force transducer. The resonant frequency of the force transducer and the attached wire hook was approximately 250 Hz, and the compliance of this arrangement was about 0.01 mm/g-force. A silver-silver chloride electrode was lowered into the pool of Ringer's solution in the container, and a similar electrode was lowered into the pool of Ringer's solution contained within the depression in the plexi-glass block. The completed preparation, illustrated in Figure 5.1. was at room temperature (21°-23°C) throughout the experiment.
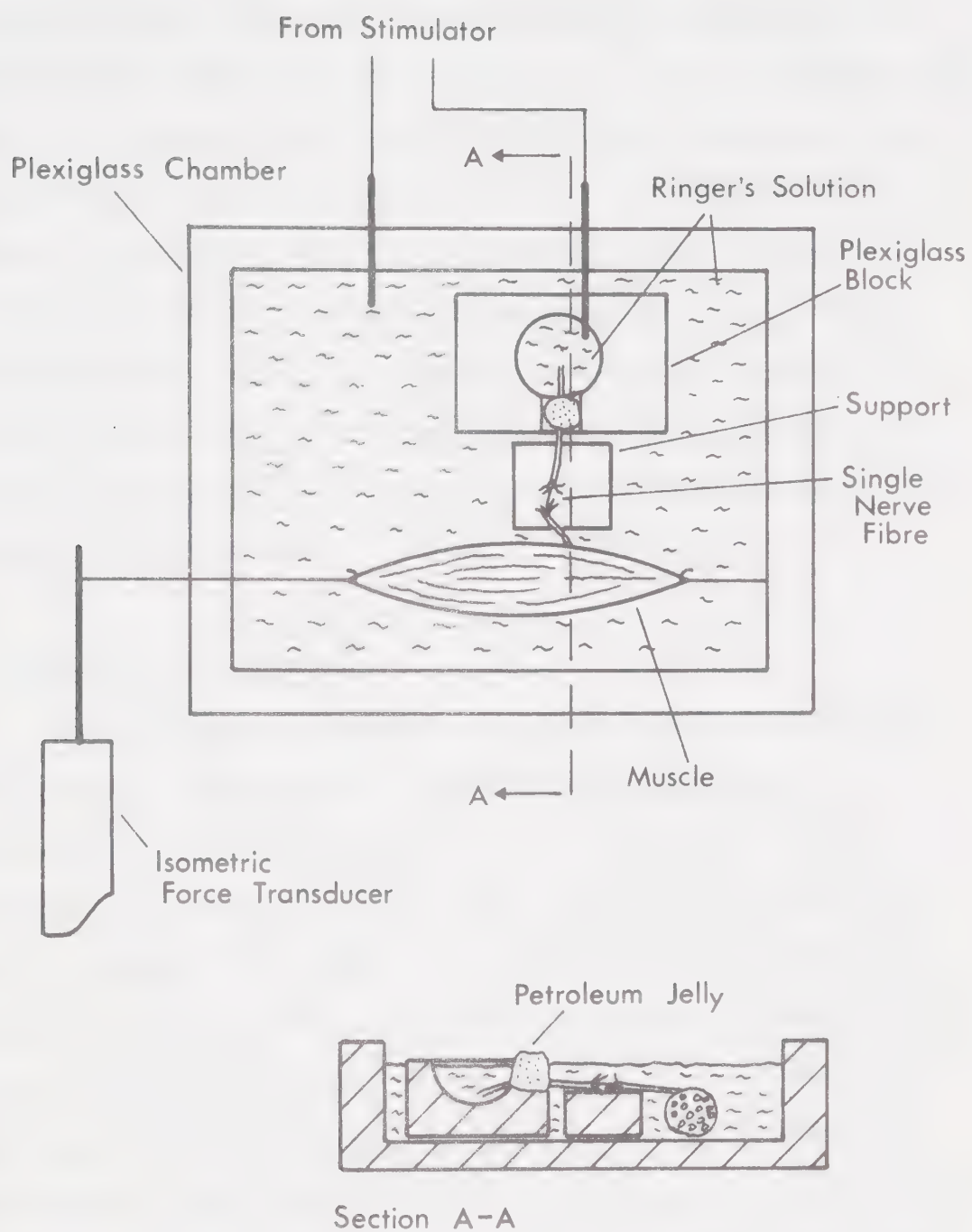
FIGURE 5.1 The Nerve-Muscle Preparation

The input signal was applied to the preparation by means of the two silver-silver chloride electrodes which were connected to one output of an Ortec 4710 dual-channel stimulator. Action potentials were generated in the motoneuron by applying a potential difference across the petroleum jelly seal with the stimulator. Such a potential difference caused current to flow along the axoplasm of the various nerve fibres and through the nerve cell membranes, thereby creating a potential difference across each membrane. When this potential difference reached the threshold potential, an action potential was generated and propagated along the axon, but only those action potentials generated in the intact fibre could reach the muscle.

5.2 Stimulation and Recording

The stimulator consisted of two separate pulse generators triggered from a common source. The second output was connected through one of two identical low-pass filters described in Appendix 1 to one input of a 16-channel Hewlett-Packard 5610A analog-to-digital converter. If desired, the output of the stimulator could be gated with an externally applied signal. The stimulator could be triggered either by means of an internal clock or by an external signal. The external trigger signal was provided by a Precision Instruments PI-6200 tape recorder with an analog tape recording of a random pulse train. Several different pulse trains were recorded on the tape so that a pulse train with interpulse intervals distributed according to a particular probability distribution could be selected by positioning the tape at the desired point. The procedure for generating these pulse trains is described in Appendix 2.

The force transducer was connected to the input of a Tektronix 3C66 carrier amplifier, and the output of this amplifier was passed through a low-pass filter to the second input of the analog-to-digital converter. The output of the carrier amplifier was also connected to one channel of a dual-channel Sanborn 320 chart recorder. The second channel of this recorder displayed the output of a frequency-to-voltage converter [101] which measured the instantaneous pulse rate at the stimulator output. An audio amplifier and loudspeaker were connected to the stimulator output so that this signal could be monitored aurally. The arrangement of the equipment used in the experiments is illustrated in Figure 5.2

Note that the input signal applied to the motor unit and the input signal sampled by the analog-to-digital converter originate from different outputs of the stimulator. This arrangement was adopted as a matter of convenience because the magnitude of the pulse required to initiate an action potential in the motoneuron varied with each preparation. The second channel of the stimulator produced a pulse at the same time as the first channel, but the magnitude of the pulse was not changed from experiment to experiment and, as a result, the magnitude-dependent scaling factor mentioned in Chapter 4 was the same for every experiment. In addition, the width of the stimulating pulse could be changed without affecting the results of the analysis.

The threshold voltage for the preparation was considered to be the minimum stimulator voltage required to produce an observable contraction of the motor unit muscle fibres. Those motor units which produced a muscle twitch in response to a 1 msec stimulus pulse were
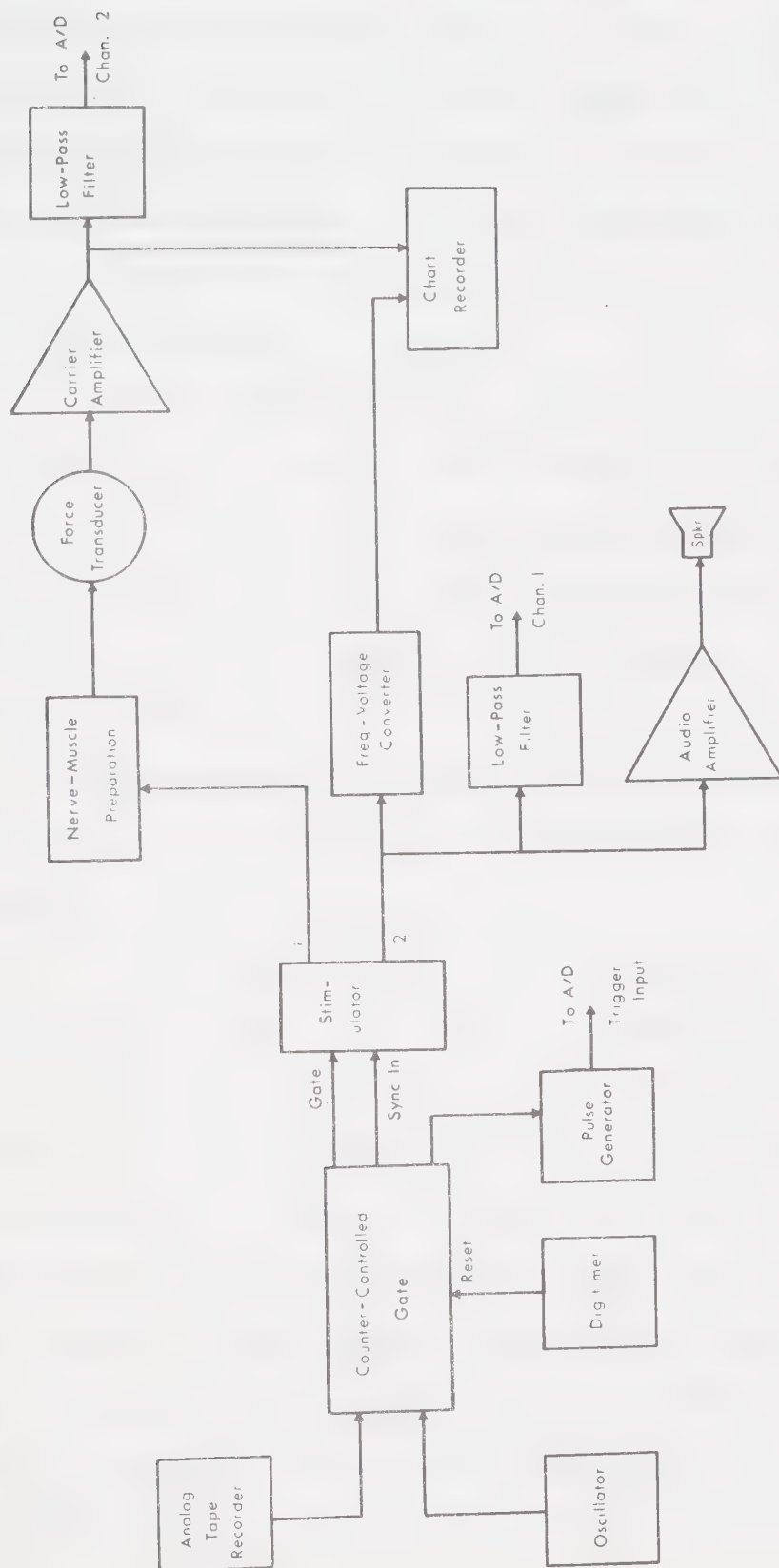
FIGURE 5.2 Apparatus for Data Collection

assumed to be fast motor units. Slow motor units were considered to be those which exhibited no twitch response but which responded with a slow muscular contraction to a train of 1 msec stimulus pulses at a rate of about 20 pulses per second. Any preparation which produced no observable single motor unit response was discarded. The intact nerve axon of such a preparation was assumed either to belong to a sensory neuron or to be damaged.

Once the threshold voltage had been determined, the responses of the motor unit to a series of constant-rate pulse trains were recorded on the chart recorder. For these measurements and all succeeding measurements, the stimulating pulse amplitude was set at approximately twice the measured threshold voltage. Generally, the stimulating voltage could be increased to a level at least 10 times higher than the threshold voltage before current spread resulted in the initiation of action potentials in the cut ends of the axons leading to the muscle.

Next, data required for the estimation of motor unit transfer functions were collected. The motor unit was subjected to periods of continuous stimulation, and its response to this stimulation was measured and recorded according to the procedure to be described below. Both the length of the stimulation periods and the specific stimulating signals employed varied from experiment to experiment, but, in most cases, periods of stimulation exceeding 1 min. in length were avoided. In an attempt to reduce the effects of muscle fatigue, the muscle was allowed to recover for several minutes after any prolonged period of stimulation.

5.3 Data Analysis During the Experiment

Data collection for the evaluation of transfer function estimates was controlled by a Hewlett-Packard 2100S computer. The computer program which performed this data collection is illustrated by means of a flow chart in Appendix 3. The sampling times of the analog-to-digital converter could be controlled either by the computer or with a pulse train from a Hewlett-Packard 2781A pacer. In either case, a command to initiate sampling caused the analog-to-digital converter to sequentially sample the two signals applied to inputs 1 and 2 with a time interval between the two sequential samples of about 12 μsec. Each sample was converted to a 10-bit binary number which was passed to the computer as part of a 16-bit binary number. The additional 6 bits carried control information.

The sample values were collected as paired blocks of data. All of the points in one of these blocks represented samples from Channel 1 of the analog-to-digital converter, and all of the points in the other block represented samples from Channel 2. For each data block, the mean value of all the points was subtracted from every point in the block, the resulting series of values was Fourier transformed, and the results of this operation were stored on a disc memory. The collection of any data block pair and the Fourier transformation of the previously collected pair of data blocks proceeded simultaneously. In addition, an average power spectrum estimate was calculated for the signal representing the motor unit output. This estimate was displayed on the oscilloscope as a plot of power versus frequency. The average power spectrum and the display were updated every time a new pair of data blocks were Fourier transformed. The smoothness of the spectral

estimate could be judged from the display, and the sampling procedure could be stopped whenever enough data blocks had been collected to yield an acceptably smooth estimate. Alternatively, a command to collect a fixed number of data blocks could be issued if desired.

The length of the data blocks and the sampling rate were specified before sampling commenced. The number of points in any data block was limited to integral powers of two, and the maximum block size was 256 points. Samples could be collected continuously, or the pacer could be used in conjunction with the counter-controlled gate circuit described in Appendix 4 to collect samples in bursts of a specified length. With this procedure, a large number of data blocks could be collected by subjecting the motor unit to many short periods of stim-ulation. When the motor unit was allowed to rest between periods of stimulation in this way, the effects of fatigue were reduced in com-parison to the case where all of the data blocks were collected during one long period of stimulation.

The maximum possible sampling rate was limited because of the time required to calculate the Fourier transform. The collection time for a data block pair could not be any shorter than the time required to Fourier transform the previously collected pair of data blocks and write the results on the disc. With an efficient fixed-point fast Fourier transform subroutine [77] written in assembly language, data could be collected continuously on two channels at a maximum rate of 300 point pairs per second.

When enough data blocks had been collected to yield adequat-ely smooth spectral estimates, transfer function estimates based on any portion of the recorded data could be calculated and displayed on the

oscilloscope as plots of gain, phase, or coherence versus frequency. A flow chart for the computer program which controlled the production of these plots is presented in Appendix 3. The values for gain in such plots indicated the gain as calculated from the filtered input and output signals. For all subsequent analysis, these values were multiplied by the gain setting of the strain gauge amplifier. The units for gain expressed in this way are g-force/volt. Because the gain was inversely proportional to the magnitude of the input pulses, this magnitude was kept constant from experiment to experiment, as were the gains of the anti-aliasing filters. Therefore, any differences among the various gain plots were due only to differences in the responses of the motor units.

Because plots of the transfer function estimates were available immediately after each period of data collection, modifications of the experimental procedures based on the results of each transfer function estimate could be carried out during the course of the experiment. After 12 preparations had been studied in this way, it was decided that, although such plots were useful in roughly gauging the responses of single motor units, further analysis, which could only be carried out after the completion of the experiment, would be necessary. Sampling intervals for these first experiments ranged from 10 to 100 msec, and mean stimulus rates ranged from 5 to 30 stimuli/sec. In most cases, the muscle was kept at its natural resting length. The results of these experiments were used in determining a suitable experimental procedure for future studies.

Samples for subsequent experiments were collected at a rate of 50 pairs per second in blocks of 128 sample pairs. Generally, 10

block pairs were collected for each transfer function estimate. The cut-off frequency for the anti-aliasing filters was 15 Hz. The Fourier transformed sample values for this group of experiments were stored on magnetic tape for further analysis by means of the computer program illustrated by a flow chart in Appendix 3. The results of 212 spectral analysis studies for 34 preparations were stored in this way.

Because the preparations were subject to fatigue, it was not possible to study each preparation with a full range of stimulus signals and muscle lengths. The effects of changes in muscle length were studied only for mean stimulus rates of 10 stimuli/sec. This rate was high enough so that the muscle tension waveform was not simply a series of individual twitches, and low enough so that fatigue effects did not appear rapidly. Various muscle lengths spanning a range of 2 mm above and below the natural resting length were studied in 17 of the 34 preparations referred to above. The effects of changes in mean stimulus rate were studied only with the muscle at its natural resting length. Stimulus signals having mean rates of 0.2, 5, 10, 15, and 20 stimuli/sec were used. Two or more of these signals were used on 22 preparations. Continuous stimulation was used on 14 preparations, and bursts of stimuli were used on 26 preparations.

For 3 preparations, the time delay between the occurrence of the stimulus pulse and the beginning of the muscle twitch was measured by simultaneously displaying the twitch waveform and the stimulus pulse on a Tektronix 604 storage oscilloscope. When the displayed twitch responses were compared with the twitch response plotted in Figure 4.1, it was concluded that the beginning of the

twitch response could be determined to within about 0.5 msec from the oscilloscope display.

5.4 Recording Action Currents in the Muscle

In a few experiments, action currents associated with the contraction of the isolated motor unit were recorded. The level of the Ringer's solution covering the nerve-muscle preparation was lowered so that the surface of the muscle was exposed to the air. A layer of paraffin oil deep enough to cover the preparation was then floated onto the surface of the Ringer's solution, and two silver-silver chloride electrodes were placed in contact with the upper surface of the muscle.

Action currents in the muscle produced a potential difference between the two electrodes. This potential difference was amplified with a Tektronix RM122 preamplifier and displayed on a Tektronix RM502A oscilloscope. A Grass Instruments Kymograph camera was used to record the oscilloscope display.

5.5 Histological Techniques

At the completion of each experiment, the external diameter of the intact axon was measured to the nearest 0.5 μm with an ocular micrometer.

With several of the preparations, an attempt was made to identify the specific muscle fibres constituting the single motor unit. After all the transfer function measurements had been completed, the motor unit was fatigued by repeated stimulation. Alternate periods of rest and stimulation were continued until the motor unit produced no

observable tension when stimulated. This procedure was carried out with the expectation that it would cause depletion of the glycogen in the muscle fibres [103]. The muscle was then quickly frozen in a mixture of dry ice and methylbutane, and transverse sections approximately 8 μm in thickness were cut with a freezing microtome. Serial sections were stained for succinic dehydrogenase [102] and for glycogen using the periodic acid-Schiff reaction [103]. In this way muscle fibres exhibiting glycogen depletion could be related to the muscle fibre types identified by Smith and Ovalle [34].

Another approach to relating motor unit types and muscle fibre types was attempted with several preparations. A single muscle fibre from the isolated motor unit was dissected out and prepared for electron microscopy according to the procedure used by Smith and Ovalle [34].

5.6 Mechanical Properties of the Whole Muscle

A procedure similar to that used by Halpern and Alpert [104] was used in studying the effects of the muscle's dynamic mechanical properties on the observed motor unit transfer function estimates. The iliofibularis muscle was removed from the animal and placed in the same plexiglass container used for the motor unit studies. One end of the muscle was connected to the force transducer and the other end was connected directly to the shaft of a Ling Altec Ltd. three ohm vibrator. The displacement of this vibrator shaft was sensed with a Hewlett-Packard 24DCDT-050 displacement transducer, and an electronic feedback circuit [9] insured that the gain of the entire puller system was flat within 1 db for frequencies below 100 Hz. A Gaussian white noise signal[9], band-limited to the range 0.4-80 Hz, was applied to the input

of the muscle puller, and transfer function estimates describing the relationship between the displacement of the puller shaft and the change in muscle tension were determined for the frequency range 0-100 Hz. These transfer function estimates were calculated with the same set of computer programs used in the motor unit studies.

CHAPTER 6

ANALYTICAL METHODS

6.1 Time Response

In order to compare the isometric responses of the various
motor unit types, several descriptive parameters were defined. The
twitch amplitude was considered to be the maximum value of the muscle
twitch tension resulting from a single stimulus, and the time between
the initiation of tension increase and the occurrence of this peak
tension was called the twitch peak time. Since the tetanic tensions
for nearly all motor units did not increase when the stimulus rate was
raised above 50 stimuli/sec, the maximum tetanic tension was defined
as the peak tension produced in response to a burst of stimulation at
a uniform rate of 50 stimuli/sec. In order to prevent fatigue damage
to the motor unit while measuring this quantity, stimulation was
terminated as soon as an obvious peak in tetanic tension had been
reached. The ratio of twitch amplitude to maximum tetanic tension was
called twitch/tetanus ratio.

In studying the fatiguability of fast motor units, it was
found that although all motor units could quickly recover from the
effects of 10 sec of stimulation at a uniform rate of 30 stimuli/sec,
such a period of stimulation was long enough to indicate differences
in fatiguability. The fatigue coefficient was therefore defined as the
tension at the end of this period of stimulation divided by the
maximum tension produced during the 10 sec interval.

Differences in the rate of tension development in slow motor
units were most apparent at low stimulus rates, but tensions were low
at such rates, and differences in tension were difficult to measure.

63

It was therefore decided that a rate of 20 stimuli/sec was the lowest suitable rate for studying tension development in slow motor units. The initial tension ratio was defined as the ratio of tension after 1 sec to the tension after 20 sec of such stimulation.

The tension and time values required to evaluate the above parameters were measured from the strip chart records collected during the experiments. The tensions recorded on the strip chart records represented the total muscle tension minus the resting tension. Therefore, all tension measurements indicated the change in isometric tension resulting from stimulation of the motor unit.

6.2 Frequency Response

Transfer function estimates were calculated from the data which had been recorded on magnetic tape during the experiments. These estimates were calculated by a Hewlett-Packard 2100 computer and plotted on a Tektronix 4010-1 display terminal. When possible, each measured transfer function estimate was then fitted with a curve representing the frequency response of a linear system. The computer program which controlled these operations is illustrated by means of a flow chart in Appendix 3.

6.2.1 Choice of Model

Initial examination of the plotted coherence estimates indicated that they could be divided into two categories related to motor unit type. For slow motor units, the points representing the coherence were scattered between 0 and 0.5 for all frequencies, thereby suggesting that the observed responses of these motor units would not be appropriately represented by linear models. For the

fast motor units, the coherence was near some constant value (usually above 0.7) for all frequencies less than about 15 Hz, but above this frequency the coherence declined rapidly to near zero at 25 Hz.

A study of the gain and phase plots for fast motor units revealed that the gain was constant for low frequencies and decreased at a rate of 12 db/octave at high frequencies. The phase approached 0° at low frequencies and was approximately -90° at the point where the low and high frequency asymptotes to the gain curve intersected. For high frequencies, the phase was in the neighborhood of -180°. The shape of these frequency response curves was therefore similar to the shape of the gain and phase curves for a second-order low-pass filter; so, because of this similarity, such a system was chosen as a model for fast motor units.

A time delay of about 10 msec between the initiation of a nerve stimulus and the beginning of the resulting muscle twitch could be measured directly, and the effects of such a delay were observed in the transfer function estimates as an increase in phase shift beyond the expected -180° at the high frequency end of the plot. Such a time delay was therefore combined with the second-order low-pass filter to produce frequency response curves which could be fitted to the measured transfer function estimates.

6.2.2 Bias in Coherence Estimates

An electronic low-pass filter with a response similar to that of a single motor unit was used to demonstrate the existence of bias in the coherence estimates. A coherence estimate for this electronic filter was calculated according to the same procedure used for the
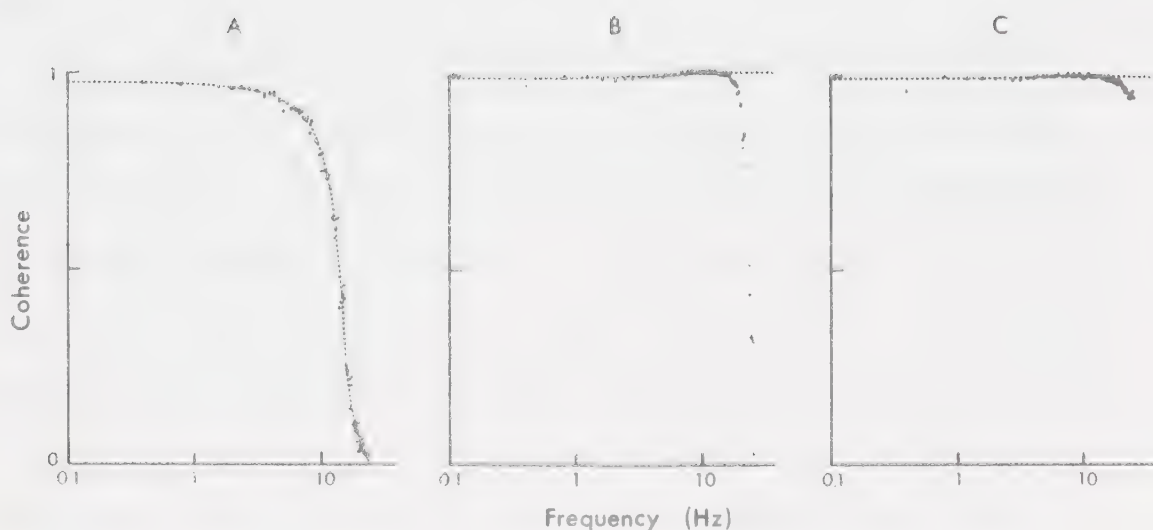
FIGURE 6.1   Coherence Estimates for Electronic Filter

motor units, but the input signal was band-limited Gaussian white

noise* [9] rather than a random pulse train. This estimate, illus-

trated by the plotted points in Figure 6.1A, represents the coherence

between a random signal passed through an anti-aliasing filter and the

same signal passed through an identical anti-aliasing filter in series

---

* The power spectrum of this signal was flat within 3 db from about
  0.04 Hz to 15 Hz. At high frequencies, the magnitude of the
  spectrum decreased at a rate of 20 db/octave.

with the electronic low-pass filter. The sharp drop in coherence at high frequencies is similar to the drop observed in the coherence estimates for single motor units when a rectangular data wandow was used.

The effect of linear filtering on the coherence estimate can be determined with Equation (3.32). For the situation described above, x(t)=y(t). Therefore $\hat{\hat{\gamma}}_{xy}(f)$ should equal 1 at all frequencies. A(f) is the transfer function of the anti-aliasing filter, and B(f) is the transfer function of the electronic low-pass filter in series with the other anti-aliasing filter. The dotted line in Figure 6.1A shows the coherence estimate for this situation calculated with Equation (3.32) for a rectangular data window. The agreement between the dotted line and the plotted points indicates that the observed drop in coherence at high frequencies is largely due to bias caused by linear filtering [90].

Jenkins and Watts [23] state that bias in the coherence estimate will increase with the length of the time delay between the two signals. The effect of the short time delay observed in single motor units was simulated by adding a 10 msec delay to the system described above, but the measured coherence estimate did not change noticeably, and the values for the theoretical estimate changed by less than 0.5%. These results indicate that the time delay associated with a single motor unit is too short to appreciably affect its coherence estimate.

The bias due to filtering can be reduced if leakage through the spectral window is decreased. This effect is illustrated in Figure 6.1B which shows the coherence estimate for the electronic

low-pass filter after the Fourier transforms of the input and output signals have been convolved with the Hanning frequency window. The dotted line shows that, in theory, the effects of bias due to filtering can be almost eliminated when the Hanning window is used. But, because of the greater width of the Hanning window's major lobe, leakage between adjacent frequencies is increased. Therefore, for this example, the coherence value nearest 0 Hz becomes slightly biased because of leakage from the 0 Hz component which has a value of zero. However, this slight bias at low frequencies is overshadowed by the improvement in the coherence estimate at high frequencies. The Hanning window is therefore highly suitable for reducing leakage in spectral estimates for single motor units.

When the Hanning window is used, the coherence estimate still decreases slightly at high frequencies even though the theoretical bias is almost zero. However, two other possible sources of bias exist--aliased power and quantization noise. The gain of the anti-aliasing filter drops sharply at high frequencies, so the effects of aliasing will be most apparent near the Nyquist frequency. As well, because the electronic filter tends to reduce the magnitude of the high frequency components, quantization noise will be more apparent at high frequencies. Since band-limited white noise was used as the input signal to the electronic filter, the anti-aliasing filters could be removed without totally degrading the spectral estimates. If aliasing is the cause of bias in the coherence estimates, removal of the anti-aliasing filters should increase the bias. As Figure 6.1C illustrates, however, the bias is greatly decreased when the anti-aliasing filters are removed. At a frequency of 23 Hz, the aliased power in the input

signal is increased by a factor of about 10, and the aliased power in the low-pass filtered version of this signal is increased by a factor of about 6. Yet the bias at 23 Hz is about 10 times smaller without the anti-aliasing filters. However, the ratio of quantization noise to signal amplitude at this frequency is decreased by a factor of about 10 when the anti-aliasing filters are removed.

The coherence between two linearly-related signals with power spectra $X(f)$ and $Y(f)$ is reduced when the signals are contaminated with added noise. If the spectra of the noise signals are $N_x(f)$ and $N_y(f)$ respectively, the coherence is [90]

$$\gamma_{xy}^2(f) = \frac{1}{\left[1+\dfrac{N_x(f)}{X(f)}\right]\left[1+\dfrac{N_y(f)}{Y(f)}\right]} \tag{6.1}$$

When this expression is evaluated at 23 Hz for a signal which spans 600 quantization levels at low frequency, the coherence is 0.956. In Figure 6.1C, the coherence at 23 Hz for signals with low frequency amplitudes spanning about 600 quantization levels is 0.95. A close agreement between measured and theoretical coherence is also apparent for other frequencies and for the situation where the anti-aliasing filters are included. It may therefore be concluded that the bias in the coherence estimate which remains after the signals are treated with the Hanning spectral window is due mainly to quantization error.

Gain and phase estimates for the electronic low-pass filter determined with and without the Hanning spectral window are illustrated in Figure 6.2. When these plots are compared with the plots of the corresponding coherence estimates in Figure 6.1, it becomes apparent that the gain and phase plots are noticeably affected only at
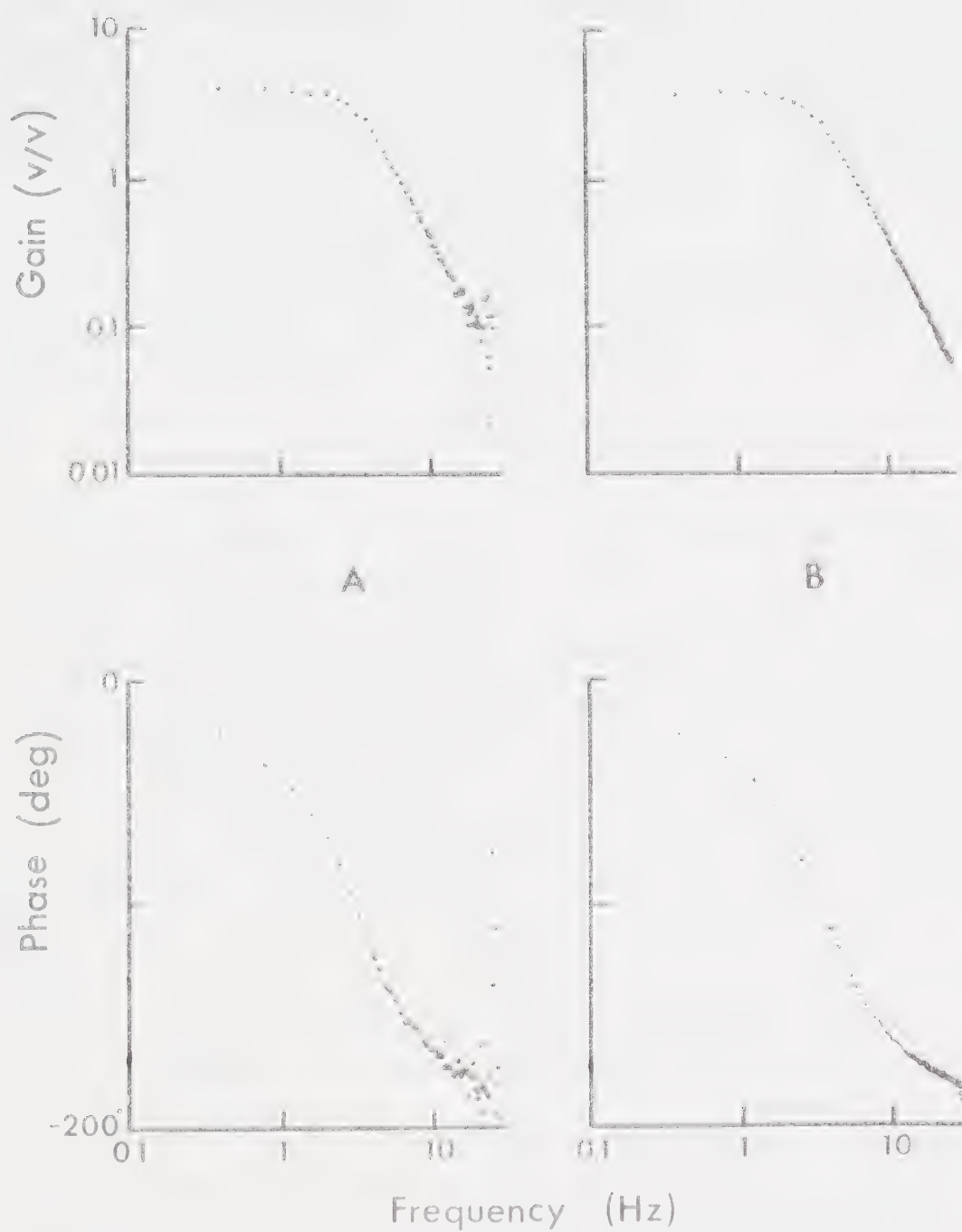
FIGURE 6.2   Transfer Function Estimates for Electronic Filter

frequencies for which the coherence estimate is severely biased. When the Hanning frequency window is used, the factors which cause the coherence estimate to become biased at high frequencies have little effect on the gain and phase estimates.

6.2.3 The Second-Order Low-Pass Filter

The transfer function of a second-order low-pass filter is [105]

$$H(jf) = \frac{k}{1 - f^2/f_n^2 + j2\zeta f/f_n} \tag{6.2}$$

where ζ is the damping ratio, and f_n is the undamped natural frequency. The gain of the filter at a frequency of 0 Hz is equal to k. Since such filters are commonly used for electrical signals, k is often called the dc (direct current) gain of the filter. Normalized plots of H(jf) versus frequency for several values of ζ are shown in Figure 6.3.

For a given filter, approximate values for k, ζ, and f_n may be obtained from a plot of the filter's frequency response. The dc gain is indicated by the low frequency asymptote, and the natural frequency is defined as the frequency at which the high and low frequency asymptotes intersect, or as the frequency where the phase is equal to -90°. The damping ratio can be estimated by comparing the plot to a series of normalized frequency response plots such as those illustrated in Figure 6.3. Note that a low damping ratio results in a peak in the gain curve and a rapid change in phase near the natural frequency.

The variability of such estimates for k, ζ, and f_n depends upon the nature of the frequency response plot. This plot is based on measurements of the system's response at a number of different
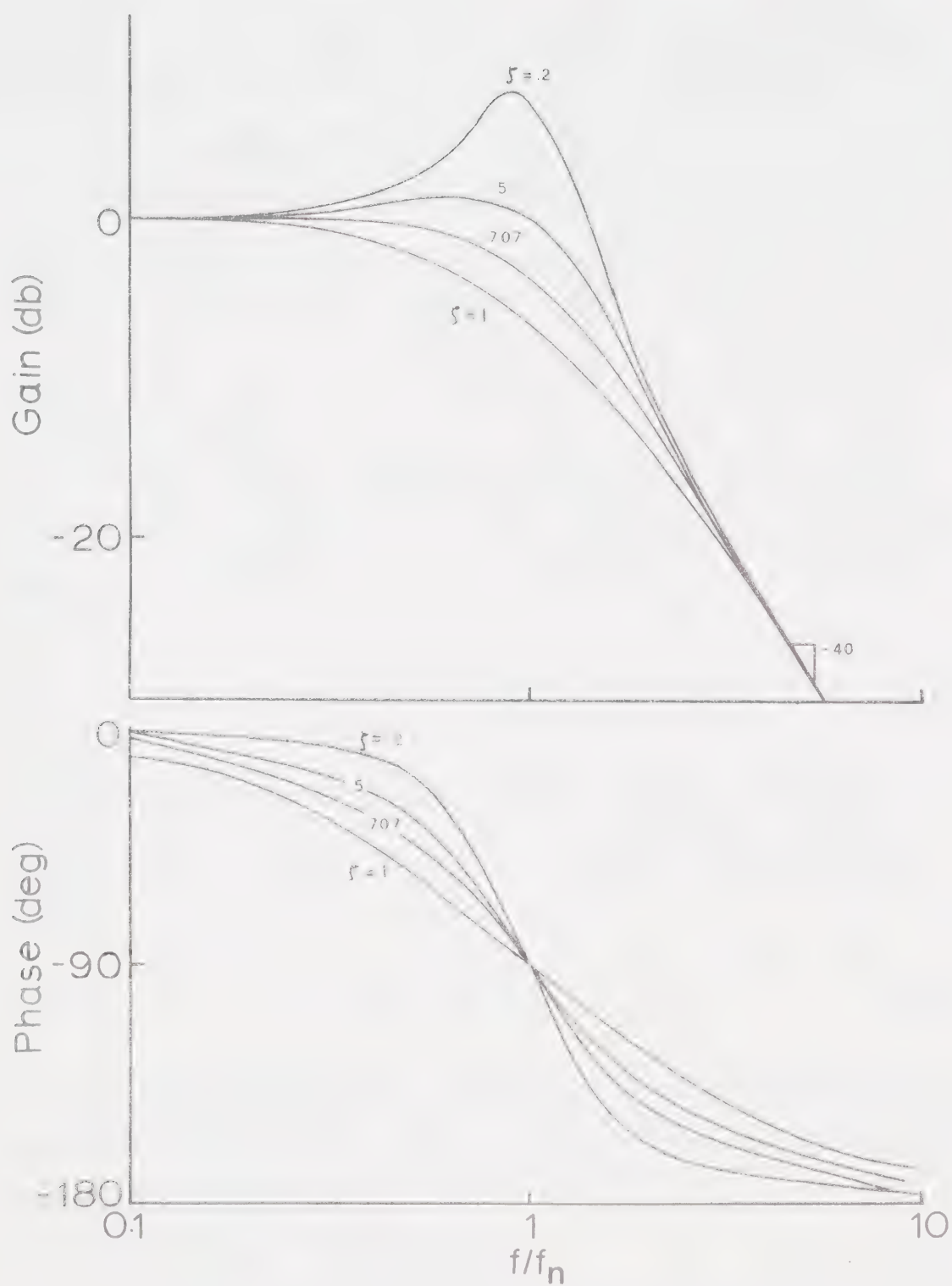
FIGURE 6.3 Frequency Response of Second-Order Systems

frequencies. If the variability of these measured values is high, or if measurements are available for only a few frequencies, the positions of the best-fitting low and high frequency asymptotes become difficult to determine. Estimation of the damping ratio also becomes difficult under such conditions. Because of these problems, a more reliable method for fitting curves to transfer function estimates is needed.

6.2.4 Curve Fitting

One scheme for fitting parameters to a transfer function estimate involves expressing the fitted transfer function, $H(jf)$, as the ratio of two polynomials:

$$H(jf) = \frac{p_0 + p_1(jf) + p_2(jf)^2 + \cdots}{1 + q_1(jf) + q_2(jf)^2 + \cdots} = \frac{P(jf)}{Q(jf)} \qquad (6.3)$$

At a particular frequency f_k, the difference between the transfer function estimate, $\hat{H}(f_k)$, and the fitted transfer function, $\overline{H}(jf_k)$, is e_k where

$$e_k = \hat{H}(jf_k) - \frac{P(jf_k)}{Q(jf_k)} \qquad (6.4)$$

Levy [106] proposed a method of evaluating $P(jf)$ and $Q(jf)$ based on minimizing the sum over all experimental points of a weighted squared error $|e_k'|^2$ where

$$e_k' = e_k \cdot Q(jf_k) \qquad (6.5)$$

With this criterion, the coefficients of $P(jf_k)$ and $Q(jf_k)$ may be obtained as the solution to a set of simultaneous algebraic equations of the form

$$[A][X] = [B] \qquad (6.6)$$

An approach similar to this was used with limited success by Kislack [107] for fitting parameters to transfer function estimates.

A technique developed by Sanathanan and Koerner [108] allows the coefficients of $P(jf_k)$ and $Q(jf_k)$ to be determined iteratively. With this procedure, the sum of $e_k'' {}^2$ is minimized where

$$e_k'' = \frac{e_k \cdot Q(jf_k)_L}{Q(jf_k)_{L-1}} \tag{6.7}$$

and L is the iteration number. Since this expression converges rapidly to e_k, the weighting function associated with the error term is unity rather than $Q(jf_k)$ as used by Levy [106]. Sanathanan and Koerner demonstrated that curves fitted on the basis of an unweighted error term follow the transfer function estimate of a complex system more closely than do curves fitted according to an error term which is weighted with $Q(jf_k)$.

The iterative procedure has been applied by Streets and Hemphill [109] to the problem of fitting parameters to systems which include a time delay. With this approach, the time delay is approximated as an all-pass filter [2] for which several parameters must be determined. This means that, for a simple system, the total number of polynomial coefficients which must be evaluated is greatly increased by the addition of a time delay. Because of this disadvantage, a different approach was adopted for fitting parameters to the motor unit transfer function estimates.

If $\hat{\hat{H}}(jf_k)$ is the transfer function estimate and $\overline{H}(jf_k)$ is the transfer function which is fitted to this estimate, a complex error term e_k may be defined as

$$e_k = \hat{\hat{H}}(jf_k) - \overline{H}(jf_k) \tag{6.8}$$

The best-fitting transfer function over the frequency range f_1 to f_m was defined as the transfer function for which ε is minimized where

$$\varepsilon = \sum_{k=1}^{m} |\epsilon_k|^2 \tag{6.9}$$

This quantity is a function of four parameters: k, ζ, f_n, and τ--the time delay. Starting with a set of approximations for these parameters, values for the fitted transfer function at frequencies f_1, f_2, ...f_m were determined. The parameters were then modified according to the Fletcher-Powell method [110] until a minimum for ε was reached. The parameter values at this point were considered to be those of the transfer function which most closely approximated the transfer function estimate.

The Fletcher-Powell method is a numerical technique for determining the minimum of a function of several variables. Because the minimum can be found quickly with this approach, the Fletcher-Powell method was selected in preference to other available minimization techniques [111]. Appendix 5 describes the details involved in applying this method to the problem of fitting transfer function estimates.

6.2.5 Confidence Intervals for Fitted Parameters

A computer simulation of the input-output relationship for a single motor unit was used to derive approximate probability distributions for the fitted parameters.

For the situation illustrated in Figure 6.4, the coherence between the input and output is [88]
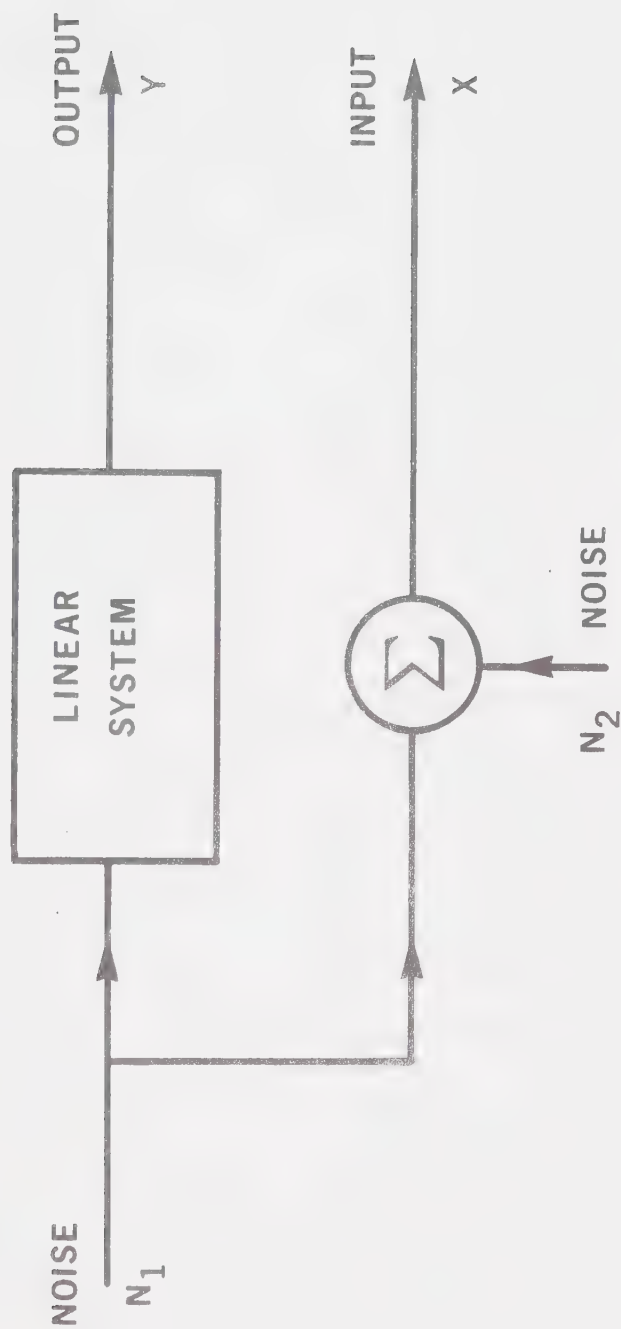
FIGURE 6.4 Simulation of a Linear System with Variable Coherence

$$\gamma_{xy}^{2}(f) = \frac{1}{1 + \kappa(f)} \qquad (6.10)$$

where κ is the ratio of the power spectra of the uncorrelated noise signals, $N_2(f)/N_1(f)$. The linear system was simulated by means of the digital second-order low-pass filter derived in Appendix 6 according to a method presented by Radar and Gold [112]. With this approach, the filter parameters could be independently varied by adjusting the digital filter constants, and the coherence could be varied by changing the relative amplitude of the added noise, N_2. The ratio $N_2(f)/N_1(f)$ was constant at all frequencies, so the coherence of the simulated motor unit was independent of frequency.

Approximate probability distributions for the various fitted parameters were obtained from 100 independent transfer function estimates for the simulated motor unit. These estimates were calculated according to the same procedure used to calculate the transfer function estimates for actual motor units. Specifically, records consisting of 128 evenly-spaced samples of $x(t)$ and $y(t)$ were Fourier transformed, smoothed estimates were calculated by averaging the results from consecutive records, and estimates for the system transfer function and coherence were calculated from the smoothed spectral estimates. The parameters which best described these transfer function estimates were determined according to the technique described in Section 6.2.4, and histograms such as the one illustrated in Figure 6.5 were plotted to show the distributions of the parameters. The same procedure was repeated for transfer function estimates simulating a variety of motor units, and, in all cases, the shape of the histograms suggested that the fitted parameters are approximately normally distributed. This
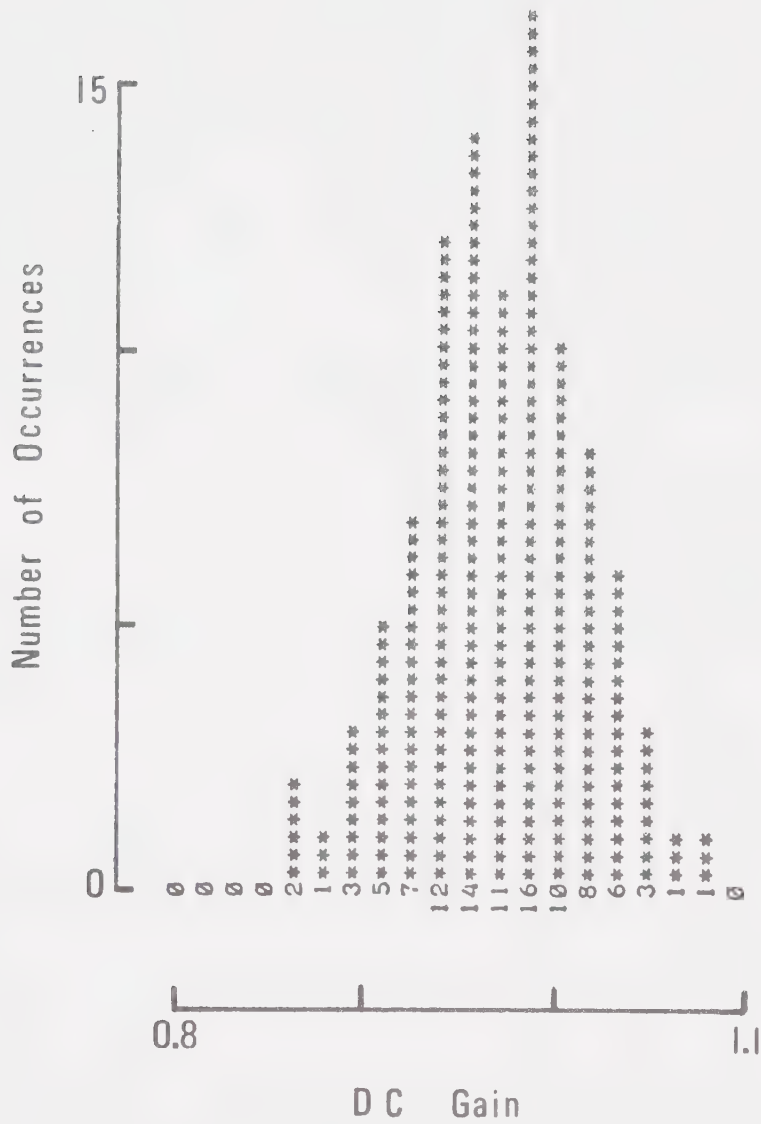
FIGURE 6.5 Distribution of DC Gain

assumption was verified with a chi-squared goodness of fit test [14] for several randomly-selected histograms. The test indicated that the distributions described by the histograms could not be differentiated from normal distributions at confidence levels of 90% or higher.

Figure 6.6 shows how the number of periodograms which are averaged to yield a single spectral estimate affects the distribution of fitted damping ratio for a system with a response similar to that of a fast motor unit. (The damping ratio for this system was 1.0, and the coherence was 0.8.) Results similar to this were obtained for all parameters and for systems with coherences ranging between 0.5-1.0. It is apparent that a substantial decrease in standard deviation can be achieved by increasing the number of periodograms associated with each spectral estimate from 5 to 10, but the standard deviation decreases much less sharply when the number of periodograms is increased further. Because an increase in the number of periodograms requires a longer period of motor unit stimulation, spectral estimates based on the average of 10 periodograms represent a good compromise between the desire for low standard deviation and the need to keep the stimulation period as short as possible. Such estimates were used for all subsequent studies.

Since the variances of spectral estimates for systems with low coherence are high, the parameters fitted to such spectral estimates have high standard deviations. This effect is illustrated for a typical situation in Figure 6.6 which shows that the standard deviation increases rapidly as the coherence decreases from 1.0. Expressions which show the effect of coherence on the distributions of each fitted parameter will be presented later in this chapter.
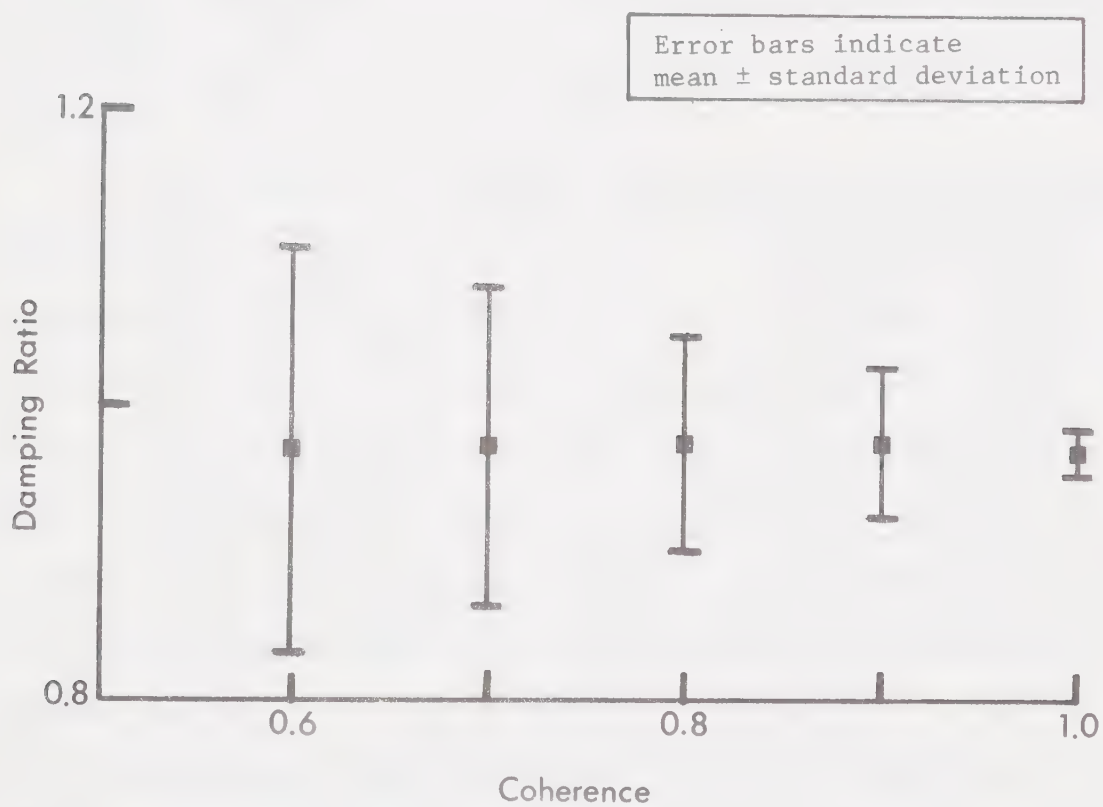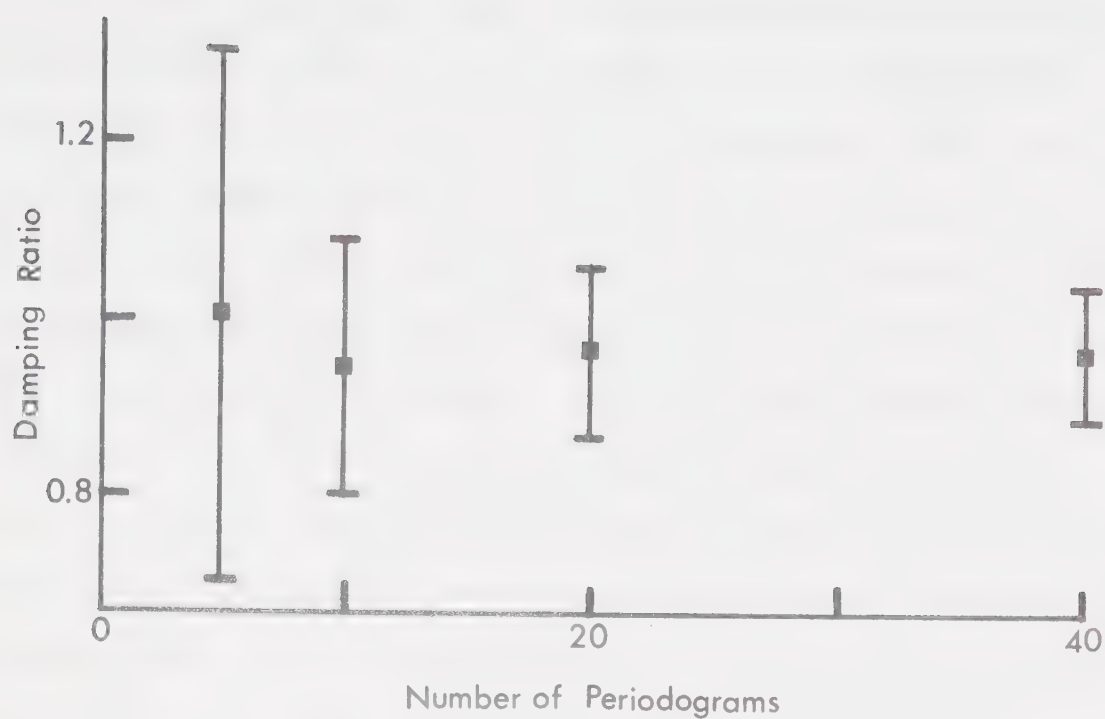
FIGURE 6.6 Effects of Record Length and Coherence on
The Value of Fitted Damping Ratio

For single motor units, the squared difference between the fitted transfer function and the transfer function estimate was much smaller for high frequencies than for low frequencies. Since curves were fitted to the transfer function estimate so that the sum of these squared differences was minimized, the low frequency components of the transfer function estimate had a much greater effect on the sum than did the high frequency components. Therefore, when the high frequency portion of the transfer function estimate was neglected during the fitting procedure, the effect on the fitted parameters was small. Because motor unit transfer function estimates tended to become unstable near the Nyquist frequency (as in Figure 6.2A) the last 20 points of the 64 point transfer function estimate were not used in the fitting procedure. This maneuver did not greatly affect the distributions of the fitted parameters, and it yielded a reduction in the computing time required to complete the calculations.

The scaling of statistical data so that it fits a standard distribution is a common procedure. An equivalent approach involves scaling the standard distribution so that it fits the data. Such a scaling procedure was applied to the normal distributions of fitted dc gain and natural frequency. That is, standard distributions of fitted parameters were calculated for a simulated motor unit with a dc gain of 1 and a natural frequency of 1 Hz. Distributions for motor units with any other values of k or f_n were obtained by scaling the standard distributions. This procedure was adopted when it was found that distributions obtained by scaling closely matched distributions which were obtained directly for a variety of simulated motor units.

Distributions for fitted time delay were determined for

simulated motor units with delays equal to zero and half the sampling

interval. Since the standard deviations of the fitted delay differed

by only about 20% for the two situations, and since the time delays

for actual motor units were usually about half the sampling interval,

the distribution calculated for this value of delay was assumed to be

valid for all responses of actual motor units. The distributions of

the other fitted parameters were negligibly affected when the delay was

changed from zero to half the sampling interval.

Because the distributions for fitted damping ratio obtained

by scaling did not match distributions which were obtained directly,

the direct procedure was used to determine distributions for a number

of different damping ratios within the range observed for actual motor

units. A linear interpolation technique, to be described below, was

then used to calculate distributions for values of damping ratio other

than these.

The distributions of the fitted parameters depended upon the

frequency range covered by the fitted transfer function. This effect

is illustrated in Figures 6.7 and 6.8 for a simulated motor unit with

the following parameter values: $k=1$, $\zeta=1$, $f_n=1$ Hz, and $\tau=25$ msec. The

Nyquist frequency for the transfer function estimates was 10 Hz, and the

upper limit of the frequency range spanned by the fitted transfer

function is designated as f_M. The plots show that moderate changes in

the ratio f_n/f_M do not greatly affect the distributions of the fitted

parameters.

For actual motor units, the ratio f_n/f_M ranged between about

0.06-0.14. Distributions were determined for a simulated motor unit

with a ratio of 0.06875, and these distributions were assumed to be
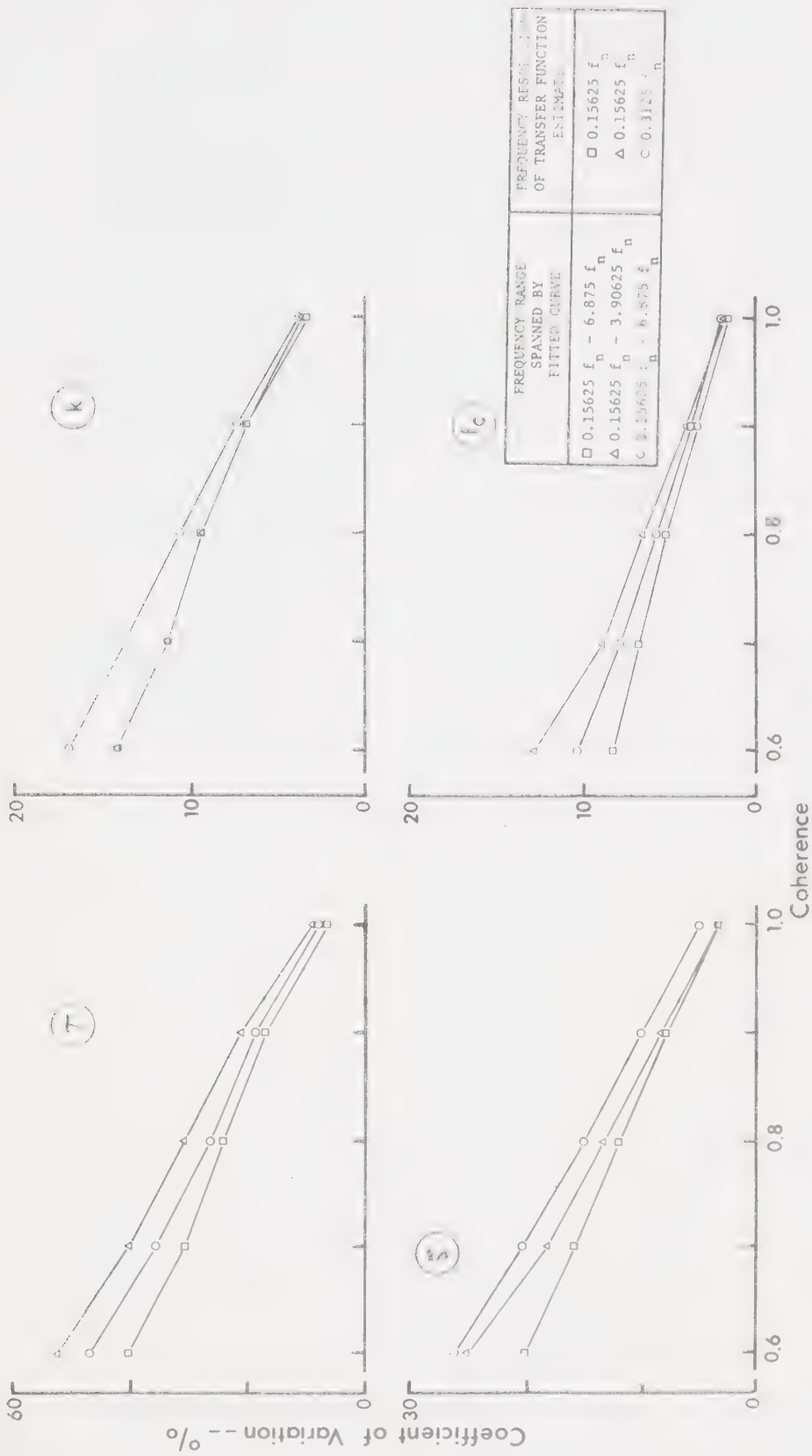
FIGURE 6.7 Coefficients of Variation for Fitted Parameters

FREQUENCY RANGE SPANNED BY FITTED CURVE	FREQUENCY RESOLUTION OF TRANSFER FUNCTION ESTIMATE
□ 0.15625 f_n – 6.875 f_n	□ 0.15625 f_n
△ 0.15625 f_n – 3.90625 f_n	△ 0.15625 f_n
○ 0.15625 f_n – 6.875 f_n	○ 0.3125 f_n

Coherence
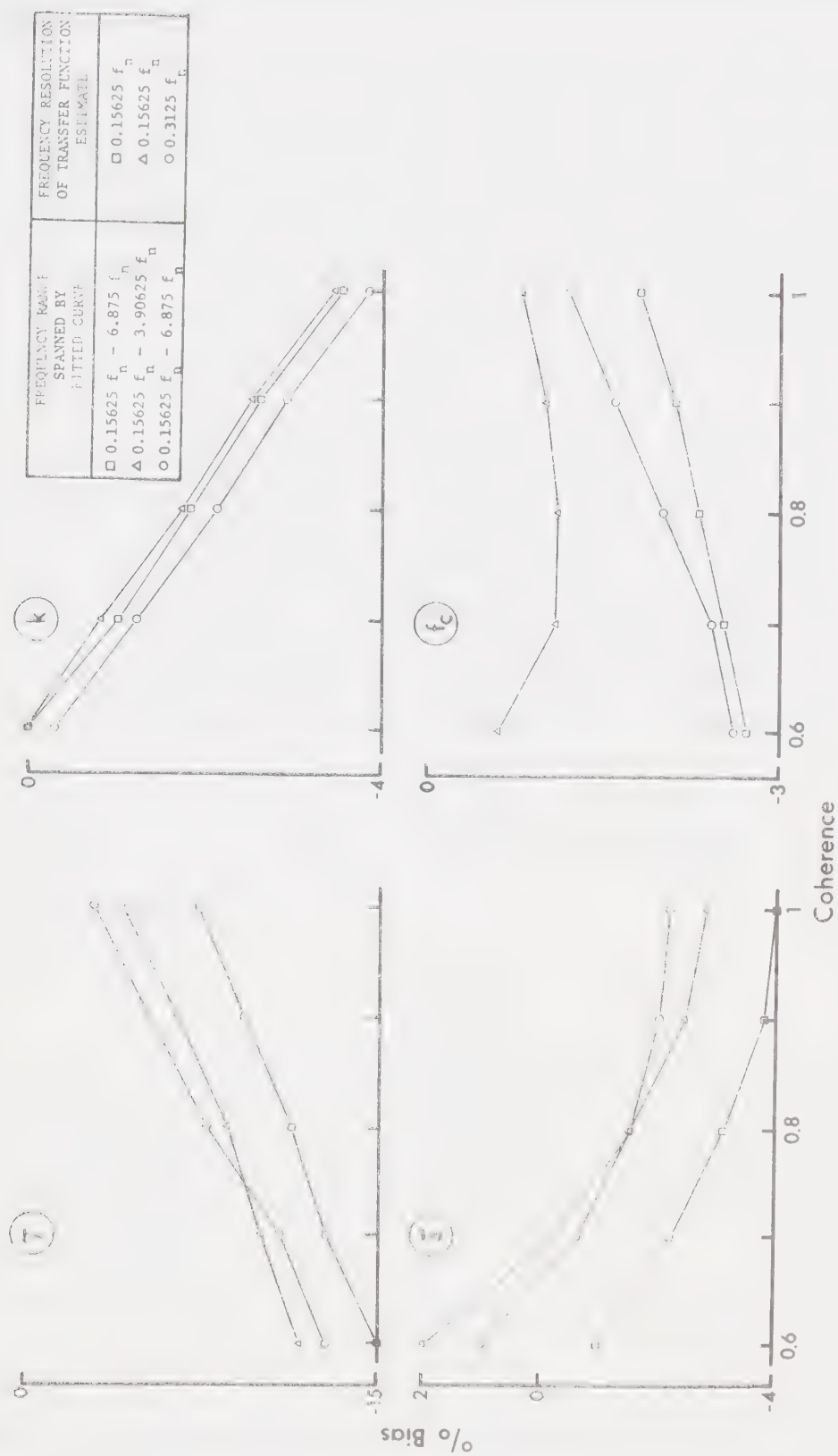
% Bias

FIGURE 6.8 Bias of Fitted Parameters

valid for all parameters fitted to the transfer function estimates of actual motor units.

Also illustrated in Figures 6.7 and 6.8 are the effects of changing the frequency resolution of the transfer function estimate. Although all of the estimates for actual motor units were determined with a frequency resolution of $f_M/40$ Hz, the figures show that, if necessary, reasonable results may be obtained with a frequency resolution as low as $f_M/20$ Hz.

The plots in Figures 6.7 and 6.8 indicate that the relationships between bias and coherence and the relationships between coefficient of variation and coherence are approximately linear for coherences between 0.6 and 1.0. The coefficients describing these relationships were calculated by applying linear regression analysis [113] to data resulting from fits to different simulated motor units with coherences between 0.6 and 1.0. If η is the mean of a fitted parameter (k, f_n, or ζ), and ξ is its standard deviation, the following relationships apply:

$$\eta = a_0 + a_1\gamma^2 \qquad (6.11)$$

$$\xi = b_0 + b_1\gamma^2 \qquad (6.12)$$

When distributions for systems with damping ratios between 0.8-1.5 were determined, it was found that the mean and standard deviations for fitted damping ratio were well described by the following relationships:

$$\eta(\zeta) = a_0 + a_1\gamma^2 + a_2\zeta \qquad (6.13)$$

$$\xi(\zeta) = b_0 + b_1\gamma^2 + b_2\zeta \qquad (6.14)$$

Values for the coefficients in these expressions are listed in Table 6.1 together with correlation coefficients.

Param.	a_0	a_1	a_2	Correl. Coeff.	b_0	b_1	b_2	Correl. Coeff.
T	18.1	4.90	-	0.908	22.4	-20.5	-	-0.998
ζ	1.04	-0.007	-	-0.949	0.300	-0.263	-	-0.998
f_n	0.640	0.033	-	0.996	0.191	-0.172	-	-0.999
ζ	0.104	-0.090	0.883	-0.999	0.150	-0.500	0.172	-0.916

(STANDARD DEVIATION)

This table is valid for:

τ = 25 msec

ζ ≤ 1

f_n = 1Hz

0.8 < ζ < 1.5

Nyquist freq. = 10 Hz

TABLE 6.1 Coefficients for Regression Equations

When curves are fitted to experimental data, the true coherence and damping ratio are not known. Estimates of these quantities must therefore be used in Equations (6.11-6.14). Coherence estimates were calculated for the simulated systems described above, and the results of these calculations indicated that the average value of the coherence estimate over the lowest 30% of the frequency range spanned by the estimate is a reasonable measure of the true system coherence. The bias in this coherence measure is less than 3%, and the standard deviation is less than 0.03 for true coherence values between 0.6 and 1.0. The only available estimate of the true damping ratio is the fitted damping ratio, and the results for the simulated motor units indicate that the bias in this quantity can be as high as 6% and the coefficient of variation can reach 20%. Means and standard deviations predicted by Equations (6.13) and (6.14) must therefore be viewed only as approximations.

Equations (6.11) and (6.12) must be scaled if they are to be used for finding the distributions of k, f_n, and τ for systems in which these parameters have values other than those indicated in Table 6.1. The coefficients for time delay are valid for transfer function estimates based on data collected at 50 msec intervals. If a different sampling interval is used, these coefficients must be multiplied by $\Delta/(50 \text{ msec})$ where Δ is the sampling interval. The coefficients for dc gain and natural frequency are valid for systems in which these parameters have values of unity. For systems other than these, the coefficients must be multiplied by the true parameter value. Of course, in experimental situations, the true parameters are not known, so scaling must be implemented with the fitted parameters. The use of

such fitted values in scaling is the major source of error affecting the estimation of distributions for fitted parameters. This error is introduced because, for a system with a coherence of 0.6, the coefficient of variation for fitted dc gain is about 14%. For fitted natural frequency, the coefficient of variation is about 9%. The bias in fitted dc gain and natural frequency is about 1% and 3% respectively.

The coefficients in Table 6.1, when properly scaled, were used to calculate estimates of the means and standard deviations of the distributions for fitted parameters. Since these fitted parameters were assumed to be normally distributed, approximate confidence intervals for each fitted value could be calculated. Even though these confidence intervals were only approximate, they were useful in interpreting the transfer function estimates for single motor units.

CHAPTER 7

RESULTS

7.1 Classification of Motor Units

Smith and Ovalle [34] classified muscle fibres in the
iliofibularis muscle of *Xenopus laevis* into five groups according to
histochemical and ultrastructural characteristics. Smith and Ovalle [34]
also observed that some muscles do not contain all five fibre types
found in the iliofibularis. Studies by other investigators [35,71] had
indicated the existence of histochemically-distinct muscle fibre types
similar to those identified by Smith and Ovalle [34]. As well,
Lännergren and Smith [35] had demonstrated a relationship between the
histochemical and functional properties of muscle fibres; and Smith and
Lännergren [72] had classified motor units into four groups, two fast
and two slow, according to functional characteristics. Smith and
Lännergren [72] had also concluded that all the muscle fibres comprising
a given fast motor unit are histochemically and functionally similar.

Based on the above evidence, Smith and Ovalle [34] proposed
that skeletal muscle fibres in the Anura may be separated into five
structurally and functionally distinct classes consisting of three
types of fast muscle fibre and two types of slow muscle fibre. An
advantage of this hypothesis is that it can be tested experimentally.
If it proves to be correct, the problem of understanding the organiza-
tion of the motor control system will be greatly simplified.

To test the hypothesis of Smith and Ovalle [34], an attempt
was made to classify the motor units studied in this investigation into
five groups, three fast and two slow. It was felt that if an approp-
riate classification scheme could be developed, if it could be shown

89

that the groups are indeed different from one another, and if a correspondence between the motor unit types and muscle fibre types could be demonstrated, the hypothesis would be greatly strengthened.

Several criteria were considered during the classification procedure. Most important, were qualitative differences among the responses of the motor units to various stimulus signals. Since specific muscle fibre types appear in specific areas within the muscle [34], the location of a motor unit within the muscle was an important factor. Also of interest were quantitative differences in particular characteristics of a motor unit's response. Finally, since Smith and Lännergren [72] had previously classified motor units into groups, their classification criteria were considered with some interest.

The first step in the classification procedure involved the separation of motor units into fast and slow categories. Fast motor units were considered to be those which produced a twitch response when subjected to a single stimulus pulse. Those which responded only to repetitive stimulation were classed as slow motor units.

All slow motor units produced a gradual increase in tension in response to regularly repetitive stimulation, and a gradual decrease in tension when stimulation ceased; but some motor units responded much more quickly than others. As well, if stimulation was maintained, tension produced by the units which responded more quickly reached a plateau and then began to rise again. If stimulation was stopped during this second increase in tension, and a series of single stimuli were then applied, small discrete contractions could be observed. No such behavior was apparent in the slowly-responding motor units. Based on these differences, slow motor units were classified into two

groups. This classification procedure for slow motor units was also used by Smith and Lännergren [72]. Because the type 5 muscle fibres of Smith and Ovalle [34] are believed responsible for the type of contraction exhibited by the more slowly contracting motor units [69], these motor units were designated as type 5. As suggested by Smith and Ovalle [34], the remaining slow motor units were designated as type 4 to match the type 4 muscle fibres. The initial tension ratio, defined in Chapter 6, was helpful in separating the slow motor units. Initial tension ratios for the type 5 units were all less than 0.25, whereas those for type 4 units were greater than 0.45.

A type of response not observed by Smith and Lännergren [72] was apparent for several of the fast motor units studied. The twitch responses for these units were much smaller than for other fast motor units, and consecutive twitch responses varied widely in amplitude. These motor units were designated as type 3 because they were always located near the core of the muscle, and the only fast muscle fibres in this area were those designated as type 3 by Smith and Ovalle [34]. Although the twitches for type 3 motor units were small, the maximum tetanic tensions (defined in Chapter 6) often approached values similar to those of the other fast motor units. Therefore the twitch/tetanus ratios (defined in Chapter 6) for type 3 units were much smaller than they were for the other fast motor units. The twitch/tetanus ratios for type 3 motor units were always less than 0.09.

The greatest differences among the remaining fast motor units were in the rates at which the units fatigued when subjected to repet- itive stimulation. Following Smith and Lännergren [72], these motor units were separated into two categories on the basis of their resis-

tance to fatigue. Since all these motor units were located away from the core of the muscle, and since the only muscle fibres in this area were the types 1 and 2 of Smith and Ovalle [34], all fast motor units not classified as type 3 were classified as types 1 and 2. The more rapidly-fatiguing motor units tended to be those which produced the largest twitch responses, and these motor units were located in the outer portion of the muscle. They were designated as type 1 because type 1 muscle fibres were the largest, and on the basis of their histo-chemistry, the most susceptible to fatigue. Also, type 1 fibres were found only in the outer portion of the muscle [34]. The remaining fast motor units were designated as type 2. They were located nearer the centre of the muscle, as were the majority of type 2 muscle fibres. The fatigue coefficient (defined in Chapter 6) for type 1 motor units was less than 0.75. For type 2 units, this quantity was greater than 0.85.

It should be stressed that the above classifications were only tentative. However, because the results of frequency response studies and histological investigations, to be reported later in this chapter, supported the classification scheme, no attempt was made to revise it.

The various descriptive parameters defined in Chapter 6 served to quantitatively describe the characteristics of the various motor unit types. The values of these parameters for the five motor unit types are listed in Table 7.1 together with other characteristics which were observed. In addition, typical responses of the various motor unit types are illustrated in Figure 7.1.

Type 1 motor units were supplied by the largest motor axons.

MOTOR UNIT TYPE	AXON DIAMETER (μm)		MAXIMUM TETANIC TENSION (g-force)		TWITCH AMPLITUDE (g-force)		TWITCH-TETANUS RATIO		TWITCH PEAK TIME (ms)		FATIGUE COEFFICIENT[1]		NUMBER OF OBSERVATIONS
	MEAN	S.D.	MEAN	S.D.	MEAN	S.D.	MEAN	S.D.	MEAN	S.D.	MEAN	S.D.	
1	19.0	2.1	37.1	17.1	15.8	8.9	0.45	0.099	41.5	6.4	.542	.184	12
2	15.6	1.9	19.0	11.7	4.5	2.7	0.24	0.082	45.8	6.0	.916	.065	12
3	12.9	2.1	8.5	7.2	0.48	0.49	0.058	0.033	68.5	16.5	.933	.110	12

MOTOR UNIT TYPE	AXON DIAMETER (μm)		MAXIMUM TETANIC TENSION (mg force)		INITIAL TENSION RATIO		NUMBER OF OBSERVATIONS
	MEAN	S.D.	MEAN	S.D.	MEAN	S.D.	
4	8.0	1.0	.95	.44	.490	.112	4
5	6.3	0.9	1.38	.16	.146	.078	5

NOTES:

1. Based on 6, 6 and 4 observations for motor unit types 1, 2 and 3 respectively.

TABLE 7.1

Characteristics of Single Motor Unit Twitch and Tetanus Responses
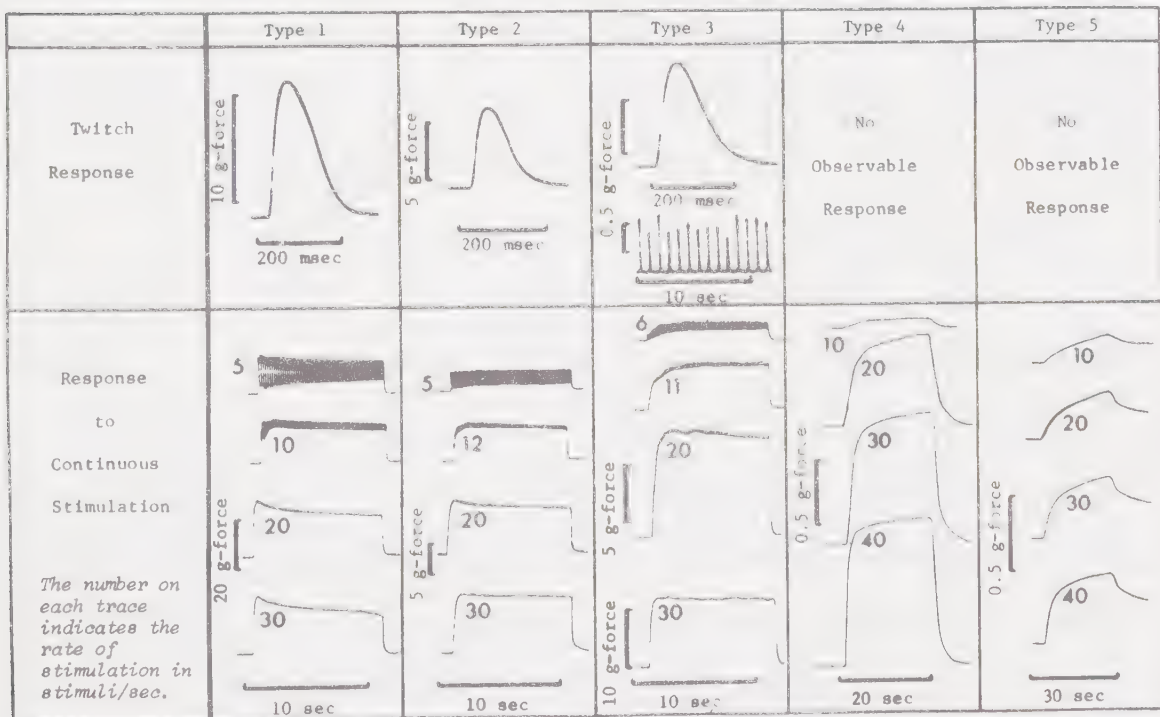
FIGURE 7.1 Responses of Single Motor Units to Stimulation with Trains of Evenly-Spaced Pulses

They developed high tetanic tensions, but they fatigued rapidly. Of all the fast motor units, the twitch/tetanus ratios for type 1 units were highest.

Type 2 motor units developed smaller tetanic tensions than type 1 units, and they exhibited lower twitch/tetanus ratios. They were supplied by medium-size motor axons. With maintained stimulation, the decrease in tetanic tension due to fatigue occurred more slowly than for the type 1 units.

Type 3 units were innervated by axons with diameters ranging from 10-15 μm. Their resistance to fatigue often approached that of type 2 motor units. The coefficients of variation for twitch amplitude were calculated for a series of fifty consecutive twitches of a type 3 motor unit at various muscle lengths. The results of these calculations are plotted together with the mean twitch amplitudes in Figure 7.2. This plot illustrates that the twitch amplitude became less variable as muscle length increased, and that the mean twitch amplitude was highest when the muscle was near its natural resting length, l_o.

In one experiment involving a type 3 motor unit, a small biphasic longitudinal current record was recorded at the surface of the muscle in association with the twitch response. On tetanic stimulation, the amplitude of the longitudinal current record increased as the tetanic tension developed. If this stimulation was continued, the muscle tension eventually began to drop, presumably because of fatigue, and the drop in muscle tension was accompanied by a decrease in the magnitude of the longitudinal current. This suggests that the fatigue effects may be largely electrical in origin, and that they are not the result of failure in the muscle contractile mechanism. A similar set

95
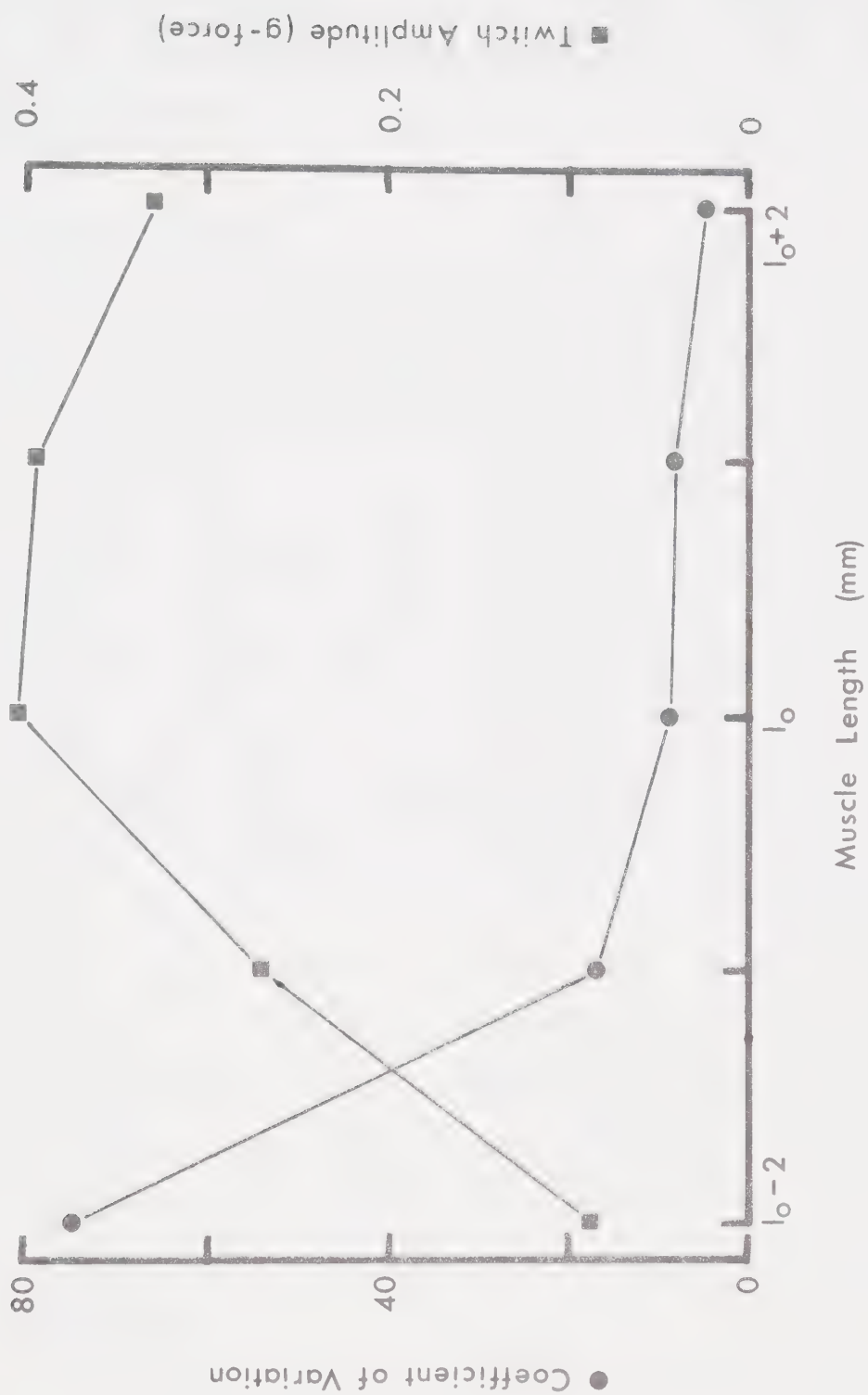
FIGURE 7.2 Effect of Muscle Length on the Mean Twitch
Amplitude of a Type 3 Motor Unit

of measurements for a type 2 motor unit agreed with observations made
by Lännergren and Smith [35]. These observations indicate that the
contractile mechanism begins to fail before the electrical activity is
noticeably affected.

7.2   Frequency Response

Transfer function estimates were calculated for several
examples of each motor unit type. Typical examples of these transfer
function estimates are plotted in Figure 7.3 for the slow motor unit
types and in Figure 7.4 for the fast motor unit types. Also shown in
Figure 7.4 are curves representing the best-fitting transfer functions
calculated according to the method outlined in Chapter 6. The horizon-
tal line on the coherence plots represents the average coherence over
the frequency range spanned by the line. For the fast motor units, the
coherence remained high for frequencies below about 15 Hz, and a second-
order model seemed appropriate for this frequency range. Above 15 Hz,
the drop in coherence could be attributed to the effects of quantization
error as discussed in Chapter 6. Because the last 20 points of the
transfer function estimates were neglected during the fitting procedure,
this drop in coherence had little effect on the shapes of the fitted
curves. Curves are not fitted in Figure 7.3 because the low coherence
associated with the slow motor unit types indicated that the transfer
functions for these motor units would not be appropriately represented
by a linear model.

The results of fits to transfer function estimates for the
three fast motor unit types are listed in Table 7.2. These transfer
function estimates were determined with the muscles at their natural
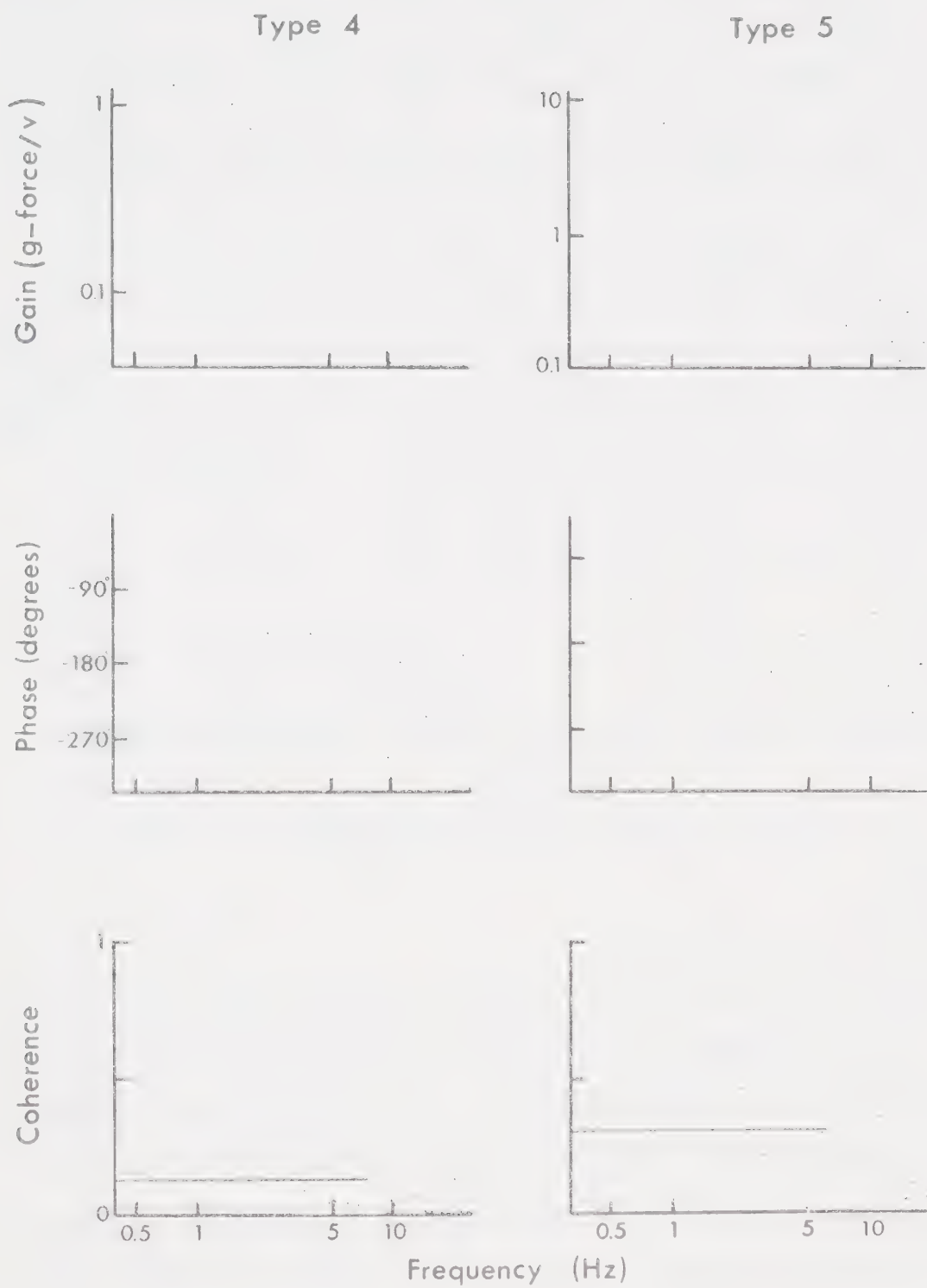
FIGURE 7.3 Transfer Function and Coherence Estimates
for Slow Motor Units
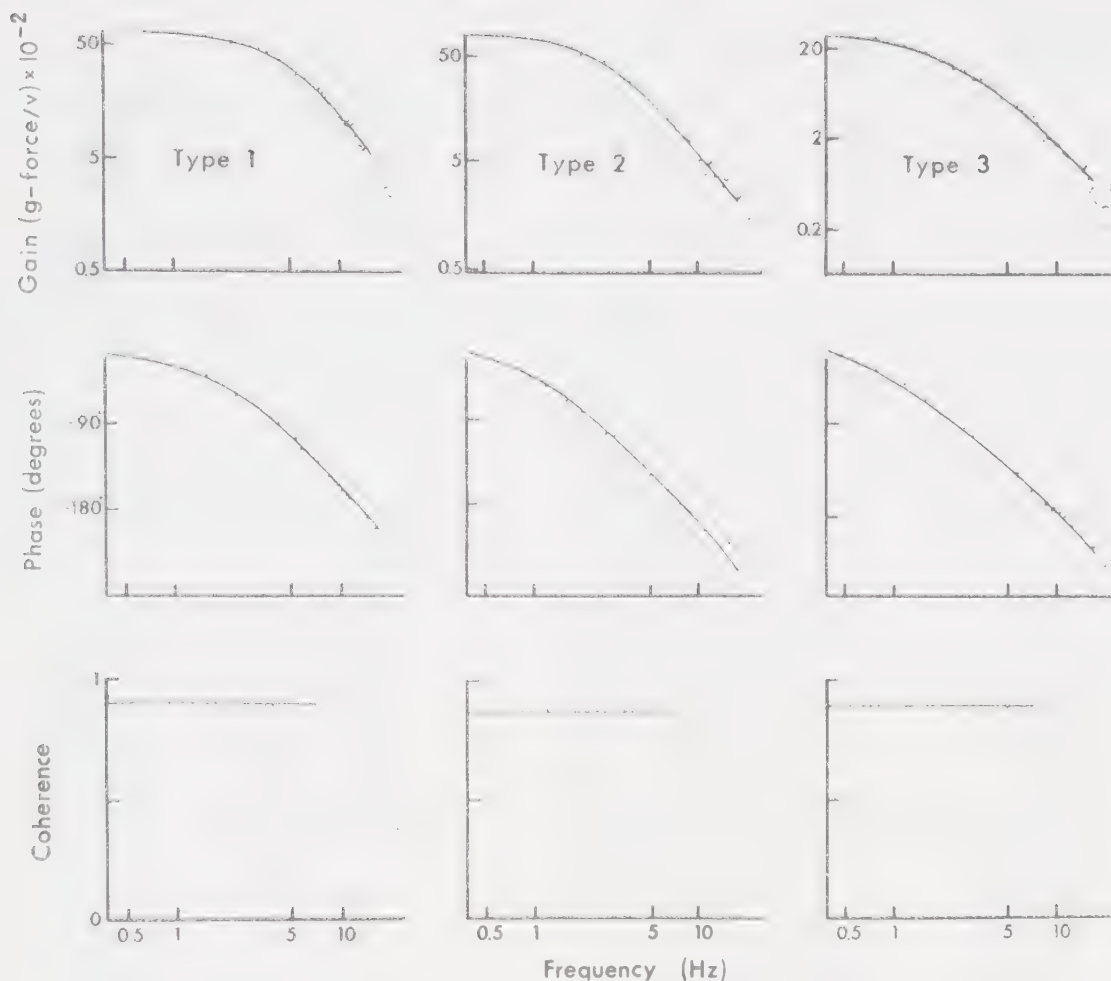
FIGURE 7.4   Transfer Function and Coherence Estimates
for Fast Motor Units

resting lengths. The interpulse intervals of the stimulus pulse train

were approximately exponentially distributed with a mean of 0.1 sec.

Interpulse interval distributions describable by gamma distributions

of orders 1-8 were tested on a few preparations. These variations in

the order of the gamma distribution seemed to have little effect on the

transfer function estimates, so the exponential distribution was used

for all subsequent studies. Stimulation and sampling were controlled

so that bursts of stimulation 2.56 sec in length occurred every 20 sec.

Comparison of transfer function estimates calculated from the

MOTOR UNIT TYPE	τ(ms)		k^1 (g-force/v)		ζ		f_n(Hz)		COHERENCE[2]		MEAN ERROR[3] (% of dc gain)		NUMBER OF OBSERVATIONS
	MEAN	S.D.	MEAN	S.D.	MEAN	S.D.	MEAN	S.D.	MEAN	S.D.	MEAN	S.D.	
1	6.61	3.33	7450	3620	1.00	0.15	3.05	0.58	0.72	0.17	5.84	2.16	8
2	10.8	3.85	4820	2680	1.14	0.21	2.44	0.29	0.72	0.15	5.43	1.15	9
3	14.2	3.68	2520	1560	1.51	0.32	2.06	0.33	0.76	0.07	3.50	2.23	4

NOTES:

1. The actual value for dc gain is arbitrary since it depends upon the amplitude of the stimulus pulse. The same pulse height was used for all experiments, however, so the relative differences in dc gain are significant.

2. Average coherence for the lower 30% of the frequency range.

3. Average difference between fitted curve and points representing transfer function estimate.

TABLE 7.2

Fitted Parameter Values for Fast Motor Units

first and last halves of groups of 20 power spectrum estimates obtained with continuous stimulation and with stimulus bursts proved to be an inconclusive means of demonstrating the advantages of stimulus bursts in reducing the effects of fatigue. This comparison indicated that the transfer function estimates were insensitive to such differences in the stimulation procedure over the time required to collect 20 records. Therefore, the justification for using stimulus bursts is based solely on the subjective observation that, with this technique, more samples could be collected over the course of the experiment before the reduction in twitch amplitude due to fatigue became unacceptable. Generally, a 20% decrease in twitch amplitude over the course of the experiment was considered acceptable

The values for each parameter fitted to the transfer function estimates were grouped according to motor unit type, and analysis of variance [138] was used to test the null hypothesis that, for each parameter, the groups came from the same population. This procedure uses an F test [138] to compare two quantities. The first quantity gives the average dispersion of the items in each group about the group means and the second quantity gives the dispersion of the group means about the mean of the entire population. If the null hypothesis is correct, these two quantities should not be significantly different. For all four fitted parameters, the F test indicated a difference at the 99% level of significance, thereby indicating that, for each parameter, at least some of the group means were different from one another. To discover which means were different from one another, comparisons between pairs of fast motor unit types were made with the least significant range test [138]. At the 95% level of signifi-

cance, the means of all parameters for type 3 motor units differed from those of the corresponding type 1 motor unit parameters. Differences at this level of significance were also apparent for all parameters except dc gain and time delay when means for type 2 and type 3 motor units were compared. A comparison of means for type 1 and type 2 motor units indicated that the natural frequencies and time delays differed at the 95% level of significance.

The effects of changes in the muscle length and stimulus rate are illustrated in Figures 7.5-7.8 for examples of each fast motor unit type. Each figure consists of four separate plots. The two upper plots show the fitted parameter values joined with straight lines for each motor unit type, and the two lower plots indicate the approximate 95% confidence regions for the fitted values. These confidence regions are the areas between sets of straight lines joining respectively the upper and lower confidence limits for each set of data points. The confidence limits were calculated according to the procedure described in Chapter 6.

The effects of changes in muscle length were studied for a stimulus signal having a mean stimulus rate of 10/sec. Transfer function estimates were obtained for a range of muscle lengths which roughly corresponded to the range of possible lengths for an iliofibularis muscle *in vivo*.

With the muscle at its natural resting length, transfer function estimates were obtained for a variety of stimulus signals with mean stimulus rates ranging between 0.2-20/sec.

As Figure 7.5 indicates, the confidence regions for time delay were so wide that a systematic variation of this parameter in
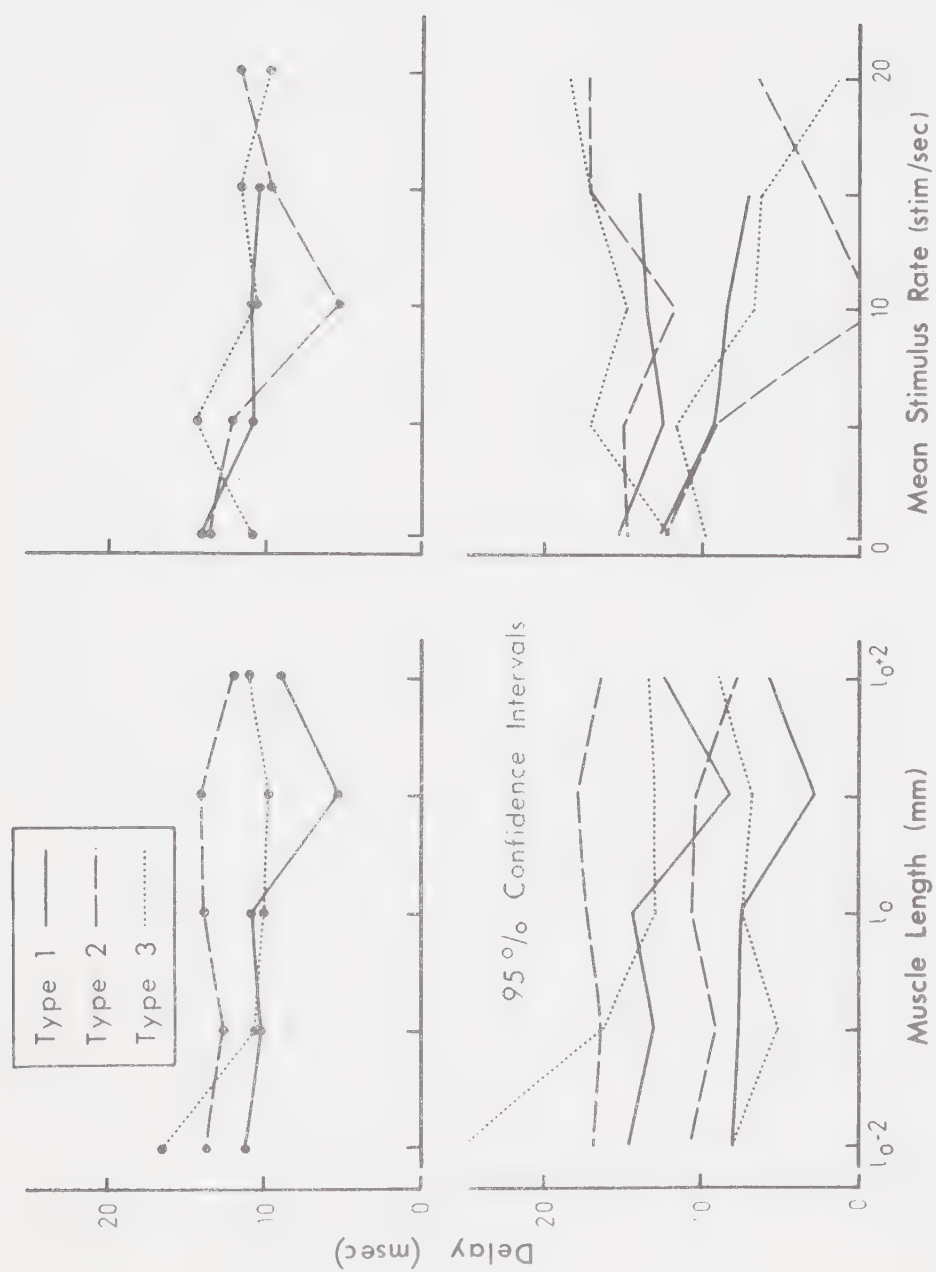
FIGURE 7.5 Effects of Mean Stimulus Rate and Muscle Length on Fitted Time Delay
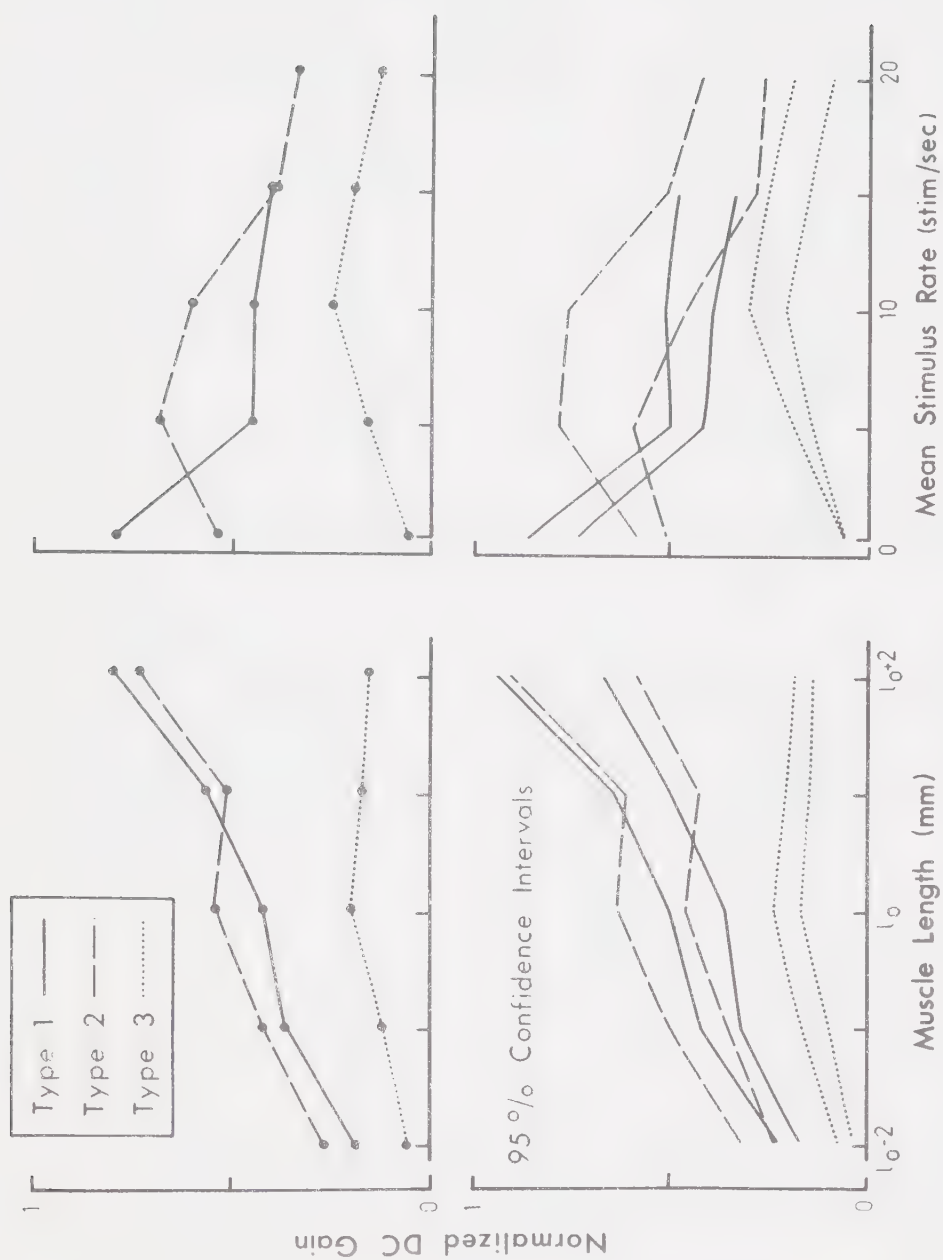
FIGURE 7.6 Effects of Mean Stimulus Rate and Muscle Length on Fitted DC Gain
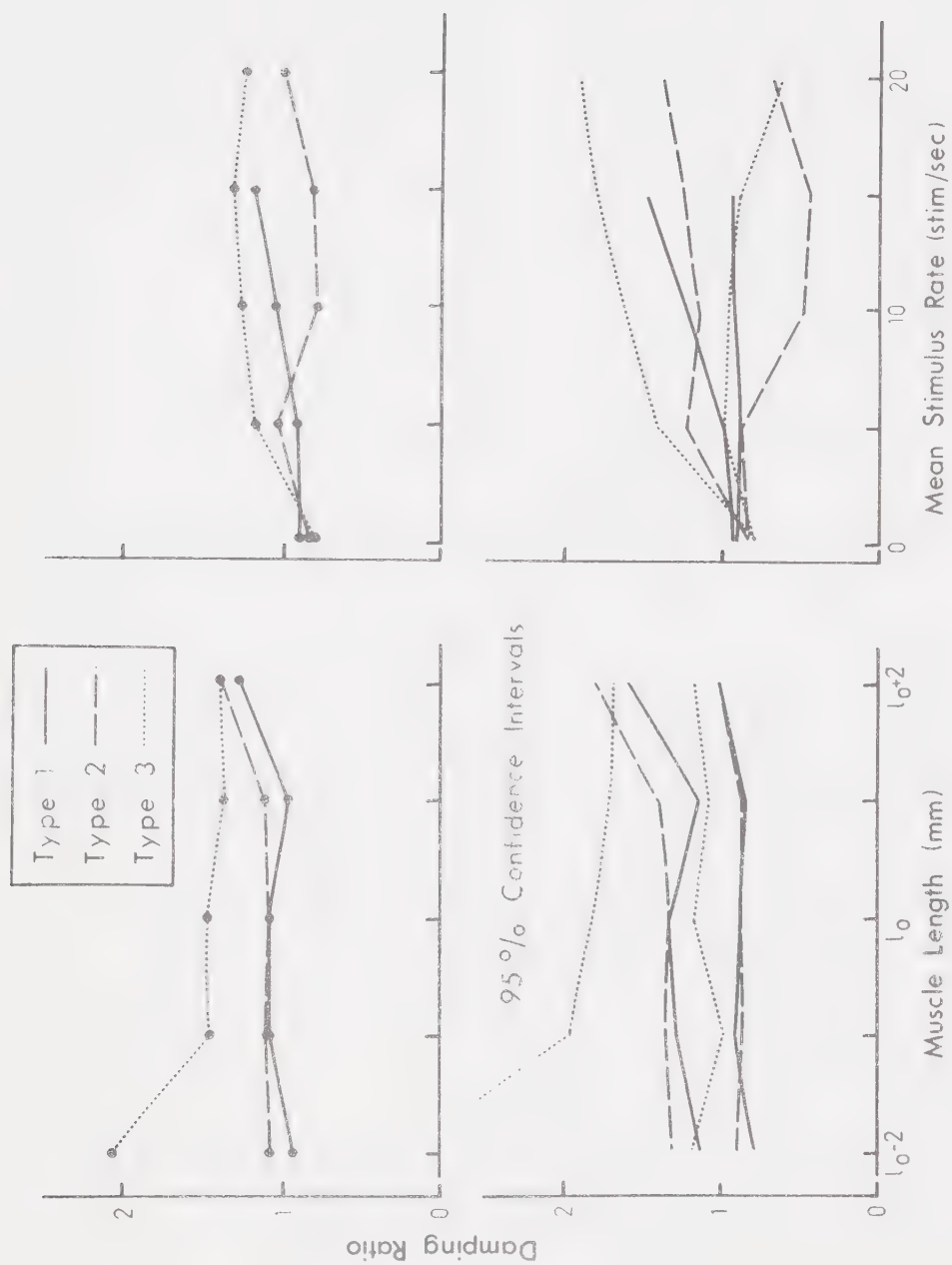
FIGURE 7.7 Effects of Mean Stimulus Rate and Muscle Length
on Fitted Damping Ratio

105
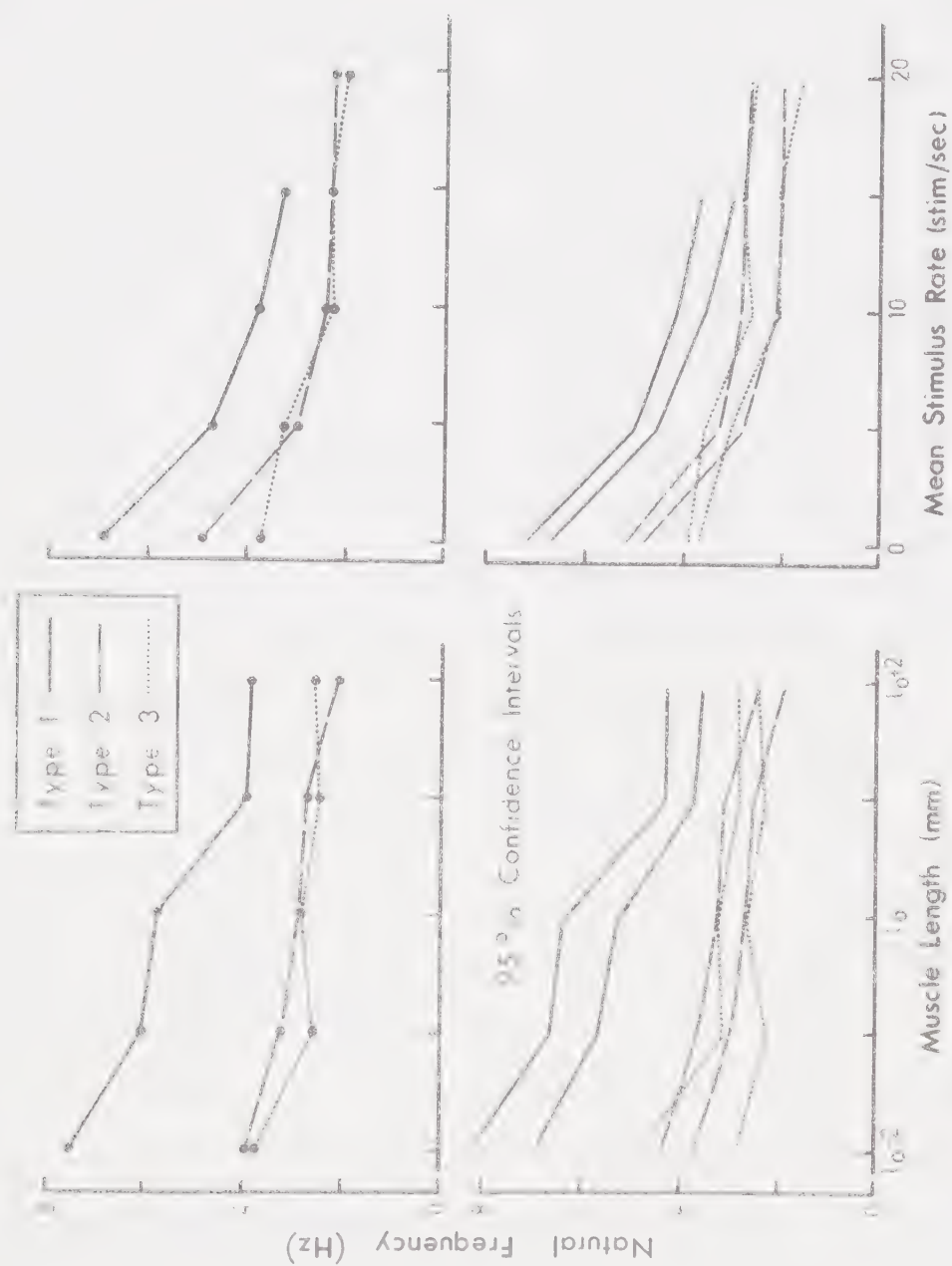
FIGURE 7.8 Effects of Mean Stimulus Rate and Muscle Length on Fitted Natural Frequency

response to changes in length or stimulus rate could not be detected. Values for fitted time delay ranged all the way from 3 to 18 msec, but in most cases, the fitted delay was in the 10 msec range. For the three preparations in which delay was measured directly, values of 8, 10, and 11 msec were obtained.

The delay consists of three components: the time required to transmit an action potential along the nerve from the point of stimulation to the neuromuscular junction, the transmission delay at the neuromuscular junction, and the delay associated with excitation and contraction in the muscle. For axon diameters between 5 μm and 20 μm, the value of the first component ranged between 1-4 msec [116], and the synaptic delay was 0.5-0.8 msec [117], so the value of the remaining component had to be near 10 msec. An experimentally-determined value in the 10 msec range for this last component of the time delay is apparent in the results of Rüdel and Taylor [46]. Differences among the mean time delays for the various motor unit types were too great to be accounted for completely by differences in the travelling times of the nerve action potentials. It therefore seems likely that differences in excitation-contraction delay exist among the various muscle fibre types.

Figure 7.6 shows that the dc gain for the type 1 motor unit was highest at very low stimulus rates whereas the dc gain for the type 2 and type 3 units reached a peak near 5 stimuli/sec. The dc gain for the type 3 motor unit was highest when the muscle was near its natural resting length, whereas the gain for the type 1 and type 2 motor units continued to increase as the muscle was lengthened.

The damping ratios for all three fast motor unit types,

plotted in Figure 7.7, increased slightly as the stimulation rate was increased, and the damping ratios for the type 1 and type 2 motor units increased slightly for increasing muscle length. For the type 3 motor unit, the damping ratio was very high when the muscle was short, and it decreased sharply as muscle length was increased. When the muscle was 2 mm longer than its resting length, the damping ratios for all three motor unit types were near 1.25.

Figure 7.8 shows that the natural frequencies for all three fast motor unit types were highest for short muscle lengths or low stimulus rates. The value of this parameter decreased as muscle length or stimulus rate was increased.

Values of the coherence estimates for each motor unit type are plotted in Figure 7.9 together with approximate 95% confidence intervals derived from the computer simulation of the fitting procedure. The plotted values represent the average of the coherence estimate over a frequency range between about 0.4 Hz and 12 Hz. The coherence for the type 1 motor unit remained above 0.8 for all muscle lengths studied, and the coherence for the type 2 motor unit remained near this value for muscle lengths below l_o +1 mm. At the longest muscle length, the coherence for the type 2 motor unit dropped to near 0.6. For the type 3 unit, the coherence was less than 0.5 when the muscle length was short. As muscle length was increased, the coherence value gradually increased to a plateau of about 0.8 for a muscle length of l_o +1 mm. The coherence for all three motor unit types in response to widely-spaced single stimuli was near 1.0, but this value dropped steadily as stimulus rate was increased.
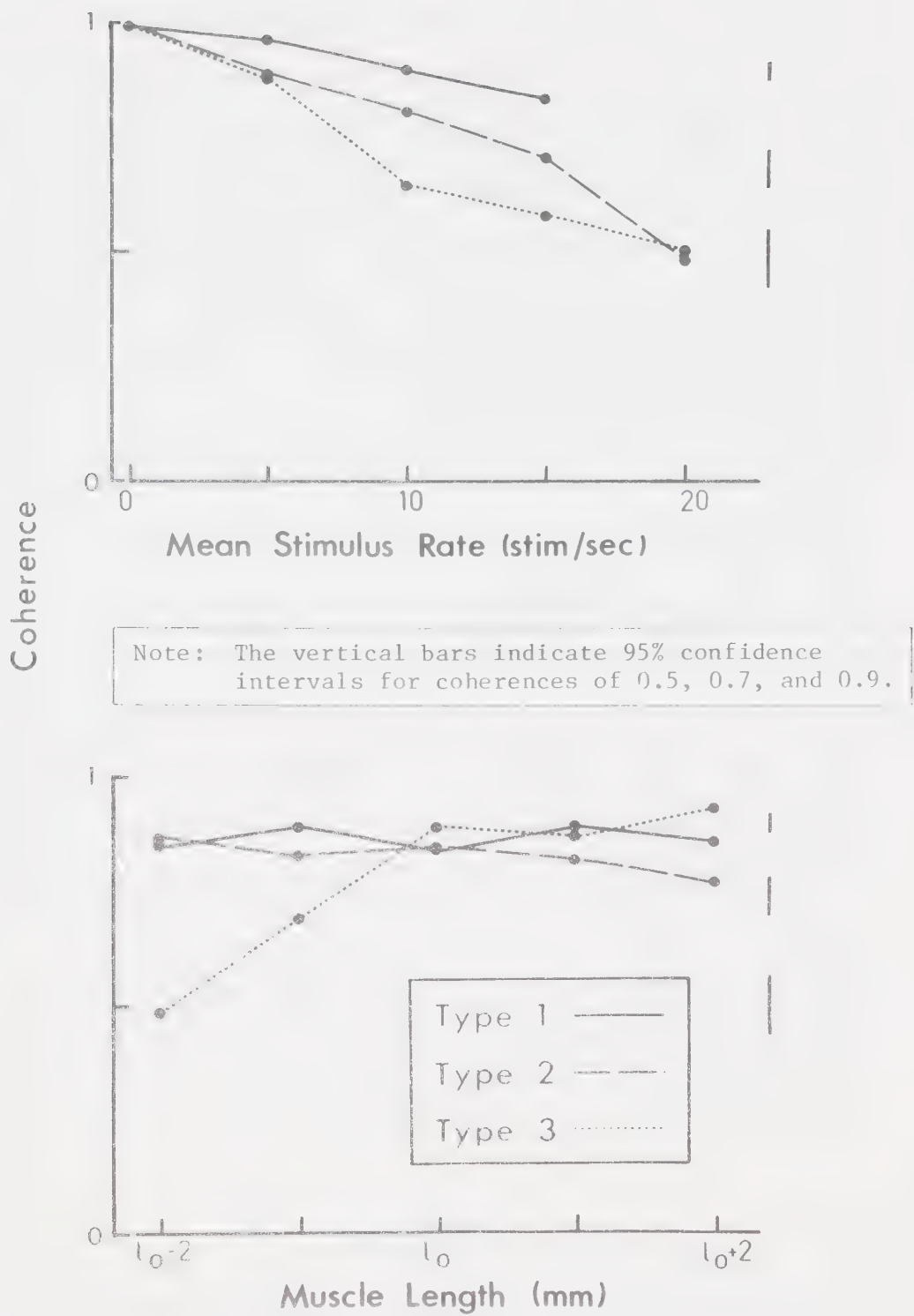
FIGURE 7.9   Effects of Mean Stimulus Rate and
Muscle Length on Average Coherence

7.3 Mechanical Properties

The transfer functions relating small changes in muscle length to changes in tension were similar to those obtained by Halpern and Alpert [104] for the sartorius muscle. A typical example, illustrating the response to random length changes never greater than about 80 μm, is shown in Figure 7.10. This maximum displacement is similar to that observed for the so-called "isometric" force transducer during the measurement of motor unit transfer function estimates. For frequencies below 20 Hz, the coherence was near 1.0, the gain was constant to within about 2 db, and the phase changed by less than 20°. This means that the mechanical response of the muscle can be approximated by that of a spring for frequencies below 20 Hz. Each transfer function estimate which was calculated for a single motor unit can therefore be viewed as the response of the motor unit's muscle fibres in parallel with a spring representing the remainder of the muscle. At low frequencies, the compliance of the whole muscle ranged between about 0.1-0.35 mm/g-force for muscle lengths between 1_o-2 mm and 1_o+2 mm.

If $1/K_2$ is the compliance of the force transducer, $1/K_1$ is the compliance of the muscle, and $F(t)$ is the force generated by the single motor unit, the force indicated by the transducer will be

$$\tilde{F}(t) = F(t) \frac{K_2}{K_1+K_2} \tag{7.1}$$

Therefore, for a force transducer compliance of 0.01 mm/g-force, the maximum attenuation of the force generated by any motor unit was only about 7% and this attenuation was constant for all frequencies below 20 Hz. For this reason the effect of the mechanical properties of the
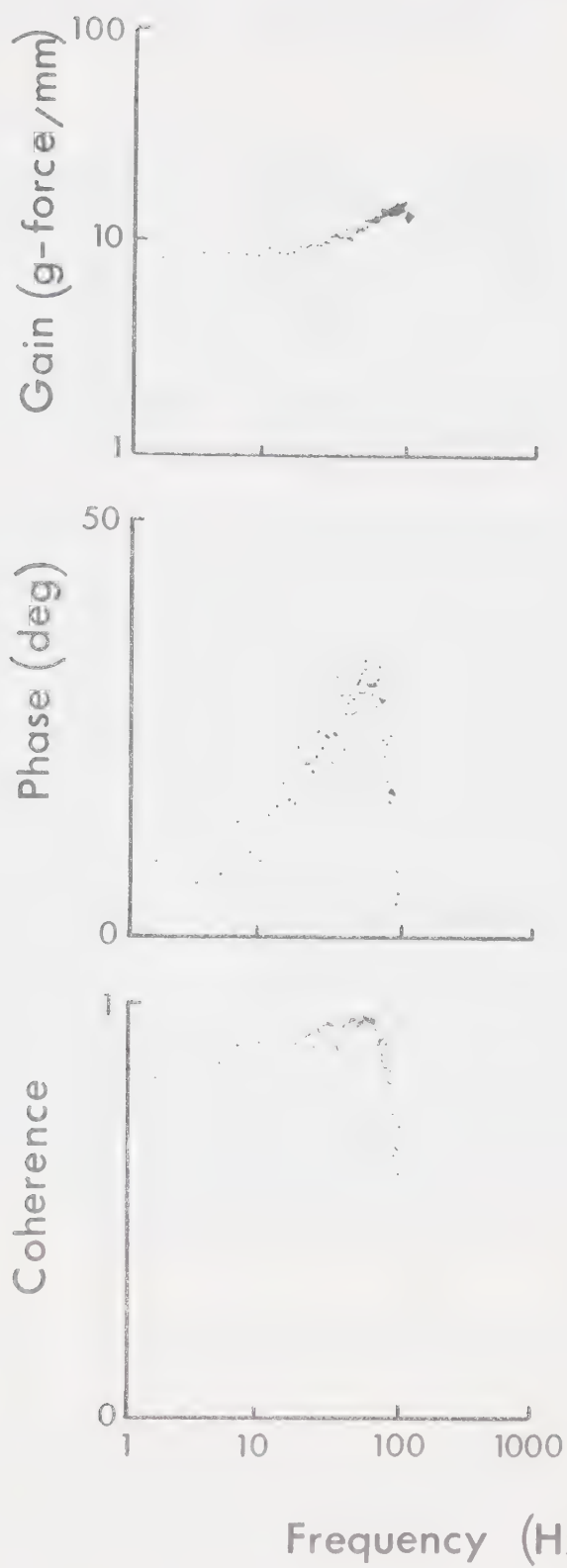
FIGURE 7.10 Relationship Between Muscle Length and Tension
for Small Random Perturbations in Length

passive muscle fibres on the frequency response of single motor units was not subtracted from the transfer function estimates.

7.4 Histochemical Studies

The photographs in Figure 7.11 show the results of studies in which single fast motor units were continually stimulated in order to deplete the glycogen in their muscle fibres. These studies were carried out on 2, 3, and 3 examples of motor units of types 1, 2, and 3 respectively. Certain muscle fibres in the photographs of sections stained for SDHase are marked with numbers which indicate the fibre type according to the designation scheme used by Smith and Ovalle [34]. The same fibres in the sections stained for glycogen are marked with letters indicating the degree of glycogen depletion. The letter U indicates a fibre in which no depletion is apparent, P indicates a partially depleted fibre, and D indicates a fibre for which the degree of depletion is substantial. Depleted, partially depleted, and undepleted fibres of the same type were found in each preparation, but the numerical designation for those fibres exhibiting any evidence of glycogen depletion always matched the numerical designation applied to the isolated motor unit. No depleted fibres were found in a control preparation which was not stimulated before being fixed.
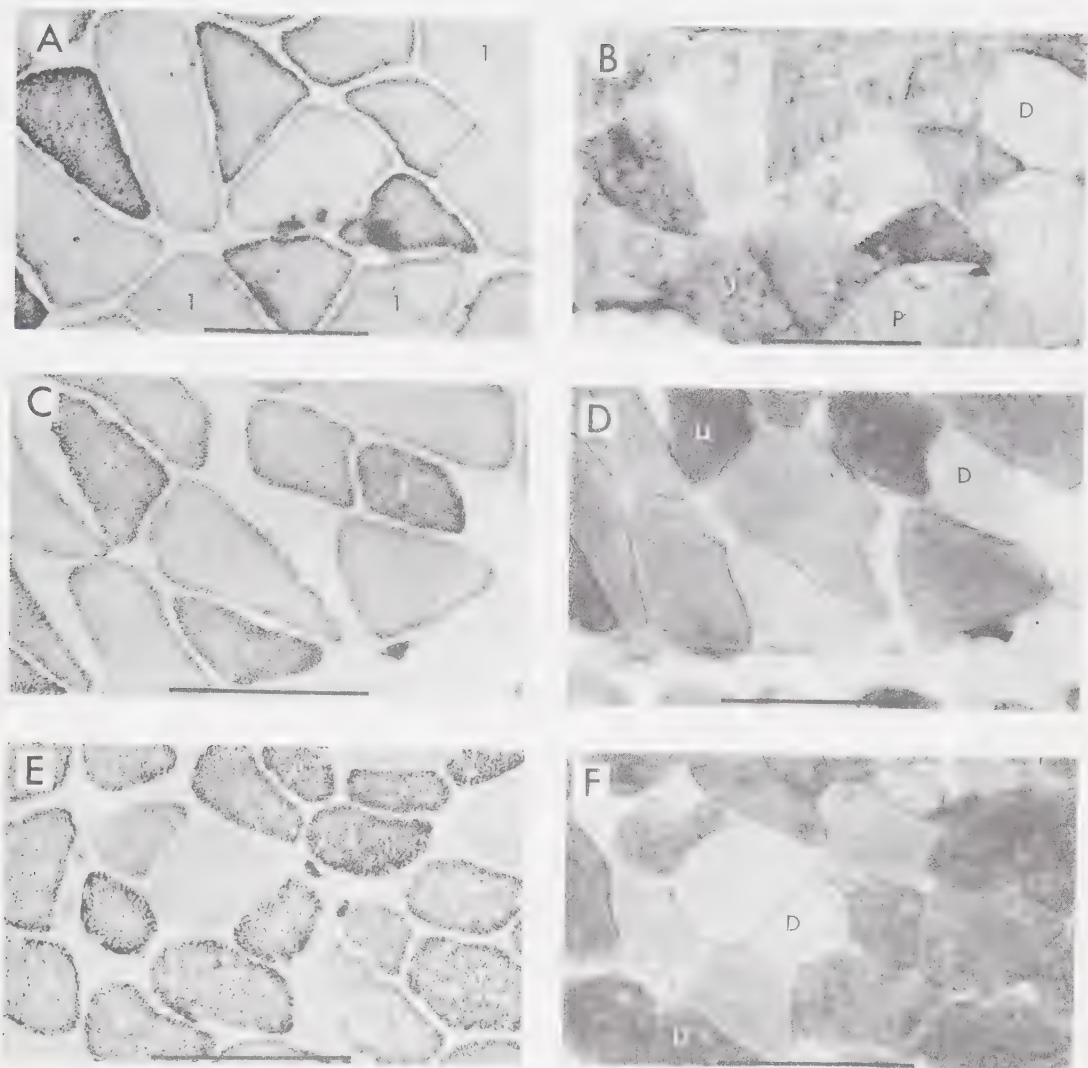
FIGURE 7.11   Transverse Sections of Muscle Fibres From Three
                Different Nerve-Muscle Preparations.

                The isolated motor units were identified as
                Type 1 (A,B), Type 2 (C,D), and Type 3 (E,F).
                Serial sections were stained for SDHase
                activity (A,C,E) and glycogen (B,D,F). The
                scale bars indicate 200 μm.

CHAPTER 8

DISCUSSION

8.1 Significance of Transfer Function Estimates

This investigation was designed to determine if spectral analysis methods can be profitably applied in studying the input-output relationships of single motor units. The iliofibularis muscle of *Xenopus laevis* was known to contain motor units of several different types, and it was felt that the effectiveness of spectral analysis could be assessed from the results of *in vitro* studies involving these motor units. It was also hoped that such studies would provide information concerning the function and organization of the various motor unit types.

Spectral analysis was used for calculating transfer function estimates from which linear models could be derived. A simpler approach to estimating the transfer function would involve Fourier transforming the waveform of a single twitch. This approach is possible because a single twitch is equivalent to the impulse response of the system, and the impulse response is the inverse Fourier transform of the transfer function [118]. Unfortunately, as the results in Chapter 7 indicate, such a transfer function estimate is a poor representation of the response to stimulation at higher rates. Therefore, the use of spectral analysis to study the responses for a variety of stimulus rates seems reasonable.

The linear models presented here for the stimulus-response relationships of single motor units have several limitations. They are only applicable to certain motor unit types, they are useful only for predicting isometric muscle tension, they depend upon such factors

as stimulus rate and muscle length, and they neglect the effects of fatigue. Despite these limitations, however, such models are useful because they provide a standard basis for describing experimentally-observed responses. The parameters associated with each model can be used to compare the response of a particular motor unit with the responses of other motor units, with theoretical responses derived from mathematical models, or with responses of the same motor unit under different experimental conditions. It should be stressed that the linear models presented here are valid only for signals having perturbations in interpulse interval similar to those of the stimulus signals used in developing the model. For such signals, the standard deviation of the interpulse interval is equal to the mean interpulse interval [135].

8.2   The Coherence Estimate

Coherence estimates for fast motor units differ from those of linear, noise-free systems in two ways: the coherence drops sharply at high frequencies, and, although the coherence at low frequencies is approximately constant, its value is less than unity.

Quantization noise seems to be the major cause of the drop in coherence at high frequencies, and this means that the coherence estimate could be improved by pre-whitening the system output signal [73]. Pre-whitening involves passing the signal through a well-designed filter so that the spectrum of the resulting filtered signal is approximately flat over the band of frequencies below the Nyquist frequency. The level of this signal may then be adjusted so that

components at all frequencies are digitized using the maximum resolut-
ion of the analog-to-digital converter. Of course, the effects of the
pre-whitening filter would have to be removed from the resulting
transfer function estimate. Pre-whitening is not required for the
input signal because a signal with a flat spectrum may be chosen as an
input.

The results in Chapter 7 suggest that the coherence for a
fast motor unit is approximately constant with a value close to that of
the low frequency coherence estimate. This value is less than unity
presumably because of the combined effects of added noise and system
nonlinearity. The response of type 1 and type 2 motor units to trains
of uniformly-spaced impulses did not appear to be contaminated with
added noise. No spurious or missing twitches were apparent, and the
twitches were all the same size. For higher stimulus rates resulting
in fused muscular contractions, no sudden changes in muscle tension
could be observed. Similar observations applied for type 3 motor units
at long muscle lengths. For short muscle lengths, however, the coeff-
icient of variation for twitch amplitude was high, and tetanic muscular
contractions were not smooth. The low frequency coherence for the type
1 and type 2 motor units was not greatly affected by changes in muscle
length, but, for the type 3 unit, this value dropped sharply at short
muscle lengths. It therefore appears that the coherence of fast motor
units is less than unity because of the nonlinear response exhibited
by these motor units. In addition, the coherence of type 3 motor units
at short muscle lengths is further reduced because of the noise-like
effects which are observed under these conditions.

Experimental measurements of the responses of a few examples

of each motor unit type have led to the assumption that the response of a fast motor unit is similar to that of a second-order low-pass filter with a time delay. Based on this assumption, simulation studies of the type described in Chapter 6 have provided useful information concerning the application of spectral analysis to the study of fast motor units. Such simulation studies would not be needed if experimental data could be obtained for a large number of single motor unit preparations, but such preparations are difficult, and the amount of information which can be obtained from each one is limited because of the effects of fatigue.

The responses of simulated motor units only crudely approximate the responses of real motor units, but these crude approximations are sufficient for studying the spectral analysis procedure. Neglecting the effects of fatigue, the greatest difference between the responses of the real and simulated motor units can be related to the coherence estimate. For real motor units, the coherence is reduced from unity largely because of the nonlinear relationship between stimulus rate and muscle tension. For the simulated motor units, the coherence depends upon random noise which is purposely introduced into an otherwise linear stimulus-response relationship. However, the probability distributions of transfer function estimates for a noisy system and a nonlinear system are identical if the coherences of the two systems are the same [23] (so long as the same spectral analysis procedure is used in both cases). Therefore, parameters fitted to a transfer function estimate for a simulated motor unit will be statistically equivalent to parameters fitted to a transfer function estimate for a real motor unit with the same coherence.

8.3   Relationships Between Motor Units and Muscle Fibres

Because the location of each motor unit type within the muscle matches the location of a particular type of muscle fibre, and because the isometric contractile properties of the various motor unit types are unique, it appears that a motor unit contains muscle fibres of only one type. The numerical designation which was assigned to each motor unit type indicates the type of muscle fibre from which the motor unit is presumably composed [34]. Direct evidence for such a relation- ship was provided by the glycogen depletion studies. These direct results are based on a limited number of experiments, and not all motor unit types were studied; but, in every case, the hypothesis that single motor units are composed only of muscle fibres of one particular type was supported. Both motor units and muscle fibres can be classified into two major groups--fast and slow, but as more criteria are consid- ered, each of these groups can be subdivided. The possibility of further subdivision still exists, but, in the absence of any evidence suggesting the existence of additional sub-groups, the present classifi- cation of motor units into five distinct groups must be accepted.

Although amphibian and mammalian muscle fibres are classified differently, the results of Weurker et al. [119] are applicable to this discussion. They proposed that single motor units in the medial gastrocnemius muscle of the cat are composed of muscle fibres which resemble one another very closely, and they suggested that the similarity among muscle fibres of the same motor unit is due to some type of neural influence. The results of cross-innervation experiments by Buller et al. [120,121], for the cat, and Elul et al. [122], for the frog, support this theory.

Other similarities between mammalian and amphibian motor unit organization are apparent. The largest motor units are, in general, innervated by the thickest nerve fibres. This relationship was observed in the cat by McPhedran et al. [57] and by Weurker et al. [119]. Since, in the frog at least, the largest motor units tend to be those which contract most rapidly, and since the conduction velocity of a nerve increases with its diameter [116], the relationship between motor unit size and axon diameter insures that the most rapidly contracting muscle fibres are capable of receiving stimuli as quickly as possible.

In both mammals [119] and amphibians, the largest, fastest motor units fatigue more rapidly than do the smaller motor units. The large differences in the fatigue rates of fast muscle fibres in the frog, noted by Grabowski et al. [96], can be explained by the existence of three fast muscle fibre types with different fatigue rates. Lännergren and Smith [35] showed that fatigue in type 1 muscle fibres is not due to failure of propagation of the muscle action potential, and a similar situation is apparent for type 2 motor units. Fatigue in type 3 units, on the other hand, develops very slowly and is accompanied by a decrease in the magnitude of the propagated action potential. It therefore seems possible that fatigue effects related to the propagation of the muscle action potential occur at the same rate for all fast motor units. The observed differences in the rates of fatigue for the three motor unit types are probably related to differences in the structure of their muscle fibres. The rapidly fatiguing type 1 muscle fibres are poorly supplied with mitochondria, and their content of glycogen and fat droplets is low, whereas type 2 muscle fibres,

which fatigue slowly, are well equipped with all of these elements. Fatigue in the contractile mechanism of type 3 motor units occurs very slowly, and type 3 muscle fibres carry an extremely abundant supply of these energy-producing elements.

8.4 Interpretation of Transfer Function Estimates

The low coherences associated with slow motor units indicate that the responses of such motor units to random stimulation are poorly represented by linear transfer functions. This result is not unexpected. Earlier investigations [50,58,72] have shown that slow motor units with responses similar to those of type 5 units exhibit nonlinear character- istics such as the absence of a twitch response and the ability to maintain relatively high tensions at low stimulus rates. As Samosudova et al. [123] suggest, this nonlinear behavior probably results from the absence of propagated action potentials and the existence of a sparse sarcoplasmic reticulum which neither supplies nor reabsorbs calcium ions quickly. It is interesting that type 4 motor units also exhibit non- linear characteristics even though these motor units can shorten much more rapidly than can type 5 units. Although nothing is known about the function of single type 4 muscle fibres, one can predict that these fibres will be found to share many of the physiological properties of the type 5 muscle fibre.

In studying the function of slow motor units, the response to stimulation of a single nerve fibre is of interest; but, because these motor units are innervated by several motoneurons, a more detailed study of their function will require a different stimulation procedure.

When muscle fibres contract in response to stimulation of

their motoneurons, a chain of complex processes is involved. However, for fast motor units, the combined effects of all these processes may be approximated with a second-order system and a time delay. The time delay appears to be associated with the events leading up to the release of calcium in the muscle and its subsequent contraction; and the second-order behavior can be simulated with the Huxley-Julian model for muscle activation and contraction outlined in Appendix 7. Although the model is a complex one involving several interacting variables, Stein and Wong [124] have shown that its frequency response is similar to that of a critically-damped second-order system. They proposed that this behavior is due to the limiting effects of two parameters. According to this proposal, the relaxation of the twitch is limited by the slower rate constant of activation (β in Appendix 7), and the rising phase of the twitch is limited by the rate constant for forming cross bridges (f_1), the rate constant for breaking cross bridges (g_1) or the series stiffness (k_s).

Since the input signals to motor units normally consist of trains of narrow pulses, a study of the impulse response of a second-order system can be helpful in interpreting the frequency response plots which were measured experimentally. The form of the impulse response depends upon whether the damping ratio is less than or greater than unity [2]. Plots of the impulse response, $h(t)$, for various values of ζ are illustrated in Figure 8.1. The response for $\zeta=1$ is of particular interest. For this situation, known as critical damping, the impulse response decays from its peak value as rapidly as possible while still remaining monotonic.

The effects of k and f_n on the impulse response can be
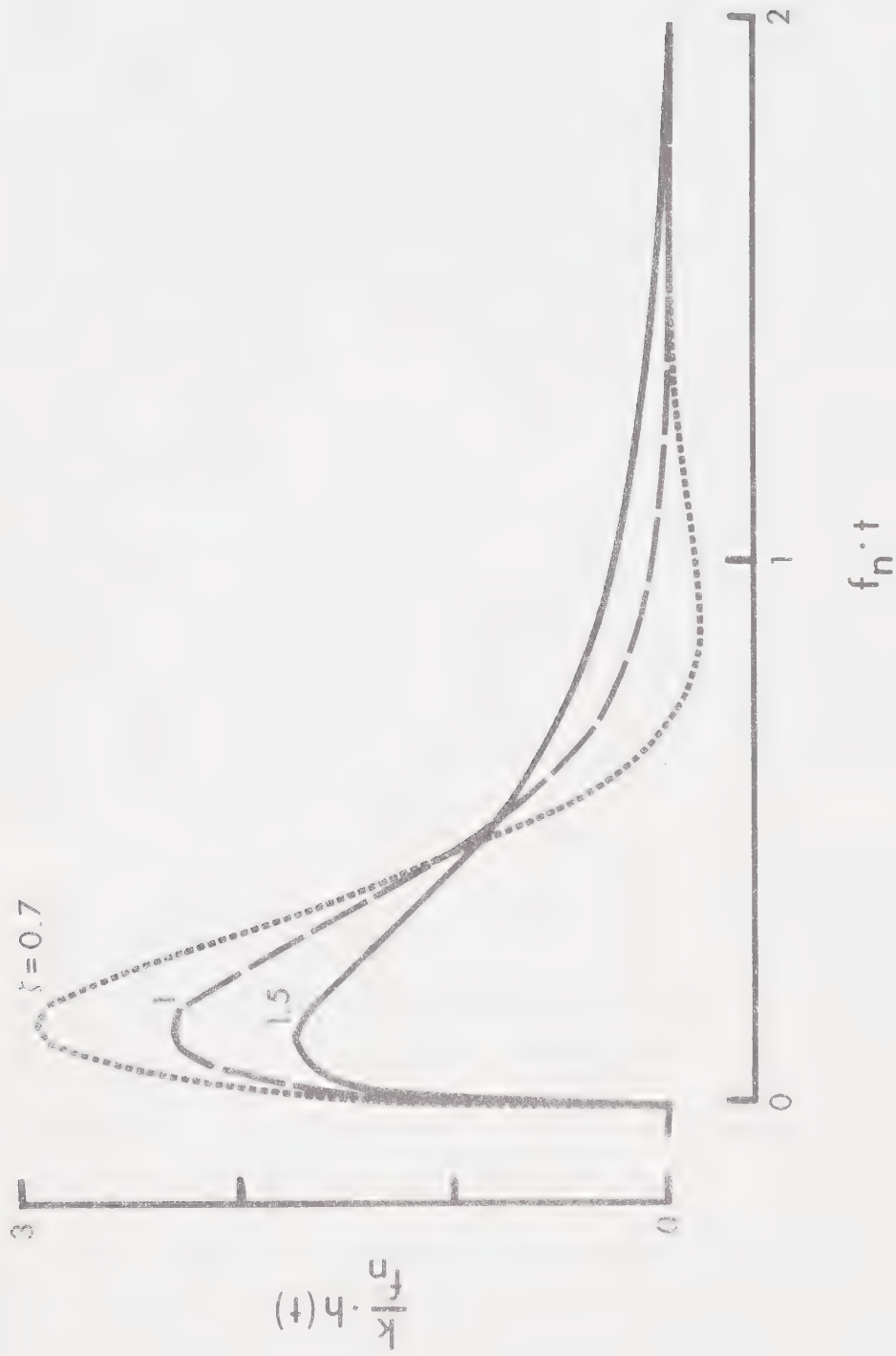
FIGURE 8.1 Impulse Response of Second-Order System

determined from Figure 8.1. An increase in k will result only in an increase in the overall magnitude of the impulse response, thereby increasing the average value of the response. An increase in f_n causes the peak value to increase and the time course of the response to shorten, but the average value remains unchanged.

Certain characteristics of the response to a train of narrow pulses can be deduced from the shape of the impulse response. If the natural frequency is low, summation of the individual impulse responses will be apparent at low stimulus rates, and the output waveform will be relatively smooth. For such a situation, the output at any time will be noticeably influenced by impulses which occurred earlier in time, and the response to a sudden change in stimulus rate will therefore be slow. If the natural frequency is high, however, the output waveform for low stimulus rates will appear more like a series of distinct impulse responses, and the response to a sudden change in stimulus rate will occur more quickly.

For all but the longest muscle lengths, the responses of type 1 and type 2 motor units were close to being critically damped. The slightly higher damping ratios which occurred at long muscle lengths and for type 3 motor units are indicative of a more slowly declining twitch which results in a slightly lower speed of response to changes in stimulus rate.

The increase in damping ratio and the decrease in natural frequency which occurred for type 1 and type 2 motor units as the muscle was stretched indicate that, as the muscle becomes longer, its speed of response decreases; and the higher dc gains at long muscle lengths show that the average force generated per stimulus pulse is

higher. These observations agree with the results presented by Close [94] for the frog sartorius muscle which contains only type 1 and type 2 muscle fibres [34]. He observed that the maximum twitch tension and the twitch contraction time increased as the muscle was stretched, and he concluded that these increases are due to length-dependent changes in the contractile process.

The unusual behavior of type 3 motor units at short muscle lengths (low coherence, high damping ratio, variability of twitch amplitude) may be due to stretch sensitivity of the motor nerve endings. The effects of such stretch sensitivity have been noted by Kuffler and Williams [62] and by Ralston and Libet [64]. Orkand [65] proposed that these effects are due to the small amount of neuromuscular transmitter substance released at the motor endplate by an individual nerve impulse. Hutter and Trautwein [125] have demonstrated that neuromuscular transmission is facilitated when the muscle is stretched. Such facilitation is apparent as an increase in the size of the local depolarization which occurs in the muscle fibre near the neuromuscular junction when a stimulus pulse is applied to the nerve. At short muscle lengths, the local depolarization may not be great enough to cause a propagated muscle action potential. However, as Nasledov [63] suggests, the local depolarization could produce a small local contraction of the muscle fibre, and the effects of such a local contraction may possibly be great enough to increase the damping ratio. The muscle fibres affected in this way would not contribute to the twitch response of the motor unit, so this response would be smaller than usual. Since the response of type 3 motor units at short muscle lengths is highly unpredictable, it seems probable that these motor units are normally activated only

at muscle lengths greater than the natural resting length.

Because the input-output relationships for fast motor units appeared to be noise-free when the muscle was at its natural resting length, the decrease in coherence observed for all three fast motor unit types as the mean stimulus rate was increased can be interpreted as a decrease in linearity resulting from the development of tetanic muscular contractions. Also common to all fast motor units at increased stimulus rates was a systematic decrease in natural frequency. When considered together with the increase in damping ratio which was only slight, this drop in natural frequency indicates that the motor units respond more quickly to a single stimulus than to variations in some mean stimulus rate.

The peak in the dc gain versus mean stimulus rate curve occurred at very low stimulus rates for the type 1 motor units and at higher mean rates for the type 2 and type 3 units. Since the dc gain can be viewed as a measure of the average force generated per stimulus pulse, it appears that type 1 motor units respond most effectively when they are stimulated at low rates, and type 2 and type 3 motor units are most effective when stimulated at higher rates. In other words, the type 2 and type 3 motor units seem to be best suited to the detection of variations in some mean stimulus rate, whereas the type 1 units operate most effectively in an on-or-off manner. One effect which might be associated with this difference in rate sensitivity is the facilitation which has been observed at the frog neuromuscular junction in response to repetitive stimulation [126,127]. Repetitive stimulation also affects the electrical and contractile processes in frog muscle [128-130]. Stein and Wong [124] demonstrated with a mathematical model

for muscle activation and contraction that saturation of the calcium re-uptake process could be responsible for the observed changes in muscle frequency response at high stimulus rates.

In summary, an overall view of the possible functions of the various motor unit types can be presented. Slow motor units seem to have little influence on the control of normal movement. They produce very little force, and they cannot respond quickly enough to influence movements which occur at normal speed. Probably, the major function of these motor units is the maintenance of posture. Type 1 units appear to be designed to produce large, rapid muscular contractions in response to short bursts of stimuli. These motor units cannot be used effectively for repetitive movements because they fatigue rapidly, so they are probably used only when a quick powerful movement is required. Repetitive movements such as those required for normal swimming are most likely produced by type 2 and type 3 motor units with the type 2 units dominating at shorter muscle lengths. The mechanism for generating an increase in muscle tension therefore seems to depend upon the type of movement involved.

In human muscle, when force is gradually increased from zero, the smaller motor units are the first to become active [131]. At low levels of force, recruitment of additional motor units is the major mechanism for increasing force, but at higher levels, increased firing rate becomes more important [132]. For twitch contractions, however, a different mode of activation is apparent [133]. Twitch contractions involving only the large motor units are commonly observed.

If frog motor units are activated in a similar manner, the tension developed during rapid, powerful movements must be controlled

mainly by the recruitment of additional type 1 motor units. Stereo-
typed, repetitive movements may be slightly influenced by variations in
the stimulus rate, but movements of this type probably depend largely
on the recruitment of additional motor units when increased force is
needed. Movements requiring fine control of force probably use both
recruitment and variation of firing rate depending on the level of
force being produced.

8.5 Conclusions and Recommendations

Several conclusions resulting from this investigation have
been presented in Chapters 6, 7, and 8. These conclusions are
summarized below:

1. Motor units in the iliofibularis muscle of *Xenopus laevis*
   can be classified into 5 types--3 fast and 2 slow. Each
   motor unit contains muscle fibres of one type only. The
   histochemical characteristics of each muscle fibre type are
   consistent with the observed behavior of the corresponding
   motor unit type.

2. If a single motor unit is stimulated with a train of narrow,
   randomly-occurring pulses, spectral analysis methods can be
   used to determine a transfer function estimate for the motor
   unit. This estimate relates the low frequency components of
   the stimulus train to the resulting isometric muscle tension.

3. The results of such spectral analysis studies indicate that
   slow motor units are poorly-modeled by linear, noise-free
   systems at frequencies associated with normal movement.

4. Because the transfer function estimates for fast motor units

are similar to the transfer functions of second-order low-pass filters, a curve representing the response of such a filter with an added time delay can be fitted to each transfer function estimate. In this way, each input-output relationship for a fast motor unit can be represented by a linear model with four parameters.

5. Because the input-output relationship is affected by such factors as muscle length and mean stimulus rate, a set of linear models is required to represent the motor unit's response to changes in these factors. Such linear models are only approximate, and they are subject to many restrictions. However, they are useful because they provide a standard basis for describing motor unit responses. They also provide information which can be used to supplement the results of studies involving stimulation with trains of regularly-occurring pulses.

6. Computer simulations of fast motor units, based on the experimentally-determined linear models, can be used to demonstrate the effects of various modifications to the spectral analysis procedure. Such simulations can also be used to estimate confidence intervals for the parameters describing the linear models.

Future applications of spectral analysis to the study of muscle function should yield useful quantitative information on the responses of fast motor units to various combinations of length, load, and stimulus pattern. As well, the effects of other factors such as

temperature or drugs could be quantitatively assessed with this technique.

BIBLIOGRAPHY

[1] H.T. Milhorn, *The Application of Control Theory to Physiological Systems*. Philadelphia: W.B. Saunders, 1966.

[2] J.H. Milsum, *Biological Control Systems Analysis*. Toronto: McGraw-Hill, 1966.

[3] L. Stark, *Neurological Control Systems, Studies in Bioengineering*. New York: Plenum Press, 1968.

[4] R.B. Stein, "The role of spike trains in transmitting and distorting sensory signals," in *The Neurosciences - Second Study Program*, F.O. Schmitt, Ed. New York: Rockefeller University Press, 1970, pp. 597-604.

[5] L.D. Partridge, "Modification of neural output signals by muscle: A frequency response study," *J. Appl. Physiol.*, Vol. 20, pp. 150-156, 1965.

[6] N.P. Rosenthal, T.A. McKean, W.J. Roberts and C.A. Terzuolo, "Frequency analysis of stretch reflex and its main subsystems in triceps surae muscles of the cat," *J. Neurophysiol.*, Vol. 33, pp. 713-749, 1970.

[7] E.J. Bayly, "Spectral analysis of pulse frequency modulation," in *Proceedings of the Conference on Systems Analysis in Neurophysiology*, (Brainerd, Minnesota), 1969, pp. 48-59.

[8] Z.J. Koles and R.S. Smith, "Characteristics of the sensory discharge of the muscle spindle in *Xenopus laevis*," *Kybernetik*, Vol. 15, pp. 99-110, 1974.

[9] Z.J. Koles, *A Study of the Sensory Dynamics of a Muscle Spindle*. Ph.D. Thesis, Dept. of Electrical Engineering, University of Alberta, 1970.

[10] A.V. Holden, *Linear Analysis of Two Insect Mechanoreceptors.* Ph.D. Thesis, Dept. of Physiology, University of Alberta, 1971.

[11] H.S. Milner-Brown, R.B. Stein and R. Yemm, "The contractile properties of human motor units during voluntary isometric contractions," *J. Physiol.*, Vol. 228, pp. 285-306, 1973.

[12] A. Mannard and R.B. Stein, "Determination of the frequency response of isometric soleus muscle in the cat using random nerve stimulation," *J. Physiol.*, Vol. 229, pp. 275-296, 1973.

[13] N.R. Goodman, "Measurement of matrix frequency response functions and multiple coherence functions," *Air Force Flight Dynamics Laboratory Research and Technology Division Technical Report,* AFFDL-TR-65-56, 1965.

[14] J.S. Bendat and A.G. Piersol, *Measurement and Analysis of Random Data.* New York: John Wiley and Sons, 1966.

[15] D.H. Perkel, G.L. Gerstein and G.P. Moore, "Neuronal spike trains and stochastic point processes--I. The single spike train," *Biophys. J.*, Vol. 7, pp. 391-418, 1967.

[16] D.H. Perkel, G.L. Gerstein and G.P. Moore, "Neuronal spike trains and stochastic point processes--II. Simultaneous spike trains," *Biophys. J.*, Vol. 7, pp. 419-440, 1967.

[17] P.A.W. Lewis, "Remarks on the theory, computation and application of the spectral analysis of series of events," *J. Sound. Vib.*, Vol. 12, pp. 353-375, 1970.

[18] G.P. Moore, D.H. Perkel and J.P. Segundo, "Statistical Analysis and functional interpretation of neuronal spike data," *Ann. Rev. Physiol.*, Vol. 28, pp. 493-522, 1966.

[19]   A.S. French and A.V. Holden,   "Alias-free sampling of neuronal
       spike trains," *Kybernetik*, Vol. 8, pp. 165-171, 1971.

[20]   W.T. Cochran, J.W. Cooley, D.L. Favin, H.D. Helms, R.A. Kaenel,
       W.W. Lang, G.C. Maling, D.E. Nelson, C.M. Rader and P.D. Welch,
       "What is the fast Fourier transform?" *IEEE Trans. Audio and
       Electroacoustics*, Vol. AU-15, pp. 45-56, 1967.

[21]   J.W. Cooley, P.A.W. Lewis and P.D. Welch, "Historical notes on
       the fast Fourier transform," *IEEE Trans. Audio and Electro-
       acoustics*, Vol. AU-15, pp.45-56, 1967.

[22]   G.D. Bergland, "A guided tour of the fast Fourier transform,"
       IEEE Spectrum, Vol. 6, pp. 41-52, 1969.

[23]   G.M. Jenkins and D.G. Watts, *Spectral Analysis and its Applications*.
       San Francisco:Holden-Day, 1968.

[24]   G.E. Blinston, "A procedure for applying spectral analysis tech-
       niques to the study of motor unit properties in skeletal muscle,"
       in *Proceedings of the Fourth Canadian Medical and Biological
       Engineering Conference*, (Winnipeg, Manitoba), 1972, pp. 46a-46b.

[25]   R.B. Stein, A.S. French, A. Mannard and R. Yemm, "New methods for
       analyzing motor function in man and animals," *Brain Res.*, Vol. 40,
       pp. 187-192, 1972.

[26]   T.A. McKean, R.E. Poppele, N.P. Rosenthal and C.A. Terzuolo,
       "The biologically relevant parameter in nerve impulse trains,"
       Kybernetik, Vol. 6, pp. 168-170, 1970.

[27]   V.B. Mountcastle, *Medical Physiology*.SSt. Louis: C.V. Mosby, 1968.

[28]   G.H. Bell, J.N. Davidson and D. Emslie-Smith, *Textbook of
       Physiology and Biochemistry*. Edinburgh: Churchill Livingstone,
       1972.

[29] H. Davson and M.G. Eggleton, *Principles of Human Physiology.*
      London: J. and A. Churchill, 1968.

[30] E. Henneman and C.B. Olson, "Relations between structure and
      function in the design of skeletal muscles," *J. Neurophysiol.*,
      Vol. 28, pp. 581-598, 1965.

[31] C.B. Olson and C.P. Swett, "Effects of prior activity on pro-
      perties of different types of motor units," *J. Neurophysiol.*,
      Vol. 34, pp. 1-16, 1971.

[32] J.M. Stein and H.A. Padykula, "Histochemical classification of
      individual skeletal muscle fibres of the rat," *Am. J. Anat.*,
      Vol. 110, pp. 103-124, 1962.

[33] R.E. Burke, D.N. Levine, P. Tsairis and F.E. Zajac,
      "Physiological types and histochemical profiles of motor units in
      the cat gastrocnemius," *J. Physiol.*, Vol. 234, pp. 723-748, 1973.

[34] R.S. Smith and W.K. Ovalle, "Varieties of fast and slow extra-
      fusal muscle fibres in amphibian hind limb muscles," *J. Anat.*,
      Vol. 116, pp. 1-24, 1973.

[35] J. Lännergren and R.S. Smith, "Types of muscle fibres in toad
      skeletal muscle," *Acta Physiol. Scand.*, Vol. 68, pp. 263-274, 1966.

[36] A. Hess, "Vertebrate slow muscle fibres," *Physiol. Rev.*, Vol. 50,
      pp. 40-62, 1970

[37] M. Nowogrodzka-Zagórska, "The organization of extraocular muscles
      in Anura," *Acta. Anat.*, Vol. 87, pp. 22-44, 1974.

[38] H.E. Huxley, "Muscle cells," in *The Cell*, J. Brachet and A.E.
      Mirsky, Eds. New York: Academic Press, 1960, Vol. 4, pp. 365-481.

[39] A. Sandow, "Skeletal muscle," *Ann. Rev. Physiol.*, Vol. 32,
      pp. 87-138, 1970.

[40] H.E. Huxley, "Evidence for continuity between the central elements of the triads and extracellular space in frog sartorius muscle," *Nature,* Vol. 202, 1067-1071, 1964.

[41] A.F. Huxley, "Muscular contraction," *J. Physiol.,* Vol. 243, pp. 1-43, 1974.

[42] A. White, P. Handler and E.L. Smith, *Principles of Biochemistry.* New York: McGraw-Hill, 1973.

[43] A.V. Hill, "The mechanics of active muscle," *Proc. Royal Soc., London, Series B,* Vol. 141, pp. 104-117, 1953.

[44] A.L. Hodgkin, "The ionic basis of electrical activity in nerve and muscle," *Biol. Rev.,* Vol. 26, pp. 339-409, 1951.

[45] B. Katz, *Nerve, Muscle and Synapse.* New York: McGraw-Hill, 1966.

[46] R. Rüdel and S.R. Taylor, "Aqueorin luminescence during contraction of amphibian skeletal muscle," *J. Physiol.,* Vol. 233, pp. 5-6P, 1973.

[47] S. Ebashi, M. Endo and I. Ohtsuki, "Control of muscle contraction," *Q. Rev. Biophys.,* Vol. 2, pp. 351-384, 1969.

[48] W. Burke and B.L. Ginsborg, "The electrical properties of the slow muscle fibre membrane," *J. Physiol.,* Vol. 132 pp. 586-598, 1956.

[49] N.V. Zimkin, V.G. Panov, V.T. Raikov, "Fast and slow fibres in human muscles." *Neurosci. and Behav. Physiol.,* Vol. 6, pp. 1-7, 1973.

[50] S.W. Kuffler and R.W. Gerard, "The small nerve motor system to skeletal muscle," *J. Neurophysiol.,* Vol. 10, pp. 383-394, 1947.

[51] L.D. Peachey, "Muscle," *Ann. Rev. Physiol.,* Vol. 30, pp. 401-440, 1968.

[52] G.C. Joyce, P.M.H. Rack and D.R. Westbury, "The mechanical properties of cat soleus muscle during controlled lengthening and shortening movements," *J. Physiol.*, Vol. 204, pp. 461-474, 1969.

[53] G.C. Joyce and P.M.H. Rack, "Isotonic lengthening and shortening movements of cat soleus muscle," *J. Physiol.*, Vol. 204, pp.475-491, 1969.

[54] P.M.H. Rack and D.R. Westbury, "The effects of length and stimulus rate on tension in the isometric cat soleus muscle," *J. Physiol.*, Vol. 204, pp. 443-460, 1969.

[55] E.E. Selkurt, *Physiology*. Boston: Little, Brown & Co., 1966.

[56] G.S. Cliff and R.M.A.P. Ridge, "Innervation of extrafusal and intrafusal fibres in snake muscle," *J. Physiol.*, Vol. 233, pp. 1-18, 1973.

[57] A.M. McPhedran, R.B. Wuerker and E. Henneman, "Properties of motor units in a homogeneous red muscle (soleus) of the cat," *J. Neurophysiol.*, Vol. 28, pp. 71-84, 1965.

[58] I. Tasaki and K. Mizutani, "Comparative studies on the activities of the muscle evoked by two kinds of motor nerve fibres," *Jap. J. Med. Sci.*, Vol. 10, pp. 237-244, 1944.

[59] S. Kuffler, Y. Laporte, and R.E. Ransmeier, "The function of the frog's small-nerve motor system," *J. Neurophysiol.*, Vol. 10, pp. 395-408, 1947.

[60] H. Sommerkamp, "Das Substrat der Dauerverkürzung am Froschmuskel," *Arch. Exp. Path. Pharmak.*, Vol. 128, pp. 99-115, 1928.

[61] S.W. Kuffler and E.M. Williams, "Small nerve junction potentials. The distribution of small motor nerves to skeletal muscle and the membrane characteristics of the fibres they innervate," *J. Physiol.*, Vol. 121, pp. 289-317, 1953.

[62] S.W Kuffler and E.M. Williams, "Properties of the slow skeletal muscle fibres of the frog," *J. Physiol.*, Vol. 121, pp. 318-340, 1953.

[63] G.A. Nasledov, "Electrical excitability of different types of frog skeletal muscle fibres," *Federation Proceedings, Trans. Supp.*, Vol. 25, pp. T443-T446, 1966.

[64] H.J. Ralston and B. Libet, "Effect of stretch on action potential of voluntary muscle," *Am. J. Physiol.*, Vol. 173, pp. 449-455, 1953.

[65] R.K. Orkand, "A further study of electrical responses in slow and twitch muscle fibres of the frog," *J. Physiol.*, Vol. 167, pp. 181-191, 1963.

[66] P. Krüger, "Grundlagen des Tetanus und Tonus der quergestreiften Skelettmuskelfasern der Wirbeltiere," *Experientia*, Vol. 6, pp. 75-80, 1950.

[67] A. Hess, "The structure of extrafusal muscle fibres in the frog and their innervation studied by the cholinesterase technique," *Am. J. Anat.*, Vol. 107, pp. 129-152, 1960.

[68] E.G. Gray, "The spindle and extrafusal innervation of a frog muscle," *Proc. Royal Soc., London, Series B*, Vol. 146, pp. 416-430, 1956.

[69] L.D. Peachey and A.F. Huxley, "Structural identification of twitch and slow striated muscle fibres of the frog," *J. Cell Biol.* Vol. 13, pp. 177-180, 1962.

[70] S.G. Page, "A comparison of the fine structures of frog slow and twitch muscle fibres," *J. Cell Biol.*, Vol. 26, pp. 477-497, 1965.

[71] G. Asmussen and A. Kiessling, "Die Muskelfasersorten des Frosches: Ihre Identifikation und die Gesetzmässigkeiten ihrer Anordnung in der Skelettmuskulatur," *Acta Biologica et Medica Germanica*, Vol. 24, pp. 871-889, 1970.

[72] R.S. Smith and J. Lännergren, "Types of motor units in the skeletal muscle of *Xenopus laevis*," *Nature*, Vol. 217, pp. 281-283, 1968.

[73] R.B. Blackman and J.W. Tukey, *The Measurement of Power Spectra.* New York: Dover Publications, 1959.

[74] M.J. Hinich and C.S. Clay, "The application of the discrete Fourier transform in the estimation of power spectra, coherence, and bispectra of geophysical data," *Rev. Geophys.*, Vol. 6, pp. 347-363, 1968.

[75] B.P. Lathi, *Communication Systems.* New York: John Wiley and Sons, 1968.

[76] R.W. Ramirez, "The fast Fourier transform's errors are predictable, therefore manageable," *Electronics*, Vol. 47, pp. 96-102, 1974.

[77] D.M. Munro, "Implementing the fast Fourier transform," *Engineering in Medicine Laboratory, Imperial College of Science and Technology, London, England, Application Report No. 3, 1973.*

[78] D.W. Tufts, H.S. Hersey, and W.E. Mosier, "Effects of FFT coefficient quantization on bin frequency response," *Proc. IEEE*, Vol. 60, pp. 146-147, 1971.

[79] C. Bingham, M.D. Godfrey, and J.W. Tukey, "Modern techniques of power spectrum estimation," *IEEE Trans. Audio and Electroacoustics*, Vol. AU-15, pp. 56-66, 1967.

[80] W.C. Orr and H.J. Hoffman, "A 90-min cardiac biorhythm: Methodology and data analysis using modified periodograms and complex demodulation," *IEEE Trans. Biomed. Eng.*, Vol. BME-21, pp. 130-143, 1974.

[81] J.W. Cooley, P.A.W. Lewis, and P.D. Welch, "The application of the fast Fourier transform to the estimation of spectra and cross-spectra," *J. Sound Vib.*, Vol. 12, pp. 339-352, 1970.

[82] T.S. Durrani and J.M. Nightingale, "Data windows for digital spectral analysis," *Proc. IEE*, Vol. 119, pp. 343-352, 1972.

[83] E.A. Sloane, "Comparison of linearly and quadratically modified spectral estimations of Gaussian signals," *IEEE Trans. Audio and Electroac.*, Vol. AU-17, pp. 133-137, 1969.

[84] P.D. Welch, "The use of fast Fourier transform for the estimation of power spectra: a method based on time averaging over short, modified periodograms," *IEEE Trans. Audio and Electroacoustics*, Vol. AU-15, pp. 70-73, 1967.

[85] R. Otnes and L. Enochson, *Digital Time Series Analysis*. New York; Wiley, 1972.

[86] R.A. Olshen, "Asymptotic properties of the periodogram of a discrete stationary process," *J. Appl. Probability*, Vol. 4, pp. 508-528, 1967.

[87] V.A. Benignus, "Estimation of the coherence spectrum and its confidence interval using the fast Fourier transform," *IEEE Trans. Audio and Electroacoustics*, Vol. AU-17, pp. 145-150, 1969.

[88] G.C. Carter, C.H. Knapp, and A.H. Nuttall, "Estimate of the magnitude-squared coherence function via overlapped fast Fourier transform processing," *IEEE Trans. Audio and Electroacoustics*, Vol. AU-21, pp. 337-344, 1974.

[89] V.A. Benignus, "Estimation of coherence spectrum of non-Gaussian time series populations," *IEEE Trans. Audio and Electroacoustics*, Vol. AU-17, pp. 198-201, 1969.

[90] M.R. Foster and N.J. Guinzy, "The coefficient of coherence: its estimation and use in geophysical data processing," *Geophysics*, Vol. 32, pp. 602-616, 1967.

[91] P.R. Roth, "Effective measurements using digital signal analysis," *IEEE Spectrum*, Vol. 8, pp. 62-70, 1971.

[92] J.W. Cooley, P.A.W. Lewis, and P.D. Welch, "The fast Fourier transform algorithm: programming considerations in the calculation of sine, cosine, and Laplace transforms," *J. Sound Vib.*, Vol. 12, pp. 315-337, 1970.

[93] A.M. Gordon, A.F. Huxley, and F.J. Julian, "The variation in isometric tension with sarcomere length in vertebrate muscle fibres," *J. Physiol.*, Vol. 184, pp. 170-192, 1966.

[94] R.I. Close, "The relations between sarcomere length and character-istics of isometric twitch contractions of frog sartorius muscle," *J. Physiol.*, Vol. 220, pp. 745-762, 1972.

[95] A.V. Hill, "The heat of shortening and the dynamic constants of muscle," *Proc. Royal Soc., London, B*, Vol. 126, pp. 136-195, 1938.

[96]   W. Grabowski, E.A. Lobsiger and H.C. Lüttgau, "The effect of
repetitive stimulation at low frequencies upon the electrical
and mechanical activity of single muscle fibres," *Pflüger's
Arch.*, Vol. 334, pp. 222-239, 1972.

[97]   S. Kita, I. Nagai, and S. Murakami, "Studies on fatigue in frog
sartorius muscle," *Sapporo Med. J.*, Vol. 39, pp. 144-155, 1971.

[98]   D.E. Nelsen, "Calculation of power density spectra for a class
of randomly jittered waveforms," *M.I.T. Res. Lab. of Electronics,
Cambridge, Mass., QPR No. 74*, pp. 168-179, 1964.

[99]   S.O. Rice, "Mathematical analysis of random noise," *Bell System
Tech. J.*, Vol. 23, pp. 284-332 and Vol. 24, pp. 46-156, 1944.

[100]   E.J. Bayly, "Spectral analysis of pulse frequency modulation in
the nervous system," *IEEE Trans. Biomed. Eng.*, Vol. BME-15,
pp. 257-265, 1968.

[101]   Z.J. Koles, E.M. Edwards, and R.S. Smith, "A method for the
measurement of instantaneous pulse frequency," *J. Sci. Inst. E,
Series 2*, Vol. 2, pp. 597-600, 1969.

[102]   M.M.Nachlas, K.C. Tsou, E. DeSouza, C.S. Cheng, and A.M. Seligman,
"Cytochemical demonstration of succinic dehydrogenase by the use
of a new p-nitrophenyl substituted ditetrazole," *J. Histochem.
and Cytochem.*, Vol. 5, pp. 420-436, 1957.

[103]   E. Kugelberg and L. Edström, "Differential histochemical effects
of muscle contractions on phosphorylase and glycogen in various
types of fibres; relation to fatigue," *J. Neurol., Neurosurg.,
and Psychiatry*, Vol. 31, pp. 415-423, 1968.

[104] W. Halpern and N.R. Alpert, "A stochastic signal method for measuring dynamic mechanical properties of muscle," *J. Appl. Physiol.*, Vol. 31, pp. 913-925, 1971.

[105] R.C. Dorf, *Modern Control Systems*. Reading Mass.: Addison-Wesley, 1967.

[106] E.C. Levy, "Complex-curve fitting," *IRE Trans. Auto. Control*, Vol. AC-4, pp. 37-43, 1959.

[107] A. Kislack, *Transfer Function Estimation Using the Fast Fourier Transform*, M.Sc. Thesis, Naval Postgraduate School, Monterey, California, 1969.

[108] C.K. Sanathanan and J. Koerner, "Transfer function synthesis as a ratio of two complex polynomials," *IEEE Trans. Auto. Control*, Vol. AC-8, pp. 56-58, 1963.

[109] R.B. Streets and G.L. Hemphill, "Advances in on-line system identification using FFT," in *Proceedings of the Symposium on Computers, Electronics and Control*, (Calgary, Alberta), 1973, pp. VI-3.

[110] R. Fletcher and M.J.D. Powell, "A rapid descent method for minimization," *Computer J.*, Vol. 6, pp. 163-168, 1963.

[111] A.P. Sage and J.L. Melsa, *System Identification*. New York: Academic Press, 1971.

[112] C.M. Rader and B. Gold, "Digital filter design techniques in the frequency domain," *IEEE Proceedings*, Vol. 55, pp. 149-171, 1967.

[113] K.W. Smillie, *STATPACK2: An APL Statistical Package*. Edmonton: University of Alberta Dept. of Computing Science, Publication No. 17, 1969.

[114] A.F. Huxley, "Muscle structure and theories of contraction,"
       Prog. Biophys. biophys. Chem., Vol. 7, pp. 257-318, 1957.

[115] F.J. Julian, "Activation in a skeletal muscle contraction model
       with a modification for insect fibrillar muscle," *Biophys. J.*
       Vol. 9, pp. 547-570, 1969.

[116] N.A. Hutchinson, Z.J. Koles, and R.S. Smith, "Conduction
       velocity in myelinated nerve fibres of *Xenopus laevis*,"
       J. Physiol., Vol. 208, pp. 279-289, 1970.

[117] B. Katz and R. Miledi, "The measurement of synaptic delay, and
       the time course of acetylcholine release at the neuromuscular
       junction," *Proc. Royal Soc., London, Series B*, Vol. 161,
       pp. 483-495, 1965.

[118] J.B. Thomas, *An Introduction to Statistical Communication Theory.*
       New York: John Wiley and Sons, Inc., 1969.

[119] R.B. Wuerker, A.M. McPhedran, and E. Henneman, "Properties of
       motor units in a heterogeneous pale muscle (m. gastrocnemius) of
       the cat," *J. Neurophysiol.*, Vol. 28, pp. 85-99, 1965.

[120] A.J. Buller, J.C. Eccles, and R.M. Eccles, "Interactions between
       motoneurones and muscles in respect of the characteristic speeds
       of their responses," *J. Physiol.*, Vol. 150, pp. 417-439, 1960.

[121] A.J. Buller and D.M. Lewis, "Further observations on mammalian
       cross-innervated skeletal muscle," *J. Physiol.*, Vol. 178,
       pp. 343-358, 1965.

[122] R. Elul, R. Miledi, and E. Stefani, "Neural control of contracture in slow muscle fibres of the frog," *Acta. Physiol. Lat. Amer.*, Vol. 20, pp. 194-226, 1970.

[123] N.V. Samosudova, R.G. Lyudkovskaya, and G.M. Frank, "Change in the ultrastructure of the slow and intermediate muscle fibres of the frog on tonic contraction," *Biofizika*, Vol. 17, pp. 1055-1060, 1972.

[124] R.B. Stein and E.Y.-M. Wong, "Analysis of models for the activation and contraction of muscle," *J. Theor. Biol.*, Vol. 46, pp. 307-327, 1974.

[125] O.F. Hutter and W. Trautwein, "Neuromuscular facilitation by stretch of motor nerve endings," *J. Physiol.*, Vol. 133, pp. 610-625, 1956.

[126] K.L. Magleby, "The effect of repetitive stimulation on facilitation of transmitter release at the frog neuromuscular junction," *J. Physiol.*, Vol. 234, pp. 327-352, 1973.

[127] M. Braun, R.F. Schmidt, and M. Zimmermann, "Facilitation at the frog neuromuscular junction during and after repetitive stimulation," *Pflüger's Arch.*, Vol. 287, pp. 41-55, 1966.

[128] J. Hanson and A. Persson, "Changes in the action potential and contraction of isolated frog muscle after repetitive stimulation," *Acta Physiol. Scand.*, Vol. 81, pp. 340-348, 1971.

[129] R. Connolly, W. Gough, and S. Winegrad, "Characteristics of the isometric twitch of skeletal muscle immediately after a tetanus," *J. Gen Physiol.*, Vol. 57, pp. 697-709, 1971.

[130] A. Isaacson, "Post-staircase potentiation, a long-lasting twitch potentiation of muscles induced by previous activity," *Life Sciences*, Part 1, Vol. 8, pp. 337-342, 1969.

[131] H.S. Milner-Brown, R.B. Stein, and R. Yemm, "The orderly recruitment of human motor units during voluntary isometric contractions," *J. Physiol.*, Vol. 230, pp. 359-370, 1973.

[132] H.S. Milner-Brown, R.B. Stein, and R. Yemm, "Changes in firing rate of human motor units during linearly changing voluntary isometric contractions," *J. Physiol.*, Vol. 230, pp. 371-390, 1973.

[133] J. Hannerz, "Discharge properties of motor units in relation to recruitment order in voluntary contraction," *Acta Physiol. Scand.* Vol. 91, pp. 374-384, 1974.

[134] R.S. Smith, G. Blinston, and W.K. Ovalle, "Skeletomotor and fusimotor organization in amphibians," in *Control of Posture and Locomotion*, R.B. Stein, K.B. Pearson, R.S. Smith, and J.B. Redford, Eds. New York: Plenum, 1973, pp. 105-117.

[135] G.A. Mihram, *Statistical Foundations and Methodology.* New York: Academic Press, 1972.

[136] International Business Machines Corporation, *System 360 Scientific Subroutine Package (360A-CM-03X) Version II Programmer's Manual.* New York: 1967.

[137] B.C. Kuo, *Analysis and Synthesis of Sampled-Data Control Systems.* Englewood Cliffs, N.J.: Prentice-Hall, 1963.

[138] R.R Sokal and F.J. Rohlf, *Biometry.* San Francisco: W.H. Freeman and Co., 1969.

APPENDIX 1

LOW-PASS FILTER

The circuit in Figure A1.1 consists of a voltage follower and two identical second-order low-pass filters cascaded together. The transfer function of the first filter is

$$H(s) = \frac{-R_3}{R_1} \cdot \frac{1}{1+[C_1 R_2 R_3 (\frac{1}{R_1} + \frac{1}{R_2} + \frac{1}{R_3})]s + R_2 R_3 C_1 C_2 s^2} \qquad (A1.1)$$

If the component values are selected so that the filter frequency response is maximally flat, the transfer function has the following form

$$H(s) = \frac{a}{1 + \frac{\sqrt{2}s}{2\pi f_c} + \frac{s^2}{(2\pi f_c)^2}} \qquad (A1.2)$$

where a is the gain of the filter and f_c is its cutoff frequency. The component values required for cutoff frequencies of 3, 15 and 30 Hz are listed in Table A1.1.

When two such filters are cascaded, the resulting magnitude and phase characteristics are respectively

$$M(f) = \frac{1}{1+(\frac{f}{f_c})^4}$$

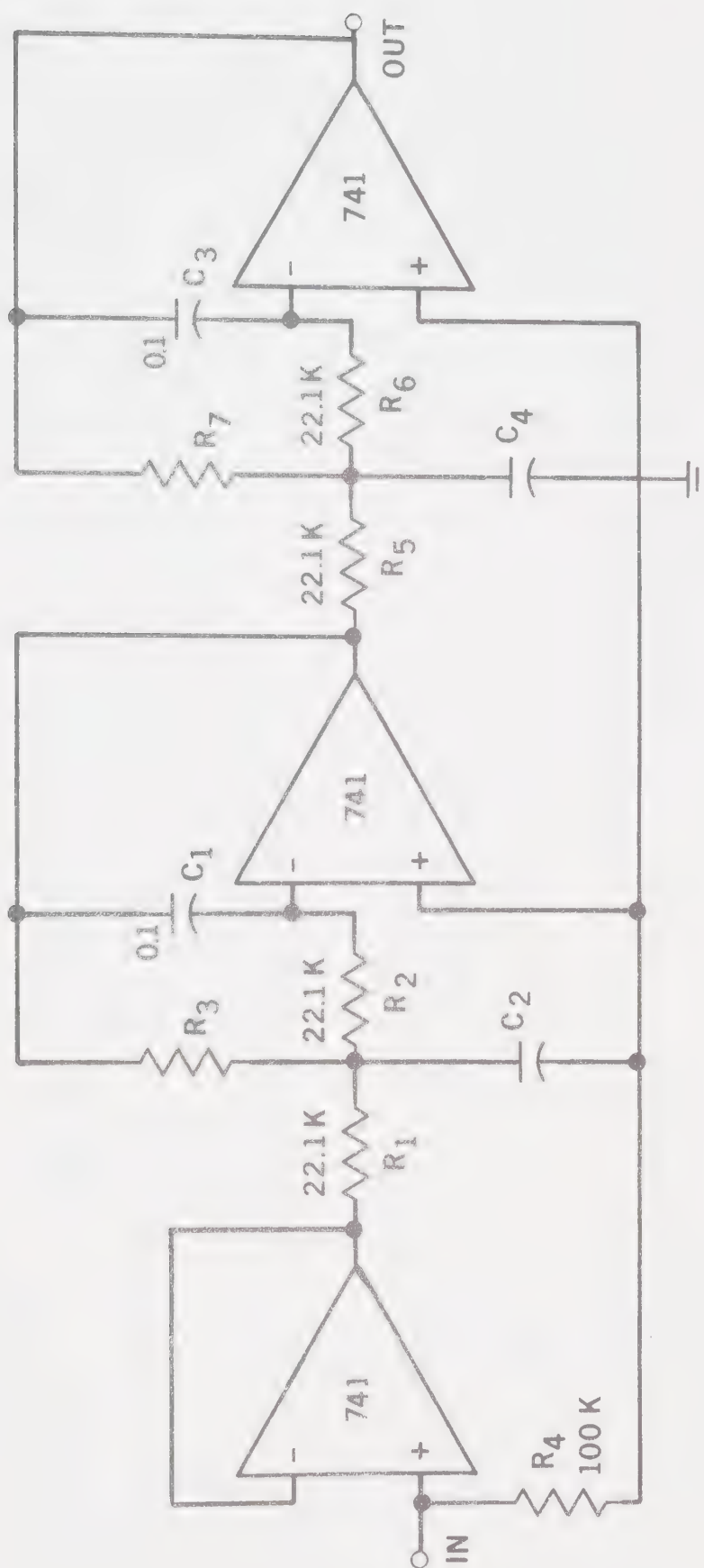$$P(f) = - \tan^{-1} \left[\frac{\frac{\sqrt{2}f}{f_c}}{1 - (\frac{f}{f_c})^2} \right]$$

(A1.3)

FIGURE A1.1 Circuit Diagram for Anti-Aliasing Filter

R_1, R_2, R_5, R_6 = 22.1kΩ

C_1, C_3 = 0.1μf

f_c (Hz)	a	R_3, R_7	C_2, C_4
3	16.5	365kΩ	3.5μf
15	2.87	63.4kΩ	0.82μf
30	1.21	26.7kΩ	0.47μf

TABLE A1.1

Component Values for Low-Pass Filter

APPENDIX 2

GENERATION OF RANDOM PULSE TRAINS

Random pulse trains with interpulse intervals distributed as gamma distributions were generated by a Hewlett-Packard 2100 computer with a digital-to-analog converter. The interpulse intervals for each pulse train were derived from uniformly distributed pseudo-random numbers created by the power residue method [135]. The particular set of pseudo-random numbers created consisted of integers with values between 1 and 32767. A series of numbers distributed as a gamma distribution could be derived from these integers in the following manner:

If x_i is any number (not necessarily integer) from a population distributed uniformly between x_{max} and x_{min}, and

$$y_i = - \frac{1}{\beta} \cdot \ln(\frac{x_i - x_{min}}{x_{max} - x_{min}}) \tag{A2.1}$$

the probability density function for y is [135]

$$p(y) = \beta e^{-\beta y} \tag{A2.2}$$

Now if

$$t_j = y_1 + y_2 + \ldots y_g \tag{A2.3}$$

the probability density function for t is [135]

$$p(t) = \frac{\beta^g t^{g-1}}{\Gamma(g)} \cdot e^{-\beta t} \tag{A2.4}$$

where $\Gamma(g)$ is the gamma function of g. This expression is the probability density function for a gamma distribution of order g with a scaling factor β.

If x_i belongs to a population of uniformly distributed integers, the values of y_i are limited to

$$y_i = -\frac{1}{\beta} \cdot \ln\left(\frac{n}{x_{max}-x_{min}}\right) \qquad n = 0,1,\ldots x_{max}-x_{min} \qquad (A2.5)$$

and the values of t_j must be derived from these y_i. This means that the value of any interpulse interval created from a series of uniformly distributed integers in the above manner must be one of a specific set of values. No other interpulse intervals are permitted. In addition, interpulse intervals which are infinite or equal to zero must be eliminated if the pulse train is to be physically realizable.

The power spectra for a set of such pulse trains with values of g ranging from 1 to 8 were estimated from modified periodograms according to the methods outlined in Chapter 3 and compared with the corresponding theoretical spectra calculated from Equation (4.2). Differences between the actual and theoretical spectra were negligible.

APPENDIX 3

FLOW CHARTS FOR COMPUTER PROGRAMS

The following terms, used in the flow charts, are entered on
the teletype when required:

Data Collection Program (Figure A3.1)

        ITIME Sampling interval (msec)

        NPTS Number of points per data block

        NRECS Number of data blocks to be collected

    Sampling Control Commands

        AB Abort

        RS Restart

        GO Begin sampling

        MT Stop

        PA Pause--temporarily stop sampling until CO command

            received. Maintain scope display.

        CO Continue

Data Analysis Program (Figure A3.2)

        RECORDS TO DISPLAY Identification numbers of first and
                          last members of a string of consecu-
                          tive data blocks. Transfer function
                          estimates are calculated by averaging
                          spectral estimates based on these
                          consecutive data blocks.

        LABEL Two numbers which will appear in the lower left
            corner of the plot to aid in identification.

    Display Commands--Indicate which plot is to be displayed on
            scope.

149

GA Gain

PH Phase

CO Coherence

NP New Plot

MT Stop

RS Restart

Data Storage Program (Figure A3.3)

LABEL Any 72 character identifying label to be stored

on the magnetic tape together with the data

NRECS Number of data blocks to be stored

Curve Fitting Program (Figure A3.4)

RECORDS TO BE DISPLAYED See data analysis program

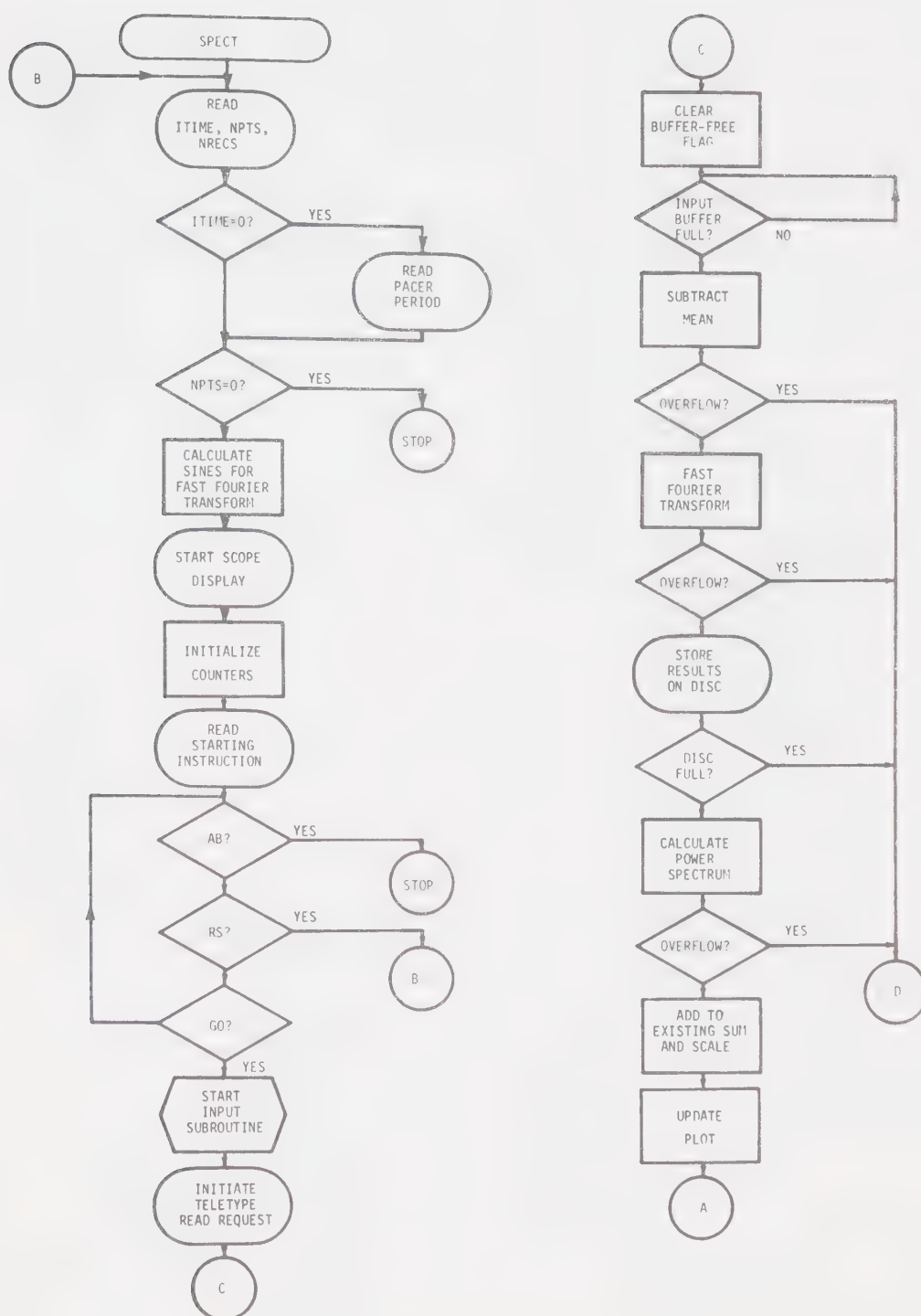Display Commands

RS Restart

PH Phase plot

NP New plot

ST Stop
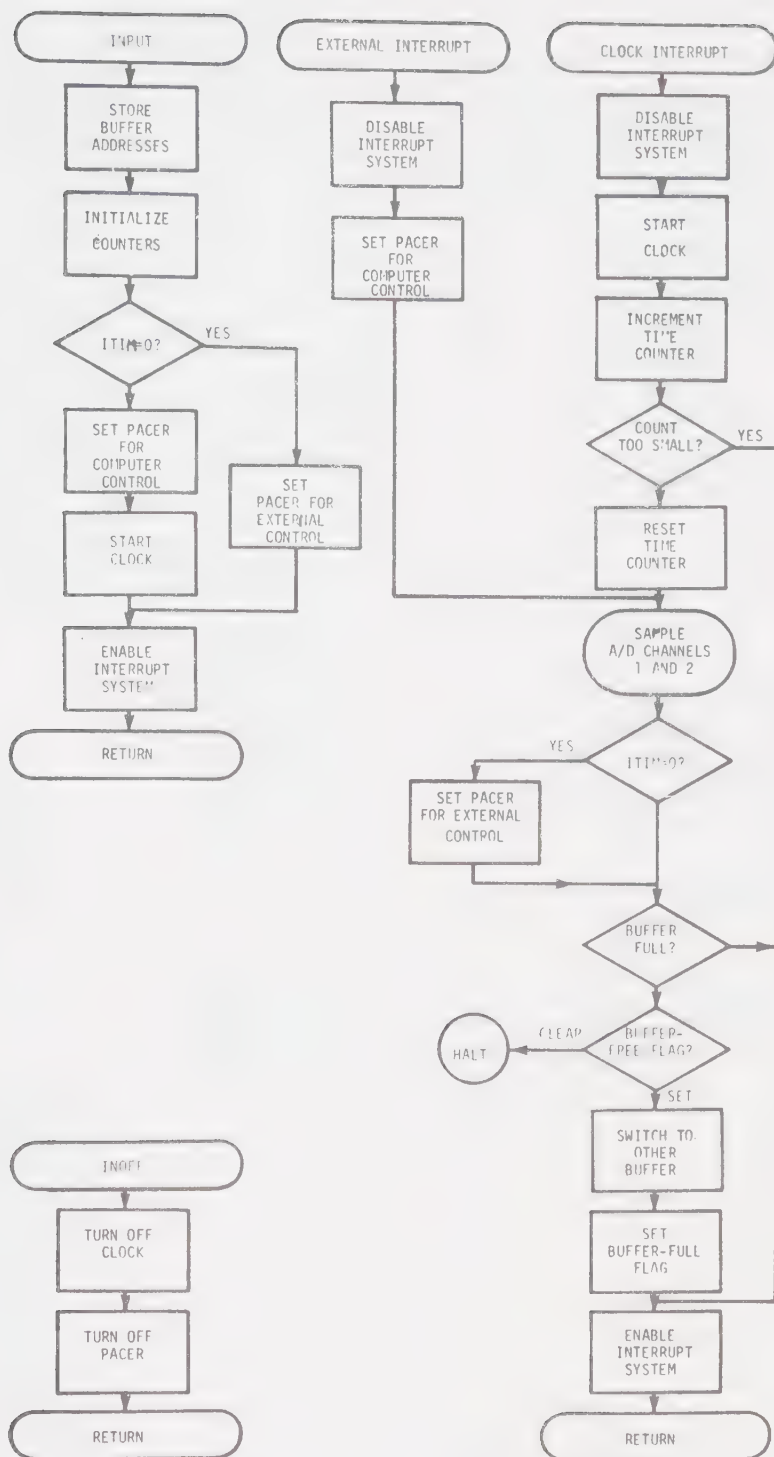
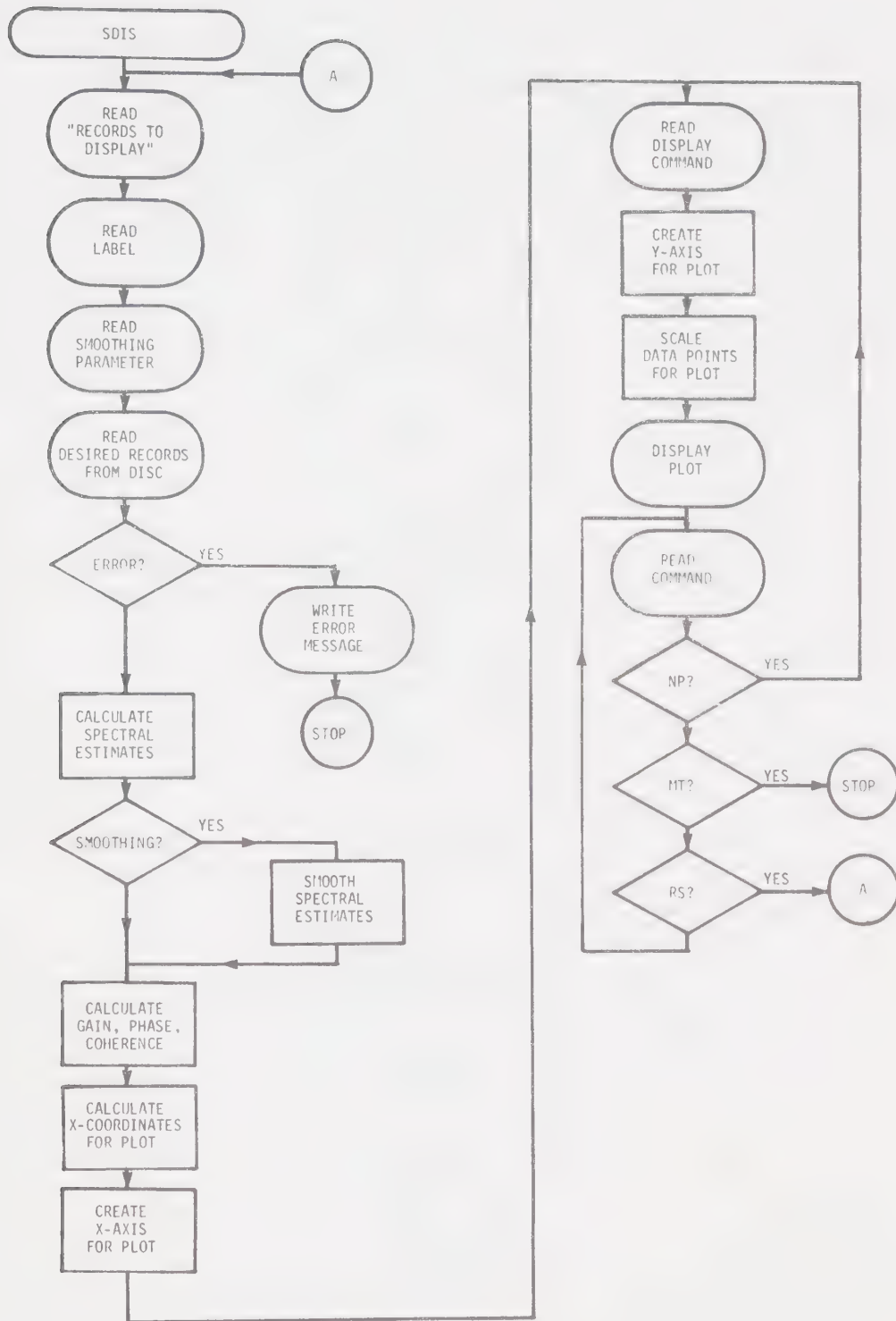FIGURE   A3.1   Flow Chart for Data Collection Program

FIGURE A3.1 continued

FIGURE A3.1   continued
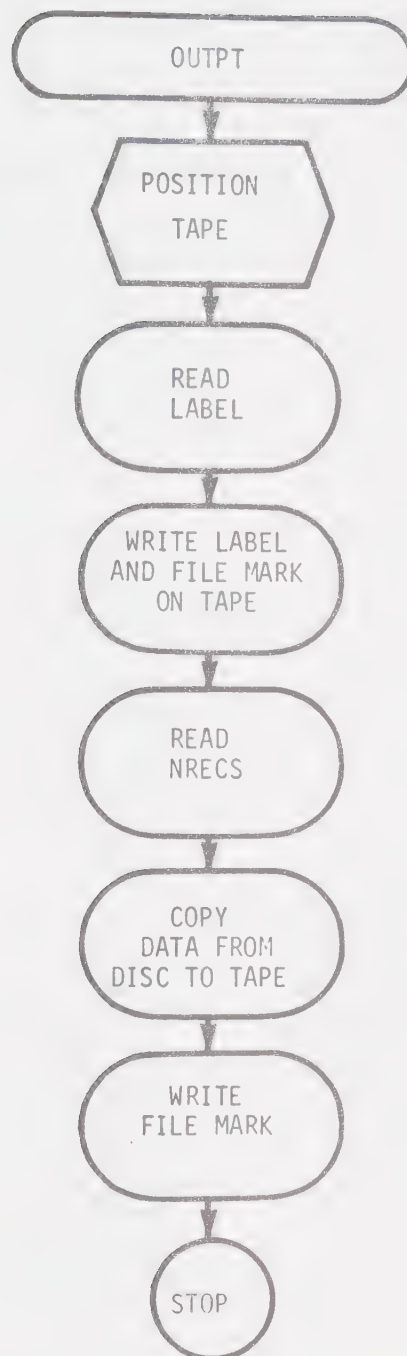
FIGURE A3.2   Flow Chart for Data Analysis Program

FIGURE A3.3   Flow Chart for Data Storage Program
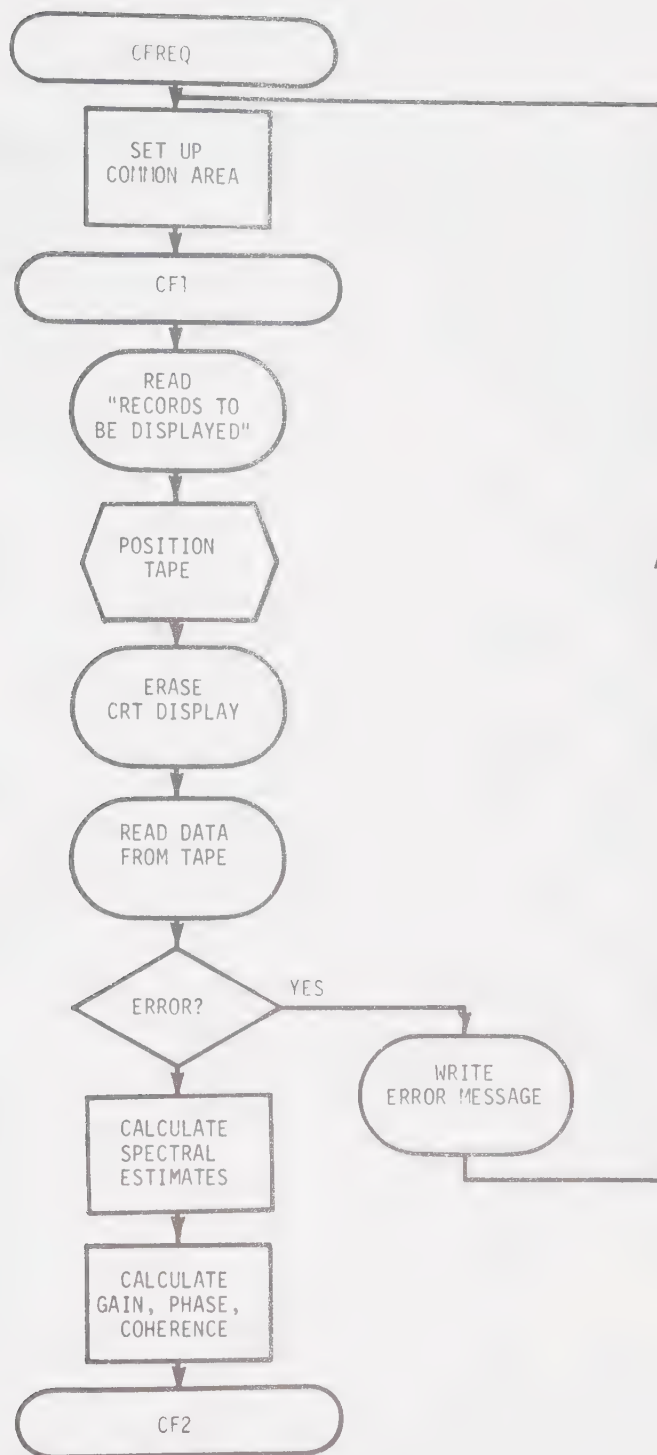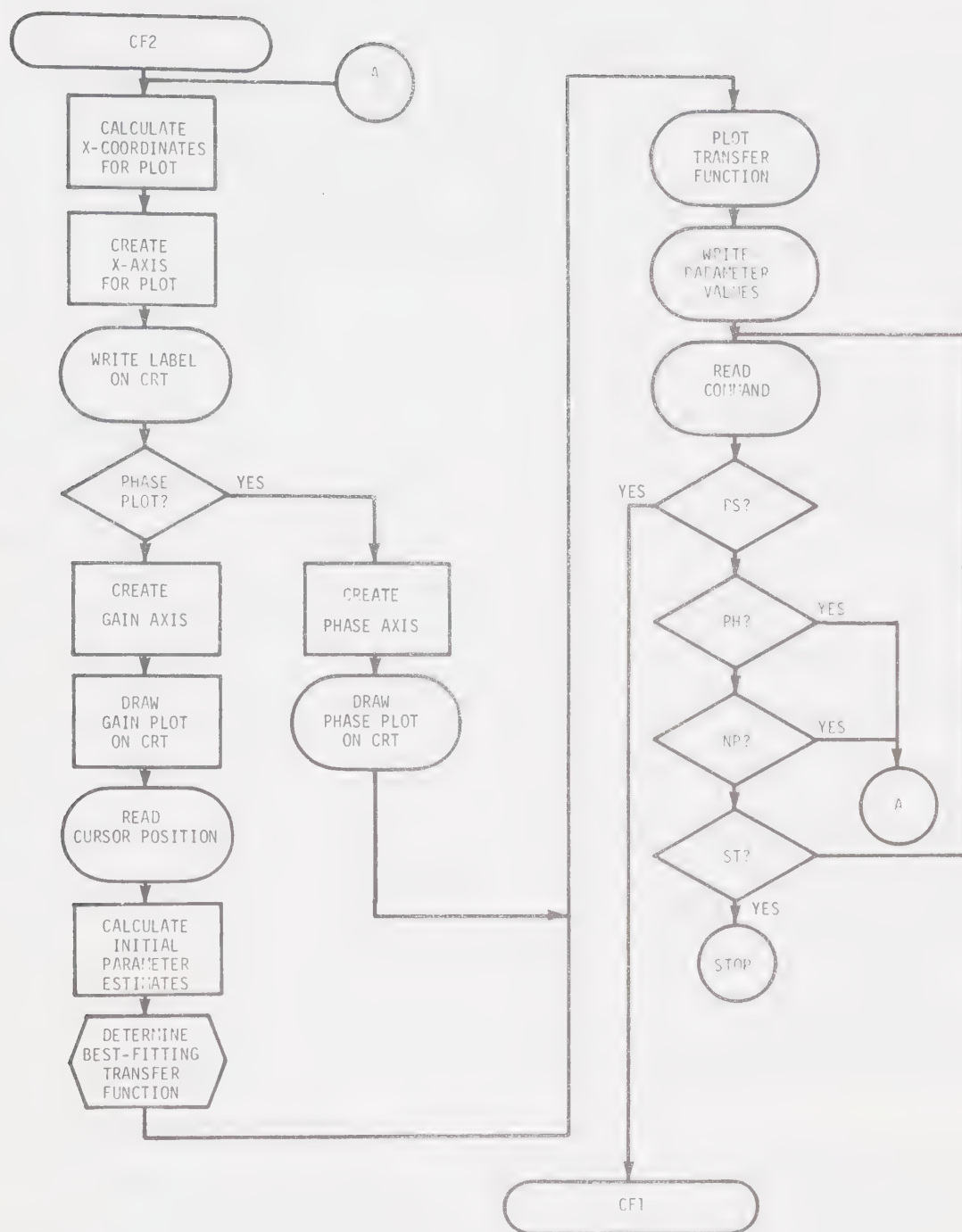
FIGURE A3.4   Flow Chart for Curve-Fitting Program

FIGURE A3.4   continued

APPENDIX 4

STIMULUS AND SAMPLING CONTROL CIRCUITRY

The circuit in Figure A4.1 provides bursts of pulses to trigger a Hewlett-Packard 5610A analog to digital converter so that it collects samples in groups of 128. In addition, gate and trigger signals for an Ortec 4710 stimulator are provided so that stimulation occurs only during these bursts.

The sine wave appearing at the base of Q_1 is converted to a pulse train by means of the shaping circuit consisting of Q_1 and Q_2. These pulses are coupled through G_1 and G_2 to the base of Q_6 and to the input of the counting circuit which consists of C_1 and the four J-K flip flops. This situation continues as long as the $\overline{Q}$ output of FF_4 is high. When this output changes state, G_2 closes and counting stops. When a reset pulse occurs at the base of Q_5, the counter and flip flops are reset, $\overline{Q}$ becomes high, and pulses may once again pass through G_2. When 128 pulses have occurred, G_2 is closed, and counting once again ceases. Thus, pulses appearing at the emitter of Q_6 will occur in bursts of 128. The pulse frequency is equal to the frequency of the sine wave, and the interval between bursts is equal to the interval between reset pulses. G_1 insures that output pulses do not occur during the reset period.

Trigger pulses for the stimulator are derived from pulses applied to the base of Q_3. These pulses are reshaped by the circuit consisting of Q_3 and Q_4, and applied to one input of G_3 which is open whenever the $\overline{Q}$ output of FF_4 is high. In this way, external trigger pulses for the stimulator are gated by G_3. If the stimulator is to be triggered internally it may be gated directly with the Q output of FF_4.
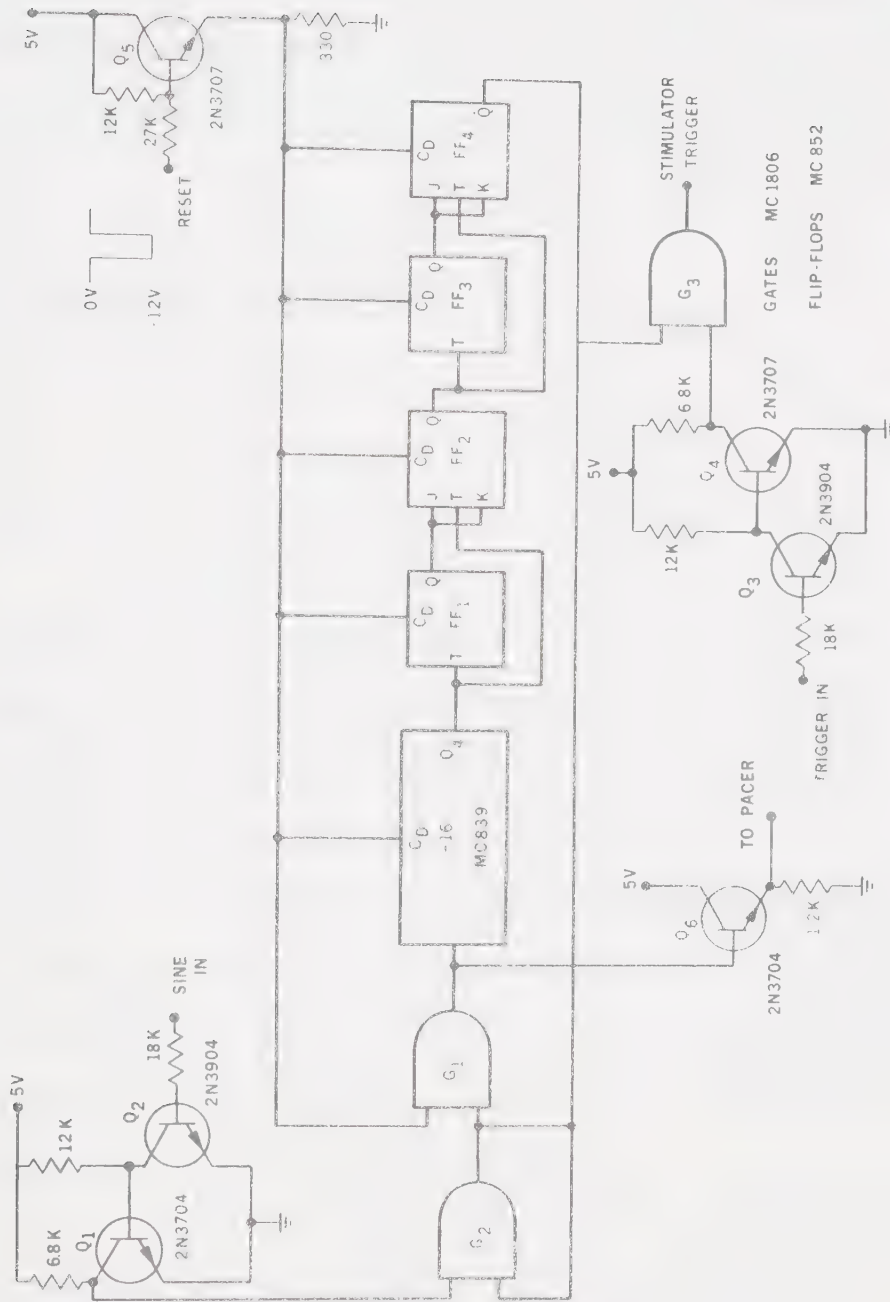
158

FIGURE A4.1 Circuit Diagram for Counter-Controlled Gate

APPENDIX 5

THE CURVE FITTING TECHNIQUE

If $\hat{\bar{H}}$ is a transfer function estimate determined at frequencies $f_1, f_2, \ldots f_N$ and $\bar{H}$ is a function of one or more parameters which is to be fitted to this estimate, the parameter values for $\bar{H}$ which result in the best fit are determined when the quantity ε is minimized.

$$\varepsilon = \sum_{q=1}^{N} \left| \hat{\bar{H}}(jf_q) - \bar{H}(jf_q) \right|^2 \tag{A5.1}$$

For single motor units, $\bar{H}$ is of the form

$$\bar{H}(jf) = \frac{kf_n^2}{f_n^2 - f^2 + j2\zeta ff_n} \, e^{-2\pi f\tau} \tag{A5.2}$$

ε is therefore a function of four parameters τ, k, ζ and f_n.

The parameter values for which ε is minimized may be calculated with subroutine FMFP from the IBM scientific subroutine package [136]. This subroutine, which uses the Fletcher-Powell method [110] for minimizing a function, requires a user-written subroutine which calculates the function value and gradient vector for a given set of parameter values. The function value may be determined by evaluating Equation (A5.2) at the desired frequencies and substituting the results into Equation (A5.1), but evaluation of the gradient vector requires a set of expressions for the partial derivatives of ε with respect to each of the four parameters.

$\hat{\bar{H}}$ and $\bar{H}$ are complex numbers with real and imaginary parts $\hat{\bar{H}}_R$, $\bar{H}_R$ and $\hat{\bar{H}}_I$, $\bar{H}_I$ respectively. For any parameter ν,

$$\frac{\partial \varepsilon}{\partial \nu} = 2 \sum_{q=1}^{N} \left[\frac{\partial \bar{H}_R}{\partial \nu} (\bar{H}_R - \hat{\bar{H}}_R) + \frac{\partial \bar{H}_I}{\partial \nu} (\bar{H}_I - \hat{\bar{H}}_I) \right] \tag{A5.3}$$

$\overline{H}$ can be written as

$$\overline{H} = AC-BD+j(BC+AD) \tag{A5.4}$$

where

$$A = \frac{kf_n^2(f_n^2-f^2)}{(f_n^2-f^2)^2+4\zeta^2f^2f_n^2} \tag{A5.5}$$

$$B = \frac{-2k\, ff_n^3}{(f_n^2-f^2)^2+4\zeta^2f^2f_n^2} \tag{A5.6}$$

$$C = \cos 2\pi f\tau \tag{A5.7}$$

$$D = -\sin 2\pi f\tau \tag{A5.8}$$

The partial derivatives are

$$\frac{\partial \overline{H}_R}{\partial \nu} = A\,\frac{\partial C}{\partial \nu} + C\,\frac{\partial A}{\partial \nu} - B\,\frac{\partial D}{\partial \nu} - D\,\frac{\partial B}{\partial \nu} \tag{A5.9}$$

$$\frac{\partial \overline{H}_I}{\partial \nu} = B\,\frac{\partial C}{\partial \nu} + \ldots \tag{A5.10}$$

Expressions for the partial derivatives of A, B, C, and D with respect to each of the four parameters τ, k, ζ and f_n are presented in Table A5.1. In order to determine the gradient vector, these expressions must be evaluated at the desired frequencies. The results may be used in Equations (A5.9) and (A5.10) and a value for each element of the gradient vector may then be determined from Equation (A5.3).

v	τ	k	ζ	f_n
$\dfrac{\partial A}{\partial v}$	0	$\dfrac{f_n^2(f_n^2 - f^2)}{G}$	$\dfrac{-8\zeta k f^2 f_n^4(f_n^2 - f^2)}{G^2}$	$\dfrac{k f_n f^2[8\zeta^2 f_n^4 - 2(f_n^2 - f^2)^2]}{G^2}$
$\dfrac{\partial B}{\partial v}$	0	$\dfrac{-2\zeta f f_n^3}{G}$	$\dfrac{-2k i f_n^3[(f_n^2 - f^2)^2 - 4\zeta^2 f^2 f_n^2]}{G^2}$	$\dfrac{2k\zeta f f_n^2[f_n^4 + f f_n^2(2 - 4\zeta^2) - 3f^4]}{G^2}$
$\dfrac{\partial \cdot}{\partial v}$	$-2\pi\sin(2\pi f\tau)$	0	0	0
$\dfrac{\partial \cdot}{\partial v}$	$-2\pi\cos(2\pi f\tau)$	0	0	0

$$G = (f_n^2 - f^2)^2 + 4\zeta^2 f^2 f_n^2$$

TABLE A5.1

Partial Derivatives For Gradient Vector Evaluation

APPENDIX 6

DIGITAL REALIZATION OF SECOND ORDER LOW-PASS FILTER

The frequency response of an analog filter with transfer function $H(s)$ is found by evaluating $H(s)$ at points along the imaginary axis of the s plane. The equivalent operation for a digital filter with transfer function $H'(z)$ consists of evaluating this function at points along the unit circle in the z plane where $z = e^{Ts}$ and T is the sampling interval. The imaginary axis on the s plane may be mapped onto the unit circle on the z plane by means of the bilinear transformation [137]

$$s = \frac{z-1}{z+1} \qquad (A6.1)$$

If the analog frequency variable is defined as ω_A and the digital frequency variable is $\omega_D T$, the functions $H(\omega_A)$ and $H'(\omega_D T)$ take on the same values when [112]

$$\omega_A = \tan \frac{\omega_D T}{2} \qquad (A6.2)$$

Therefore, a second order low-pass digital filter with natural frequency ω_c' is equivalent to an analog filter with a natural frequency of

$$\omega_c = \tan \frac{\omega_c' T}{2} \qquad (A6.3)$$

Using Equations (A6.1) and (6.2) the transfer function for the digital filter is

$$H'(z) = \frac{\omega_c^2}{(\frac{z-1}{z+1})^2 + 2\zeta\omega_c (\frac{z-1}{z+1}) + \omega_c^2} \qquad (A6.4)$$

163

This is equivalent to

$$H'(z) = \frac{\omega_c(1+2z^{-1}+z^{-2})}{(1+2\zeta\omega_c+\omega_c^2)+z^{-1}(2\omega_c^2-2)+z^{-2}(1-2\zeta\omega_c+\omega_c^2)} \qquad (A6.5)$$

and this expression is equal to the ratio of the z transforms of the output and input signals $y(nT)$ and $x(nT)$ where $n=0,1,2\ldots$

$$H'(z) = \frac{Y(z)}{X(z)} \qquad (A6.6)$$

If this relationship is substituted into Equation (A6.5) the result is

$$Y(z) = \frac{1}{A}\left[Y(z)(-Bz^{-1}-Cz^{-2})+\omega_c^2 X(z)(1+2z^{-1}+z^{-2})\right] \qquad (A6.7)$$

where

$$A = 1+2\zeta\omega_c+\omega_c^2 \qquad (A6.8)$$

$$B = 2(\omega_c^2-1)$$

$$C = 1-2\zeta\omega_c+\omega_c^2$$

The inverse z transform of Equation (A6.7) is

$$y(nT) = \frac{1}{A}\{-By[(n-1)T]-Cy[(n-2)T]\} +$$

$$\frac{\omega_c^2}{A}\{x[nT]+2x[(n-1)T]+x[(n-2)T]\} \qquad (A6.11)$$

With this equation, the value of the filtered signal at sampling instant n may be calculated when the values of the input signal and the filtered signal for the previous two sampling instants are known. Also required is the value of the input signal at sampling instant n. When n equals 0 or 1, the previous two sample values are not available, and a common practise is to set the unknown values equal to zero. This is equivalent to multiplying the continuous signals $x(t)$ and $y(t)$ by unit step functions before they are sampled.

APPENDIX 7

THE HUXLEY-JULIAN MODEL

The following is a summary of the Huxley-Julian model for
muscle activation and contraction as presented by Stein and Wong [124].

Huxley [114] proposed that muscle contraction is produced
when cross-bridges on the A filaments link with specific sites on the
I filaments. Because cross-bridges can only become linked on one side
of their equilibrium position, force is generated in only one
direction. The time course of interacting cross bridges was described
by a first-order differential equation.

$$\frac{\partial n}{\partial t} = (1-n)f - ng \qquad (A7.1)$$

where f and g are position-dependent variables for making and breaking
cross-bridges respectively, and n is the proportion of cross-bridges
that are made.

The force generated by all the interacting cross-bridges at
any time, t, is P_g where

$$P_g = \int_{-\infty}^{} k_0 nu \, du \qquad (A7.2)$$

k_0 is a normalization constant, and u is a normalized variable
representing the distance from the equilibrium position. The infinite
limits on the integral imply that integration is extended in both
directions from the equilibrium position until P_g no longer changes
appreciably. The equivalent stiffness of the interacting cross-bridges
is k_g where

$$k_g = \int_{-\infty}^{} k_0 n \, du \qquad (A7.3)$$

The variable f in Equation (A7.1) was assumed to depend on